Development of whole cell-based biosensor in 3D environment for nanoparticles cytotoxicity detection

Dissertation

To Fulfill the

Requirements for the Degree of

„doctor rerum naturalium“ (Dr. rer. nat.)

Submitted to the Council of the Faculty

of Biology and Pharmacy

of the Friedrich Schiller University Jena

by Master (MSc) biotechnologist Monika Dubiak-Szepietowska

born on 3rd of April 1989 in Sieradz (Poland)

Gutachter:

1. Prof. Dr. rer. nat. habil. Thomas Winckler, Friedrich Schiller University Jena

2. Prof. Dr. rer. nat. habil. Karl-Heinz Feller, Ernst-Abbe- University of Applied Sciences Jena

3. Prof. Dr. habil. Fred Lisdat, Technical University Wildau

Jena, 8th of December 2016

Table of contents

List of figures

List of figures in appendix

List of tables

List of abbreviations

2D - two-dimensional cell culture; monolayer cell culture

3D - three-dimensional cell culture

AP - alkaline phosphatase

AP-1- -activator protein 1

CAD - computer-aided design

CAT - chloramphenicol acetyltransferase

CBB - cell-based biosensor

DMEM - Dulbecco's Modified Eagle Medium

DMSO - dimethyl sulfoxide

EC_{50} - half maximal effective concentration

ECM - extracellular matrix

EHS - Engelbreth-Holm-Swarm mouse carinoma

GAPDH - glyceraldehyde 3-phosphate dehydrogenase

GFP - green fluorescent protein

GIT - gastrointestinal tract

GUS - β-Glucuronidase

HSP - heat shock protein

IKKα, IKK1 - kinase IκB

IKKβ, IKK2 - kinase IκB

IKKγ – NEMO, NF-κB essential regulatory protein

IL- interleukin

ISRE/IRF -IFN-stimulated response elements /interferon regulatory factor

IUPAC - International Union of Pure and Applied Chemistry

KC - Kupffer cells

lacZ - β-galactosidase

LPS - lipopolysaccharides

luc - luciferase

NEMO - NF-κB essential regulatory protein, IKKγ

NF-κB - nuclear factor kappa-light-chain-enhancer of activated B cells

NLS - nuclear localization signals

NP - nanoparticle(s)

PBS - phosphate buffered saline

PCR - polymerase chain reaction

PLAP - human placental alkaline phosphatase

*p*NPP - *p*-nitrophenyl phosphate

qPCR – quantitative (real time) PCR

REACH - Registration, Evaluation, Authorization and Restriction of Chemicals

RP - rapid prototyping

RT-PCR - reverse transcription PCR

SEAP - human secreted alkaline phosphatase

STAT3 - signal transducer and activator of transcription 3

TNF-α - tumor necrosis factor

1 MOTIVATION

Almost each day somewhere in the world, someone reveals a better technique for producing nanoparticles (NP), a better way of handling them, an even better preparation of functionalized them and application method in industry. It serves the dire need to test them in terms of toxicity in humans and to the environment. It is widely known that the same properties which provide technical benefits of nanotechnology also lead to potentially increased or unique health and safety exposures. As, the European Union postulates to reduce, refine and replace experiments on animals (3R principle; EU-Directive 2010/63), this demands the implementation of human-cell based models for toxicity assessment, which may mimic with the best possible efficiency living tissue and give highly predictive results to *in vivo*. Moreover, cell-based assays offers several advantages over the use of a whole animals or widely used molecular biology methods. Cells respond to external stimuli in a physiological manner thus, cell-based assays enable more comprehensive and complex functional information through providing insights into the mechanisms of toxicant action. Therefore, whole cell-based biosensor (CBB) was developed to monitor and screen toxic substances in *nano* range. Until today, the majority of cell-based assays take advantage of traditional two-dimensional (2D) monolayer cells cultured on flat surfaces. Although, the 2D cell culture has turned out to be a valuable method for cell-based research, its limitations have been increasingly identified. Thus, in the presented study, three dimensional cell-culture systems (3D) were incorporated as environments for sensor cells. Besides, the developed biosensor enable detection of toxicity in very early stage, before cell death, in short time even after 2 h exposure as opposed to widely used commercially available cell-based assays such as MTT, XTT Alamar Blue or LDH. Moreover, implementation of whole cell biosensors based on human cells in a three dimensional milieu and its application for screening of nanoparticle toxicity has not been investigated before. Additionally, the presented system joins the complex *in vitro* model imitating living tissue with high throughput analytical methods. Genetic modification of HepG2 cells resulted in generation novel NF-κB_HepG2 sensor cells with extracellular reporter protein (human secreted alkaline phosphatase). Finally, the selected screening pathway (NF-κB signaling) can be activated by a wide range of stimuli, which broadens application spectrum of presented CBB. Therefore, this system is well suited in nanoparticle toxicity detection but also for a wide variety of potentially

hostile compounds in basic screening to provide initial warning of adverse effects and trigger subsequent analysis and remedial actions.

The presented project aimed to improve the prediction of nanomaterial cytotoxicity on cell and tissue- level and provide the essential screening steps prior to any *in vivo* or environmental applications. Therefore, to achieve this goal, the initial objective was the use of a genetically modified human hepatoblastoma cell line (HepG2) that joins a cellular signaling system (NF-κB pathway) with a reporter gene (human secreted alkaline phosphatase) to create a whole cell-based biosensor with optical readout. This should allow the monitoring of toxic effects of chemicals in real time, in early stage before cell death. Based on these results it was intended to establish an environment for sensor cells with improved physiological relevance of cell-based assays. Since cells in the body grow in a three dimensional milieu, a 3D approach as an alternative to 2D culture was to be established to reduce the gap between cell culture and living tissue. Moreover, development of new cell models should be coupled with their usage in various quantitative measurements. Therefore, an additional objective was to transfer and optimize available analytical methods from 2D- to 3D-based cell culture.

2 INTRODUCTION

2.1 Biosensors

According to a IUPAC (International Union of Pure and Applied Chemistry) definition a biosensor is a self-contained integrated device, which is capable of providing specific quantitative or semi-quantitative analytical information using a biological recognition element which is retained in direct spatial contact with an transduction element [1]. Information is translated by the biological recognition elements from the biochemical domain (usually an analyte concentration or type), into a chemical or physical output signal with a defined sensitivity. Moreover, the purpose of the recognition system is to provide the sensor with a high degree of specificity for the analyte to be measured [2]. The transducer part of the sensor serves to transfer the signal from the recognition system, mostly to the detector domain. Widely used transduction systems are based on measurement of fluorescence, luminescence, absorbance, refractive index (optical transducers), amperometry, potentiometry (electrochemical transducers), calorimetry (thermal transducers), conductivity (electrical transducers) or quartz crystal microbalance measurements (piezoelectric transducers) [3], [4].

2.1.1 Whole cell-based biosensors

The term cell-based biosensor describes detection systems employing both prokaryotic and eukaryotic cells. Cell-based biosensors typically have three interconnected modules to accomplish the task, that is, the input of the sensor, the internal gene regulatory networks and the output system [5]. Input of the CBB is represented by receptors embedded in the cell membrane or inside the cytoplasm, which cells need to detect stimuli (e.g., chemicals, antigens, heat or light) and forward them into differential gene transcriptional levels or post-translation modifications. Next, the information is processed by the gene regulatory network, and integrated before an output decision is made. The gene expression levels are then altered to produce different proteins, which results in measurable changes [6], [7], [8]. Widely used method to create cell-based biosensors is transfection of cells with a reporter vector derived from a specific response promoter [9]. This kind of biosensors can detect biochemical effects directly via living cells and convert these effects into e.g. optical, electrical signals (Figure 1). In addition to analyte sensing and detecting, cell-based biosensors can carry the benefits of rapid and sensitive analysis

for *in situ* monitoring with cells. Compared with molecular biosensors, cell-based biosensors are expected to respond optimally to bioactive analytes. Additionally, CBB are characterized by many advantages, e.g., fast response time, long-term recording and label-free experimentation. However, cell-based biosensors still suffer from some intrinsic shortcomings. The common problems faced by the optimization of cell-based biosensors include how to achieve satisfactory stability, how to improve the selectivity of sensor cells and how to prolong the cells' lifetime [10], [11]. One of the first commercialized sensor based on single cells was naturally luminescent bacteria (Microtox® test). This simple sensor used the inhibition of the light after exposure with pollutant and was developed for monitoring of aquatic samples over 37 years ago [12]. Till now, have been published a number of reports where whole cells of microorganisms (such as bacteria, yeast and algae) were used as a screening element of environmental hazards [13], [14], [15], [16], [17] or mammalian cell-based sensors to evaluate chemical safety and their clinical potency [18], [19], [20], [21], [22] (more examples in Table 1). Nevertheless, CBB based on human cells used in nanomaterials toxicity screening represent small percentage of developed CBB. To date, all this kind of biosensors were developed and published by Peng Chen and Akiyoshi Taniguchi groups (National Institute for Materials Science, Namiki Tsukuba Japan) [9], [23]. Therefore, the project presented here will complement and expand this still novel field and will provide a step forward for a better understanding.

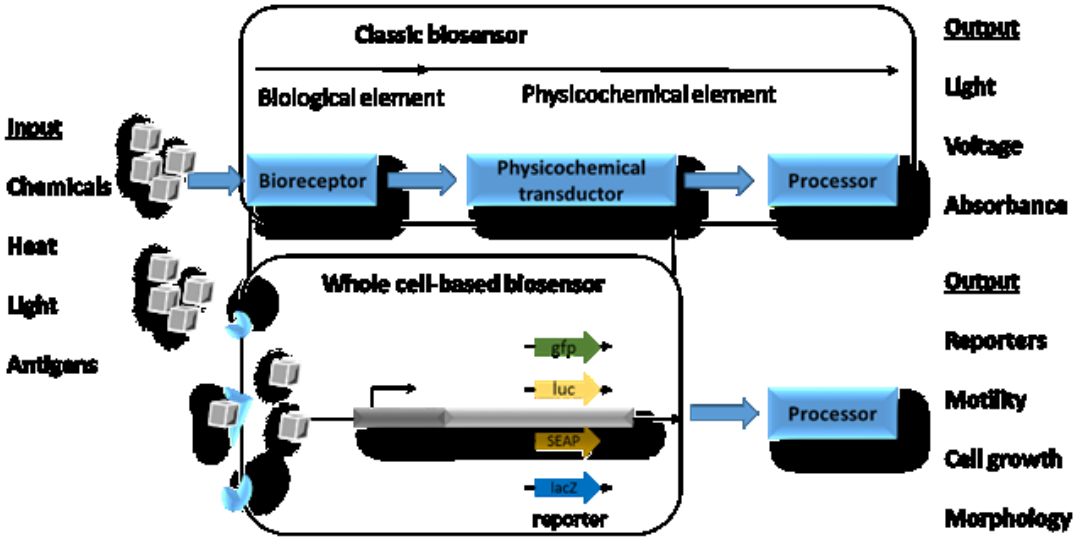

Figure 1. Schematic representation of classic and whole cell-based biosensor.

Whole cell-based biosensor	Analyte	Detection mode	Ref.
HaCaT cells (keratinocytes; human)	Heavy metals, plant extracts	Fluorescence	[24], [22]
Ped-2E9 cells (lymphocytes; murine)	*Listeria monocytogenes* strains, *Bacillus cereus* strains and toxins from *Listeria / Bacillus*	Laser scanning cytometry	[25]
Vero cells (kidney epithelial cells; monkey)	Mycotoxins (t-2, zearalenone)	Spectrophotometry	[26]
Alcaligenes eutrophus (a gram negative *Bacillus*)	Heavy metals	Bioluminescence / cyclic voltammetry	[27]
HUVECs cells (umbilical vein endothelial cells ; human)	Histamine	Ion-selective electrode (ISE)	[28]
Primary cells (cortical cells; rat)	Acetylcholine	Potentiometry	[29]
HepG2 (hepatoblastoma; human)	Copper ions	Bioluminescence	[30]
*HepG2 (hepatoblastoma; human)	Titanium dioxide nanoparticles	Bioluminescence	[23]
Chlorella vulgaris (algae)	Herbicides	Fluorescence	[31]
Pseudokirchneriella subcapitata (algae)	CuO, ZnO and TiO2 – nanoparticles	Fluorescence	[32]
NIH/3T3 (embryonic fibroblast; mouse)	Titanium dioxide nanoparticles	Bioluminescence	[33]

Table 1. Overview of the whole cell-based biosensors used in cytotoxicity assessment. * Developed CBB based on human cells used in nanoparticles toxicity screening.

2.1.1.1 Biosensing mechanism

In cell-based biosensor screening strategies, it is usually not the product of an endogenous enzyme, cell morphology or a pathway itself that comes out in a calculable output, but preferably the product of a reporter gene that provides a discriminating phenotype. Reporters such as *lacZ* (β-galactosidase), *luc* (luciferase), or *gfp* (the green fluorescent protein), can be easily screened by color formation, luminescence, or fluorescence. Promoters that are strongly activated under normal conditions (constitutive expression system) generally ensure a high basal expression level of the reporter gene. During exposure of the CBB to a potential toxic analyte, the expression dependent and inversely proportional to the tested sample toxicity. This influences the basic gene expression of the cell, inhibiting the growth, or inducing cell death and reducing the intensity of the reporter signal. Commonly, the promoters selected for designing these kind of CBB are those regulating the gene expression of constitutive genes, such as ribosomal proteins, metabolism proteins or cell structural proteins (e.g., tubulin, actin,

etc.), which maintain gene expression at a sufficiently high and constant level. Although these biosensors are not distinguished by specificity, they may be useful for screening the presence of toxic agents in an ecosystem. It should be noted that, in these sensors, any compound that affects either the cellular metabolism or causes stress in the cell induces a response.

Inducible systems use constructs which are fusions of an inducible promoter and a reporter gene. To design an inducible CBB, a specific promoter, which is only activated by a specific group of related analytes / stimuli, is selected to carry out the gene construct. The level of the gene expression controlled by these types of inducible promoters is commonly high, because the gene product originated may play an important role in the cellular defense against a particular stressor or toxic substance. Selection of the appropriate promoter demands prior examination of the transcriptional capacities of the cell under influence of that analyte. This kind of CBB represent serviceable biosensors for monitoring group of specific environmental pollutants, despite the complexity of their construction. Promoter region binds transcription factors that are usually activated in response to the stimulation of receptor-mediated or receptor-independent signaling cascade, which is initiated not exclusively by one kind of analyte but usually chemically / structurally similar compounds. Thus, their specificity will depend on the degree of the signaling cascade specificity to an exclusive analyte of a chemically related group of analytes [34], [35], [36], [37], [38], [39]. Heat shock response (HSP), the SOS controlled response (including *recA, sulA, umuCD, recN, uvrA, cda*) in connection with a reporter gene are widely developed in a semi-specific CBB. Thus, these kind of CBBs are named parallel stress response or semi-specific CBB [40].

2.1.1.2 Human secreted alkaline phosphatase (SEAP)

Widespread research in the field of molecular biology based on eukaryotic cells involves the elucidation of factors which regulate the gene expression at the transcriptional and post-transcriptional levels. The use of reporter genes which encode enzymes or proteins that can be easily quantify is a typical approach that has been used to facilitate the determination of gene expression levels. Many reporter proteins have been used in eukaryotic cells including chloramphenicol acetyltransferase (CAT) [41], β-Glucuronidase (GUS) [42], β-galactosidase (*lacZ*) [43], or luciferase (*luc*) [44] and fluorescent proteins [45], [24], [46]. However, all of these reporter systems show some disadvantages, such as the presence of similar endogenous enzyme activity, requirement

for a cumbersome assay, separation of the product from the substrate, cell lysis performance, fluorescent proteins bleaching or difficulties with high throughput screenings development. Berger et al. [47] described a reporter gene, human secreted alkaline phosphatase (SEAP), which avoids several of these limitations. The SEAP gene encodes a secreted form of the human placental alkaline phosphatase (PLAP, EC 3.1.3.1), which is a hydrolase enzyme involved in removing phosphate groups from many types of molecules, including nucleotides and proteins. PLAP is initially anchored to the membrane via a C-terminal 26-amino acid hydrophobic domain. SEAP lacks this amino acids sequence, allowing the protein to be efficiently secreted in an active form [48], [49]. SEAP is secreted by genetically modified cells and can be consequently assayed using a small aliquot of the cell culture medium. SEAP activity revealed in cell culture medium is directly proportional to changes in the intracellular amount of SEAP mRNA and protein. Another important advantage is that background noise of the endogenous alkaline phosphatases is nearly absent. Nevertheless, the activity of endogenous alkaline phosphatases (AP) present in test samples can be excluded completely by incubating the sample at 65°C and with L-homoarginine without affecting SEAP activity. The enzyme can withstand temperatures as high as 65°C and is durable to the phosphatase inhibitor L-homoarginine [50]. The secreted nature of SEAP provides several advantages for its use as a reporter gene: (i) preparation of cell lysates is not needed; (ii) the kinetics of gene expression can be easily examined by repeated series of medium from the same cultures; (iii) transfected cells are not disturbed during measurement of SEAP activity and remain intact for further investigations; and (iv) background from endogenous alkaline phosphatase can be eliminated. SEAP catalyzes the hydrolysis of *p*-Nitrophenyl phosphate producing a yellow end product that can be measured spectrophotometrically at 405 nm. Therefore, a SEAP reporter system is well-suited to high-throughput applications. As the goal of presented study was to adopt three dimensional environment for sensor cells, SEAP seems to be an ideal extracellular reporter protein for application in such a complex cell culture system, which enable measurements without the time consuming cell extraction from 3D milieu.

2.2 Nanoparticles

Nowadays nanotechnology is one of the key technologies which promises revolution in our world [51]. Materials at *nano* scale, multiply novel features and applications that vary markedly comparing to corresponding bulk counterpart. The unusual physicochemical features of engineered nanomaterials are attributable to their small size (size distribution and surface area), surface structure (inorganic or organic coatings, surface reactivity, surface groups, etc.) chemical composition (electronic properties, purity, crystallinity etc.), shape, solubility and tendency of agglomeration. The potential risks of nanotechnology are currently the topic of hundreds of studies being performed in laboratories around the world. The urgency of this research is driven by the rapid utilization of the known applications for nanotechnology by industrial and commercial entities, as well as the extensive numbers of theoretical applications that are expected to fundamentally modify the world around us [52]. Nanoscale materials are already being incorporated for the use in many commercially available products including electronics, pharmaceuticals, cosmetics and sunscreens, automobile catalytic converters, dental bonding, stain resistant clothing and fabrics, corrosion resistant paints and coating metal cutting tools [53], [54], [55], [56], [57]. Nanotechnology can be very profitable sector and already the United States government has described nanotechnology „as *the foundation for the next industrial revolution"* worth as appraised trillion dollars within the coming ten years [58].

2.2.1 Definition and classification

The term *engineered nanoparticles* applies only to particles which have at least one dimension less than 100 nm in length and does not apply to particles under 100 nm that produced naturally or are by-products of other processes such as fire smoke, welding fumes, or carbon black [52]. Nanoparticles are generally classified based on their dimensionality, morphology, surface charge, composition, size, uniformity, and agglomeration state. Depending on the physicochemical properties, nanomaterials can induce different biological effects (Table 2).

Physicochemical features		Biological effect	Cell type	Ref.
Size	5-10 nm AgNP	Oxidative stress	HepG2	[59]
	20 nm, 80 nm and 110 AgNP	Genotoxicity, inflammation	L929, RAW 264.7	[60]
	5 nm, 20 nm and 50 nm AgNP	Morphological changes and changes in membrane integrity	A549, SGC-7901, HepG2, MCF-7	[61]
	165 nm ZnONP	DNA damage, lipids peroxidation	A431	[62]
	267 nm ZnONP	Apoptosis, NP uptake	HepG2	[63]
	10 nm ZnONP	Inflammation, oxidative stress	BEAS-2B	[64]
Surface charge	Positively-, neutral- and negatively charged AuNP	Differences in potential of mitochondrial membrane	HaCaT	[65]
	Positively charged with different Z-potential ZnONP	Differences in cell death	Hut-78	[66]
	Positively-, neutral- and negatively charged AgNP	Differences in cell proliferation ,membrane damage, cell uptake, DNA oxidation	TK6	[67]
Aggregation state	Aggregates of AuNP vs monodispersed AuNP	Differences in cell uptake	HeLa, MDA-MB-435	[68]
	Aggregates of SiNP vs monodispersed SiNP	Differences cytokine levels IL-6,IL-8, IL-1β	BEAS-2B	[69]
	Aggregates of TiO_2NP with different sizes	Differences in cytotoxicity and genotoxicity (level of DNA strand breaks)	TK6	[70]
Surface coating	PEGylated PMA-coated Fe_3O_4NP vs uncoated Fe_3O_4NP	Differences in cell membrane integrity, cellular uptake, inflammatory response	HUVEC, RAW264.7	[71]
	PVP-coated 20 nm AgNP vs PVP-coated 110 nm AgNP; citrate-coated 20 nm AgNP vs citrate-coated 110 nm AgNP	Differences in cell vitality, bioavailability, inflammation	BEAS-2B	[72]

Table 2. Biological effects due to physicochemical features of nanoparticles.

Routes of exposure and bio-distribution

2.2.2

The human body contains several semi-open spaces for direct substance exchange with the external environment, i.e. the skin, respiratory tract and gastrointestinal tract (GIT) [73]. Exogenous substances are also able to translocate to secondary organs mostly with blood stream or lymph system [74],[75]. Skin is the mean border and defense organ in our body and directly interacts with many toxic agents. The skin is a structured organ containing three layers: the epidermis, the dermis and the subcutaneous layer [76]. The strongly keratinized *stratum corneum* is the primary protecting layer and may be the rate limiting obstacle to defend against the infiltration of micron sized particles and harmful toxicants. Skin exposure to nanomaterials can also take place during the intentional application of topical / sun creams and other drug treatments. The main mechanism of NP uptake by skin cells is via endocytosis of epithelial cells [77]. Second exposure rote represent the respiratory system - a mean portal for ambient particulate material. Latterly, the pathology of inhaled manufactured nanoparticles have received attention. Micron sized particles are predominantly trapped and cleared by upper airway mucociliary escalator system, but particles smaller than 1 μm can get down to the pulmonary alveolus provide their abnormal functions after longer exposure time. Additionally, the deposition of inhaled ultrafine particles with diameter < 100 nm may result besides in absorption across the lung epithelium, and later nanomaterials can enter through alveolar blood vessels the blood system and lymph to reach cells in the liver, bone marrow, lymph nodes, spleen and heart [78], [79]. Nanomaterials can fetch up the GIT from the respiratory tract through the nasal region after mucociliary clearance, or can be administrate directly with water, food, cosmetics, drugs, and drug delivery devices. In GIT the main protective barrier is mucus which is continuously secreted and traps and coats external particulates and pathogens to preserve the underlying epithelium [80]. In biodistribution of exogenous substances very important roles are played by endogenous clearance processes like mucociliary movement, interstitial translocation, lymphatic drainage, blood circulation translocation, epithelial endocytosis and chemical clearance processes such as dissolution, leaching and protein binding. Clearance and opsonization of nanoparticles depends on size and surface characteristics. De Jong et al. [81] described size dependent tissue distribution of gold nanoparticles where smaller (10 nm) nanoparticles showing the most widespread distribution (liver, blood, spleen, thymus, heart, lung, kidney, testis and brain) whereas the larger particles (50, 100 and 250 nm) were noticed only in liver, blood,

and spleen. Moreover, nanomaterials are known to activate the immune system and contribute to initiate the complement pathway or promote allergies. Furthermore, NP are readily taken up by monocytes, macrophages and dendritic cells. This may pose a hazard to these cell types and therefore, reduce the capacity of an immune response. Interferon (IFN)-γ, IL-12 and tumor necrosis factor (TNF)-α, production were induced by NP in peripheral blood mononuclear cells [82], [83], [84].

2.2.3 Uptake of nanoparticles into cells

Comprehension the way nanomaterials interact with living matter will rise substantially new opportunities in medicine and diagnostics. The same nanoparticle can be captured via different mechanisms. For example, diamond powder particle uptake is based on macropinocytosis or on cadherin-mediated endocytosis pathways and uptake type influences intracellular metabolism [85]. Membrane stability can be affected by nanoparticles directly (e.g. physical damage) or indirectly (e.g. oxidation), however, in both cases can lead to cell death. The ability of membranes to regulate intracellular homeostasis, through selective permeability and transport mechanisms [86], makes it a susceptible target for possible impairing effects of nanomaterials. Interplay between nanoparticles and membranes depend largely on the nanoparticles surface properties (hydrophilic/hydrophobic). This is the reason why surface modifications, development novel coating methods are crucial in the design of drug delivery systems due to enhancement of nanoparticle uptake into cells. Nanoparticle size also plays an important role. Nanomaterials may enter cells in various ways by known mechanisms e.g. phagocytosis which is mostly characteristic to specialized macrophage cells; macropinocytosis traps large droplets of fluid and occurs in many different types of cells; in processes mediated by proteins such as clathrin and caveolin or other less understood mechanisms that are independent of clathrin or caveolin are probably also involved with nanoparticle uptake [87, 88]. Charged nanoparticles can alter the local physical features of lipid membranes, which could shed new light on the interplay between cells and nanomaterials. Differently charged nanoparticles can actively modulate the phase structure of lipid membranes and contribute to formation of nano-sized holes. For example, cationic NP were reported as more cytotoxic compared to negatively charged or neutral nanomaterials, as they are known to disturb the integrality of negatively charged plasma membrane [89]. Gene expression analysis suggests that membrane damage is nanomaterial as well as concentration dependent [90]. Furthermore,

mitochondria, appear to be a major target for gold nanoparticles [91], magnetic iron oxide nanoparticles [92], or titanium dioxide nanoparticles [93]. Another preferential intracellular compartment is represented by lysosomes, the cell's digestive system. Nanoparticles usually end up in lysosomes where cells try to either digest or excrete them. The impact of size, shape and nanomaterial type on the cell's ability to digest or excrete nanoparticles after accumulation in lysosomes is not fully analyzed [94], [95]. Finally, the nuclear membrane with nuclear pores transport substances in and out the nucleus and some, generally smaller, nanoparticles appear able to either diffuse through these pores or be transported via receptor meditated transport mechanisms to gain access to the intra-nuclear [96]. NP-induced genotoxicity may be direct, through intercalation or physical interaction, or indirect via altering proteins involved in cell division or oxidative stress. Some research has shown that silica NP are able to enter the nucleus and change cell proliferation by inhibiting DNA replication and transcription processes [97] while quantum dots have been shown to interact with histone proteins [98]. Oxidative stress is typical and a well-described effect of the interaction NP with biological systems, which undoubtedly contribute to point mutations, DNA adducts and fragmentation of chromosomes. NP have also been shown to alter the function of DNA repair genes resulting in aberrant DNA repair such as *BRCA1, Gadd45*, *XRCC1*, *RPA1, RAD51C* and *FEN1*, providing defects in DNA repair [99], [100]. Research on the genotoxic potential of NP are conducted in many laboratories, but still very few studies, so far, have examined their epigenetic potential. Gene expression is controlled by epigenetic processes, namely DNA methylation, histone modification and miRNA. NP are able to affect both global DNA methylation levels, methylation at specific gene promoters as well as enzymes/proteins involved in regulation of DNA methylation. NP are able induced changes in histone modifications as well. Oxidative stress has been shown to increase the levels of acetylated histone H4 and therefore abnormal changes in chromatin condensation. NP interact with miRNAs, which are short, single stranded, noncoding RNA molecules that have diverse functions in cells and it is appraised that about a third of the mammalian genes are regulated by miRNAs [101], [102], [103], [104]. Furthermore, Lynch et al. [105] suggest that interaction of nanoparticles with proteins causes mainly their bioavailability for cells. Surfaces of nanomaterials that interact with a biological milieu are in a dynamic exchange with biomolecules such as proteins and lipids. Proteins that reside on the particle surface (in *in vitro* systems proteins from FBS, in *in vivo* system proteins from e.g. extracellular matrix) will influence, indeed mediate,

the nanoparticle–cell interplays. Therefore, the identity and life time of these proteins on the particle surface can affect the way cells interact, recognize and process the nanoparticles. Proteins that do not have relevant receptor-binding sequence, will make the particle less attractive for the cell, because cells associate and take up only the proteins they need. However, if a protein corona on nanoparticle surface presents the relevant receptor-binding sites and is in contact with the cells long enough, it can activate the cell's uptake machinery process known as endocytosis.

2.2.4 Cellular signaling pathway modulation

Nanoparticles activate various intracellular signaling pathways such as NF-κB, MAPK, Rho GTPase, p38-Nrf-2, and SAP/ JNK signaling [106], [107], [108]. The ability to monitor transcriptional regulators in real time after exposure with nanomaterials greatly enhances the understanding of cellular regulation and control of their toxic mechanisms. Conventional gene expression analysis usually engages measuring single-time-point with techniques such as northern blots, reverse transcription polymerase chain reaction (RT-PCR) or DNA microarrays. Taking advantage of these techniques, dynamics can only be approximated by assembling average results from separate cell populations, one for each time point. Therefore, sensor cells developed in this thesis seem to be a perfect tool to control over the time activation of specific intracellular pathway (NF-κB) after exposure of cells to nanoparticles.

2.2.5 NF-κB pathway

Different kind of response elements / biomarkers / receptors (e.g. AP-1(*activator protein 1)*, STAT3 (*Signal transducer and activator of transcription 3*), HSP (*Heat Shock Protein*), ISRE/IRF (*IFN-stimulated response elements* /*Interferon regulatory factor*) were previously developed in combination with various reporter systems [109], [22] to monitor gene expression in mammalian cells after exposure to potentially hazardous agents. Undeniably, selecting the right biomarker is necessary for the later proper assessment of the toxic effects of analyzed compounds. The presented PhD thesis aims to develop universal biosensor to analyze toxic effect of chemicals including nanomaterials and literature described the NF-κB pathway as strongly activated after exposure of various kinds of nanoparticles [110], [111], [112] therefore, the NF-κB pathway was selected, examined and implemented in sensor cells as a screening pathway /response element.

Crucial to life is the ability to sense and adjust to the environment changes. For multicellular organisms, the ability to respond to external alteration is pivotal not only for survival but also for normal development and maintenance of homeostasis. It is well known that various signaling pathways can modify cellular function, as signaling acts to alter transcriptional responses and contribute to both transient and sustained changes. Rapid, but temporary, changes in gene expression are regulated by inducible transcription factors such as NF-κB. Nuclear factor-κB is a pleiotropic mediator of inducible and specific gene regulation involving various biological activities including immune response, inflammation, cell proliferation and death. The NF-κB transcription factor family in mammals consists of five proteins, p65 (RelA), p105/p50 (NF-κB1), RelB, c-Rel, and p100/52 (NF-κB2) that associate with each other to form individual transcriptionally active homo-and heterodimeric complexes (Figure 2). They all are characterized by a conserved 300 amino acid long amino-terminal Rel homology domain (RHD), and sequences within the RHD are required for (i) dimerization, (ii) DNA binding, (iii) interaction with IκBs and (iv) nuclear translocation. Although NF-κB activity is inducible in most cells, NF-κB pathway can also be constitutively active in certain cell types, such as neurons, vascular smooth muscle cells, mature B cells, macrophages, as well as some of tumor cells [113], [114].

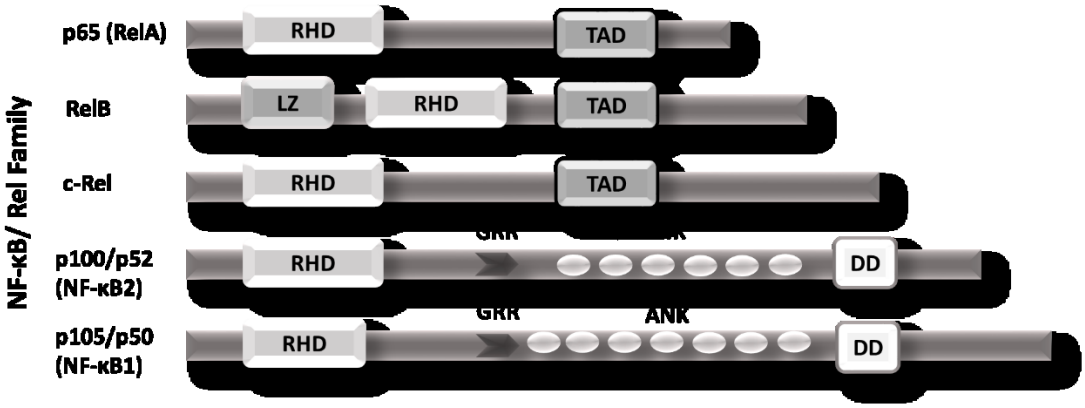

Figure 2. Members of the NF-κB family [115]: (RHD) the Rel homology domain - typical for the NF-κB proteins, (ANK) ankyrin repeats; (DD) death domain; (GRR) glycine-rich region; (LZ) leucine-zipper; (TAD) transactivation domain.

2.2.5.1 Activation of NF-κB pathway

In most cells NF-κB proteins residue in cytoplasm in an inactive form, where they are bound to inhibitors known as IκB. These proteins contain multiple copies of sequences known as ankyrin repeats, the IκB molecules mask the nuclear localization signals (NLS)

of NF-κB proteins and keep them in an inactive state. There are two activation processes of NF-κB pathway: canonical (classical) and non-canonical (alternative). In the canonical process, after activation of NF-κB pathway-specific kinases, IKKα (or IKK1), IKKβ (or IKK2) and regulatory protein NEMO (NF-κB essential regulatory protein, IKKγ) are activated to phosphorylate tandem serine residues on the N-terminal domain of IκB molecules (serines 32 and 36 for IκB-α). This leads to polyubiquitination and subsequent degradation of the inhibitor, enabling active NF-κB to translocate into the nucleus. In the nucleus NF-κB may activate the expression of a variety of genes (pro- or anti-apoptotic, it depends of: (i) kind of stimuli, (ii) concentration of stimuli or (iii) stimuli frequency) [116]. Because the NF-κB pathway controls the expression of numerous genes, the activity of NF-κB is tightly controlled at multiple levels. Several mechanisms exist to terminate NF-κB-dependent signals and avoid deleterious constitutive activation. For instance, the IKK negatively controls the duration of their activation via multiple phosphorylation of their N-terminal domain. The most efficient way to block NFκB-dependent transcription is via inducible transcription of the gene for IκB-α, the inhibitory subunit. Once expressed, IκB-α molecules translocate to the nucleus to remove NF-κB from DNA and shuttle it back to the cytosol to terminate transcription. The more NF-κB is activated, the more molecules of IκB-α are expressed, therefore the amount of IκB-α molecules is proportional to activated NF-κB. This assumption is used to measure activation of NF-κB signaling via qPCR [117]. The alternative activation process concerns nuclear translocation of dimer p52:RelB and is strictly dependent on IKK1 homodimers (activated by NF-κB inducing kinase – NIK). While the classical activation process may activate plenty of stimuli, alternative pathway is joined with lymphotoxin-α, BAFF- B cell activating factor and RANKL -receptor activator for nuclear factor kappa B ligand [118], [119].

2.3 Methods of nanoparticle toxicity assessment

Quantification is associated inseparably with reproducibility of measurements, which in biological research sometimes proves difficult, mainly because of the complexity of living matter and the often inevitable experimental variability. Quantification of nanoparticles in biological systems (i.e., cells, tissues and organs) has grown to be an essential part of nanotoxicological and nanomedical fields. Compared to *in vivo* studies, *in vitro* studies benefit from being faster, allowing greater control, lower cost, and

decreasing ethical concerns by reducing the number of laboratory animals required for experiments. However, the extension of results from *in vitro* experiments for the prediction of *in vivo* toxicity is problematic due to the *in vitro* exposure conditions which usually feature higher concentrations and exposure times than found in the cellular environment *in vivo* [120], [121], [122]. Diverse quantitative and semi-quantitative techniques for analysis of nanoparticle interaction with cells and tissues already exist (Table 3). Microscopy (mostly light microscopy and electron microscopy) enables detection and location of nanoparticles in cells. Examination of *in vitro* nanoparticle uptake and localization is intrinsically combined to cytotoxicological studies. Cell uptake provides evidence of nanoparticle-cell interaction, wherein the intracellular machinery is in contact with nanoparticles. Nevertheless, all microscopy methods demand elaborate sampling strategies in order to provide quantitative results [123]. Other methods require 'labeled' particles, fluorescently, radioactively or magnetically. However, still the most commonly used *in vitro* assessment techniques are based on the changes in cell proliferation, metabolic activity, membrane integrity, molecular biology methods or detection of apoptic markers for example anexin V.

Method	Application	Type of NP	Biosystem	Ref.
Light microscopy	Morphological Observation	Quantum Dots (QD)	NIH/3T3 cells	[124]
		Spherical silver nanoparticles 7-20 nm	primary fibroblasts and primary liver cells isolated from Swiss albino mice	[125]
	Live/dead staining	Superparamagnetic iron oxide nanoparticles 100 nm, 150 nm	HBMEC cells	[126]
	NP localisation	CdSe/ZnS QDs	MCF-7 cells	[127]
		Copper(II) oxide 12 nm, 50-80 nm	HepG2	[128]
		NaYF4:Er3+,Yb3+ up-converting nanoparticles <70nm	HeLa cells	[129]
	Changes in chromatin condensation NP exposure-immunocytochemistry	CdTe QDs	MCF7	[102]
Scanning electron microscopy SEM	Agglomeration state of nanoparticles	SilverNP 20nm and 200nm, Titanium dioxide 21nm	HepG2, A549 and THP-1 cells	[130]
	Intracellular nanoparticles localization	Iron NP	hMSCs cells	[131]
		serum-protein-coated AuNP of 10, 15, and 30 nm	A549	[132]
		TiO2 NP <25 nm	HEK-293 cells	[133]

Transmission electron microscopy TEM	Intracellular nanoparticles localization	Au NP 4, 12, or 18 nm	K562 cells	[134]
		poly(d,l-lactide-co-glycolide) nanoparticles 260 nm	VSMCs cells	[135]
Mass spectrometry	Cell uptake depended of nanoparticles concentration	yttrium oxide and zinc oxide nanoparticles 45 nm	HAECs cells	[136]
Field –flow fractionation	Particle in tissue separation, size sorting	SiO_2NP 70 nm 250 nm	HAEC cells	[137]
Radioactive labeling	Monitoring of translocation of NP to blood and secondary organs	iridium and carbon nanoparticles radiolabeled with ^{192}Ir	male WKY/Kyo@Rj rats 250±20 g	[138]
Magnetic nanoparticles	Monitoring of translocation, accumulation and increased cytotoxicity in tumor cells	Iron oxide nanoparticles 5-8 nm	Rat 9L/lacZ glioma(9L) and human D283 medulloblastoma (D283) cells	[139]
Colorimetric assays	Metabolic activity (Alamar Blue, MTT,XTT)	AgNP <100nm, ZnO, NiO, and CeO_2 different sizes, nano Metal–organic framework <200 nm	HT22, A549, MCF7, HepG2 cells	[140], [141], [142]
	Membrane integrity (LDH)	superparamagnetic iron oxide nanoparticles 10-15 nm	T3, RAW264.7,MCF7	[143]
Molecular biology techniques	DNA fragmentation after NP exposure- single cell gel electrophoresis assay (Comet assay), TUNEL	thiolated and nitrosated iron oxide NP, Nanocrystalline silve <50 nm	Human lymphocytes isolated from blood, Eight- to ten-week-old female BALB⁄c mice, weighing 16–18 g	[144], [145], [146]
	Gene expression after NP stimulation- Real-Time PCR, proteins expression- Western Blot	TiO_2NP < 600 nm, AgNP <40 nm	lung tissue from adult female C57BL/6BomTac mice, 16HBE, HepG, HUVEC, EUE	[147], [148], [149]

Table 3. Overview of analytical methods to assess nanoparticles toxicity in cells, tissues or organs.

2.4 Hepatotoxicity

2.4.1 Liver

Liver is one of the major organs of nanoparticles accumulation, has crucial role in metabolic homeostasis and is the principal detoxification center in our body. This explains the choice of hepatocyte cells (HepG2) as a model cells, described in the presented thesis. In the human body the liver is located in the upper right quadrant of the abdomen, under the diaphragm and to the right of the stomach. It weighs about 1800 grams in men and 1400 grams in women. The liver consists of two main lobes (gross anatomy) both of which consist of 8 segments. The segments contain a thousand lobules. The lobules are joined to small ducts that link with larger ducts to finally form the common hepatic duct. The common hepatic duct carries bile produced by the liver cells to the duodenum and gallbladder (the first part of the small intestine). Lobules are the functional units of the liver and each lobule contain of millions of hepatic cells (hepatocytes) which are the main metabolic cells. The lobules are combine together with accompanying the vessels (veins and arteries) ducts and nerves through the hepatic portal, as a fibrous capsule called Glisson's capsule. Two major types of cells reside liver: parenchymal cells and non-parenchymal cells. Hepatocytes represents parenchymal cells (approximately up to 70% of total liver). These cells are engaged in most of the functions that are ascribed to the liver. They play a considerable role in the metabolism of exogenous and endogenous lipids and catabolism of blood-derived protein. Hepatocytes produce important serum proteins such as complement components and acute phase proteins, as well as numerous hormones and cytokines. Non-parenchymal cells mainly represent phagocytic Kupffer cells (KC), hepatic stellate cells and intrahepatic lymphocytes [150], [151]. KCs are the resident macrophages of the liver and portray the largest number of macrophages in the mammalian body. KCs remove antigens from the circulation and are responsible for the clearance of bacteria. These macrophages are usually concentrated in the peripheral region of the liver, which enables control of the blood entering the organ. It is believed that due to the permanent exposure to low levels of gut-derived antigens, KCs are in a constant semi-activated state. Alike other macrophages, once these KCs are fully activated they are capable of phagocytosis and antigen uptake and the production of mediators involved in protein degradation, cytotoxicity and defense mechanisms. KCs are also essential in the maintenance of liver.

Models of hepatotoxicity

Almost every day somewhere in the world someone reveals a better technique for producing NP, a better way of handling them, an even better preparation of functionalized them and application method in industry. Therefore, it is in dire need to test them in terms of toxicity to humans and the environment. Nowadays consumers continually increase their expectations about the safety of products. Therefore, the European Union brought in the regulation known as Registration, Evaluation, Authorisation and Restriction of Chemicals (REACH) by legislation in 2007 [152], what is the largest safety assessment of chemicals that has ever been accomplished. REACH executes industry accountable for managing and accessing the risks posed by chemicals and providing proper safety information to their users.

2.4.2

An ideal examination to understand whether a factor is harmful to humans would require a large number of human volunteers who are representative of the heterogeneity of humans and who are in contact with examined agent under realistic conditions. All possible results should then be assessed. Therefore, a crucial question is how advantageous are the current models, which are usually animal models? It is known that the use of animals has limitations [153], [154], [155], [156]: people are not 80 kg rats; the way of consuming substances is different; metabolism shows often disparate; people live longer and are exposed to a multitude of environmental factors. Finally, people suffer from different diseases, which have as well high impact for organism sensitivity. Incorrect experimental models yield many false positive results and subsequently diminishes the correlation between findings in animal models and humans. Additionally, the European Union insists to reduce, refine and replace (3R principle; EU-Directive 2010/63) experiments on animals. This has created substantial pressure to develop human-cell based models for toxicity testing that may be able to reflect with great efficiency living tissue and give highly predictive results to simulate the *in vivo* situation [157].

2.4.3

Three dimensional cell culture

From 1997, when the pioneer in the development three dimensional cell cultures Prof. Mina Bissell published a breakthrough article [158], until present 3D cell culture technologies have revolutionized our comprehension of cellular behavior. There is a huge difference between a flat layer of cells and a complex, three-dimensional tissue. A 3D cell culture system contains an artificially created milieu in which cells are permitted to

grow or interact with their surroundings in all three dimensions. Bissell's group demonstrated that antibodies against a cell surface receptor (β1-integrin) utterly changed the behavior of cancerous breast cells grown in 3-D environment: they become non-cancerous, changing their abnormal shapes and growth patterns. This result had never been observed in 2-D cultures. Therefore, just the modification of the way a cell interacts with its environment, as Bissell had shown, can radically alter cell behavior. 3-D culture can provide a better model for what happens *in vivo*, it might allow scientists to reduce their use of experimental animals. Additionally, Mihael Polymeropoulos (chief scientific officer of Vanda Pharmaceuticals in Rockville, Maryland) predicts that "*in 10 years, anyone trying to use 2-D analyses to get relevant and novel biological information will find it difficult to get funded"* [159]. Therefore, cultures of hepatocytes in 3D environments become a more and more popular model of hepatotoxicity. Each 3D cell model comes with its own set of advantages and limitations, and one distinct model is not suitable for all applications. Models for the appraisal of testing cell toxicity must mimic the *in vivo* situation as closely as possible.

2.4.3.1 Spheroid model

Spheroid cell culture is one of the most popular models of 3D cell culture. Spheroids are self-assembled agglomerates of cell colonies that resemble avascular environments with gradients of nutrients, O_2, CO_2 and water soluble wastes, [160]. Compared to conventional 2D cell cultures, multicellular spheroids better mimic a real tissue [161], [162], [163]. Spheroid formation can be divided into three main phases: (i) formation of cell agglomerates via integrin-ECM binding; (ii) a delay period for cadherin expression and accumulation; (iii) formation of compact spheroids through homophilic cadherin-cadherin interactions[164] (Figure 3A). Several mathematical models have been applied to simulate nutrients, oxygen and waste transport and pH measurement in spheroid cell culture [165], [166]. Experimental verifications of these predictions have also been performed using methods such as microelectrodes with pH-sensitive indicators, microscopic observations and development genetically encoded sensors [167], [168], [169]. Research indicates that the spheroid model is similar to avascular tissue or tumor mass with diffusion limitation of about 150–200 μm to many molecules. Inefficient mass transport also results in metabolic waste accumulation inside the spheroids .Therefore, compacted spheroids with a size above 200-500 μm (depends mostly on kind of cells and

connections strength between cells) in diameter commonly are characterized by an outer layer of highly proliferative cells with a necrotic core inside spheroid (Figure 3B).

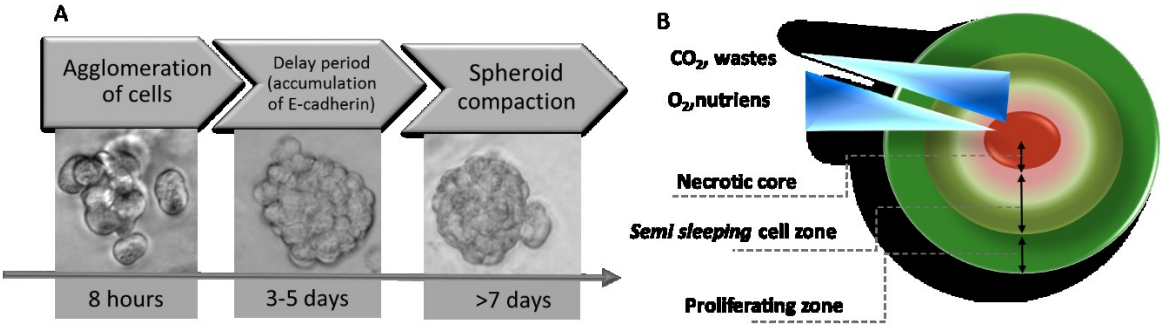

Figure 3. A model of the spheroid formation process; HepG2 cells in Collagen type I gel (A) and schematic of microenvironment inside a compacted spheroid (B) [164]

A popular method to obtain spheroid-like structures is embedding cells in different hydrogel materials. Hydrogels are water-swollen polymeric networks, usually composed of cross-linked hydrophilic polymers that can swell but do not dissolve in water. Their ability to swell under biological conditions makes them a perfect class of materials for biomedical applications, such as tissue engineering and drug delivery [170], [171], [172], [173], [174], [175]. Moreover, hydrogels portray an emerging and highly attractive class of biomaterials whose unrivaled set of properties has recently broadened their use in *in vitro* cell culture platforms. Hydrogels have a high water content, possess tissue-like elasticity, and facile transport of nutrients and waste point them out as ideal candidates for mimicking the cell's extracellular matrix (ECM). Furthermore, their optical clarity makes microscopy-based assays of cell function possible [176], [177]. Gels can be created from a multitude of sources through a variety of cross-linking methods (e.g., physical, covalent, ionic interactions) with varying degrees of success. Based on their cross- linking mechanism, hydrogels can be classified into physical and chemical. Physical crosslinks encompass entangled chains mainly by hydrophobic / hydrophilic interactions. These physical crosslinks may not be lasting junctions and may be reversible due to small changes in temperature, pH, and electrolytes content. Some hydrogels can be cross-linked by thermally induced gelation [178], self-assembling amphiphiles [179] or ionic cross-linking [180]. A popular strategy applies cross-linking with UV light through photopolymerization [181], [182], [183]. Here, free radicals released from a photoinitiator attack the organic groups, which results in covalent cross-linking of the hydrogel within seconds or minutes upon irradiation. Since the photoinitiator and its solvent, the UV light exposure, and the free radicals may be damaging to cells, application of this method in

cell-based assays has been lately declined. Chemical (or covalent) crosslinks are lasting junctions formed by covalent bonds. A common way to create a covalently crosslinked network is to polymerize end-functionalized macromeres. Hydrogel networks may include both lasting junctions and semilasting junctions. The type and degree of crosslinking effects many of the network properties, like swelling properties, elastic modulus and transport of molecules [184]. Subsequently, hydrogels can be classified by their structure (amorphous, semicrystalline and hydrogen-bond), preparation methods (homopolymer, copolymer and multipolymer) or ionic charge (cationic, anionic, neutral, and ampholytic). Hydrogels from natural polymers have been used in cell biology owing to their biocompatibility and biodegradability. There are four main types of natural polymers: (i) proteins, such as silk, fibrin , collagen, gelatin, Matrigel [185], [186] or genetically engineered proteins, such as silk-elastin like protein [187], (ii) polysaccharides, such as agarose, dextran, hyaluronic acid (HA), and chitosan; (iii) protein/polysaccharide hybrid polymers, such as collagen/HA, fibrin/alginate laminin/ cellulose and gelatin/chitosan. Despite many benefits, the application of natural hydrogels may be limited due to potential immunogenic reactions [188], [189].

Collagen-, gelatin- and Matrigel-based hydrogels were developed in this study to create 3D environments for sensor cells. Selected polymers normally build the surroundings of cells in tissues *in vivo,* therefore they nicely mimic the native system. Collagen is the main fibrous protein in mammals and the basic constituent of extracellular matrix (25% - 35% of the whole-body protein content). Three left handed polypeptide helices entwine together into a right handed triple helix create molecular structure of collagen. Obtained long fibrils can form bundles of much larger diameters, the thickness of which determines the tensile strength of the connective tissue. Cells can control locally the orientation of collagen fibrils in extra cellular matrix which affect cell polarization. Additionally, collagen contains cell-adhesion sites along their sequence which act in cell migration [190], [191]. Gelatin is the peptide mixture produced through the irreversible process of partial hydrolysis of collagen. Gelatin gels lack thermal stability; therefore, they require covalent crosslinking for applications as tissue engineering. For cell culture studies, the materials properties of gelatin gels may be improved by crosslinking the fibers using gluteraldehyde, formaldehyde or enzymatic crosslinking by transglutaminase (used in this study) [192], [193]. Finally, Matrigel (commercial name) consists of basement membrane proteins extracted from Engelbreth-Holm-Swarm (EHS) mouse sarcoma, a

tumor rich in extracellular matrix proteins. Matrigel contains a heterogeneous composition and is rich in laminin and collagen types I and IV. It also contains heparin sulphate proteoglycans, entactin/ nidogen, and usually various growth factors. Matrigel gels quickly and irreversibly between 24 °C - 37 °C, and the gelling speed is dependent on the concentration and incubation temperature [194].

Furthermore, 3D spheroids model can be formed using the hanging drop method [195], [196], [197], [198]. Cell suspension drops are deposited onto the underside of the lid of a tissue culture dish. Each drop usually is 15–30 μL in volume containing approximately 100–1000 cells. When the lid is inverted, drops are held because of surface tension. The microgravity environment in each drop results in central placement the cells, which then create single spheroids at the free liquid-air interface. This simply method is especially useful for generating spheroids of defined sizes and for studying cellular or molecular events during spheroid assembly, but is limited by difficulty in medium exchange and handling and long-term cultures. Another popular method to create spheroid system is cultivation of the cells in bioreactors [199], [200], [201], [202]. Bioreactors are usually exploited in industrial fermentation processing, wastewater treatment, food processing and production of pharmaceuticals and recombinant proteins (e.g. antibodies, growth factors, vaccines and antibiotics). The overall basis behind these methods is that a cell suspension is located into a reservoir and the suspension is maintain in motion, that is, either it is gently stirred or the reservoir is rotated. The continuous motion of the suspended cells provide that cells do not adhere to the container walls, but rather form cell–cell interactions [203], [204]. Furthermore, spheroids may be set up on commercially available well plates with modified surface e.g. SCIVAX's NanoCulture® Plate, Lipidure®-COAT Plates, Mimetix® multi-well plate, Celltreat® Scientific 3D Insert™, Alvetex Scaffold with perfused well plates and Perfecta3D® Hanging Drop Plates. Hepatocytes-based spheroids models are widely used and well described in toxicology research such as models of anti-cancer drug testing [205], platform for drug-induced hepatotoxicity analysis [206], as a functional xenobiotic metabolism model [207] as a tool for in vitro toxicity studies [208] as models to test drug delivery [209] as a platform for long-term preservation of liver-specific functions [210] or as well- defined micro-platform of liver tissue reconstruction on-a-chip [211].

2.4.3.2 3D cell culture models based on synthetic scaffold

Nowadays, synthetic polymers are an alternative choice for fabricating scaffolds for 3D cell culture. Because they can be composed with various block structures characterized by different molecular weights, mechanical strength and biodegradability. Synthetic polymers can be classified regarding their biodegrability into three main types, including nonbiodegradable, biodegradable and bioactive polymer. Typical synthetic polymers used in cell biology and tissue engineering are represent by poly(ethylene glycol) (PEG), poly(vinyl alcohol) (PVA), polypropylene furmarate-co-ethylene glycol (P(PF-co-EG)), poly(acrylamide) (PAAm), poly(acrylic acid) (PAA), poly(hydroxyethyl methacrylate) (PHEMA), poly(ethylene oxide) (PEO), poly N-isopropylacrylamide (PNIPAAm), poly(methacrylic acid) (PMMA), poly(glycolic acid) (PGA), poly(ε-caprolactone) (PCL), and poly(lactic acid) (PLA)) [212]. A major requirement is biocompatibility of material, therefore currently, material developers combine semi-synthetic hydrogels. This kind of structures usually consist of a synthetic hydrophilic polymer which is joined to a polysaccharide or protein moiety. Semi-synthetic hydrogels are produced in copolymerization reactions between the polymer precursor and the biological conjugate. Such reactions typically adapt the already mentioned cross-linking methods. In this way, it is possible to create a promoting hydrogel with highly defined technical properties [213], [214] [215]. A variety of rapid prototyping (RP) methods have been extensively used. RP implements computer-aided design (CAD) in which construction data are read and manufactured automatically layer-by-layer according to the virtual design. The main benefit of rapid prototyping is its high flexibility. Using RP, the 3D form of tissue engineered constructs can be custom-manufactured according to individual needs. Another advantage is controlled size, geometry and scaffold porosity. Furthermore, hydrogels with different mechanical features can be used to create a complex 3D scaffold resembling blood vessels or skin substitutes [216], [217], [218]. Nevertheless, due to the high number of hydrogels, there is no universal RP method which can be implemented to each hydrogel material. Additionally development of high throughput assays is challenging with 3D printed scaffolds and still mainly cell analysis precede time consuming cells extraction. [219].

Organotypic slice cultures and decellularized liver matrix

2.4.4

Organotypic models are created by culturing organ slices of microscopic thickness. Slices are usually cultured on porous membrane, on collagen-coated substrates, or within 3D collagen gel. Each cell in the slice should be not more than 200 μm apart from the media and oxygen supply. In this way, the tissue slice remains viable for many weeks or months even in serum-free media. Organotypic liver cultures are widespread in drug discovery and toxicity testing. A main benefit of adapting whole organ slices is that the basic organ architecture is preserved. A drawback is that the data processing and the interpretation of experiments based on complex tissue specimens can be challenging [220], [221], [222], [223]. Other complex liver model is presented by decellularized liver matrix. The decellularized liver graft is characterized by the functional and structural similarities to the native microvascular network. Efficient recellularization of the liver matrix with differentiated hepatocytes and following perfusion for *in vitro* culture allows to maintain liver-specific function including albumin, urea synthesis and cytochrome P450 enzyme expression at approximate levels to native liver [224], [225]. Isolated tissue slice models and perfused are the closest *in vitro* models of the *in vivo* state. Nevertheless, these models are costly, the organs are hard-to-reach and preserving the tissue's viability *ex vivo* is intractable. This rise isolated perfused organs and tissue slice models unsuitable for routine testing purposes. Organotypic 3D cell cultures could offer an attractive alternative to animal models for both ethical and economic grounds.

2.5 Three dimensional environment for cell-based biosensor

Developed and presented in this study cell-based biosensors use living cells to monitor physiological and functional changes induced by external stimuli. The cultured cells are the most critical part of a cell-based biosensor. Therefore, adoption of three dimensional cell culture to biosensor is anticipated to provide more predictive results for *in vivo* analysis, as three dimensional cultures resemble closer to *in vivo* conditions than traditional monolayer cell culture. To date, almost all cell- based biosensors use traditional cells cultured on flat materials. Although the time-honored 2D cell culture has proven to be a prominent technique for cell-based research, its limitations have been

increasingly noticed. In *in vivo* milieu, most of the cells are surrounded by other cells and extracellular matrix in a 3D fashion. As a result, monolayer cell culture analysis may rise misleading and non-predictive results for *in vivo* responses. On the other hand, 3D cell culture provides a more physiologically relevant environment for cells and allows the study of cellular responses in a setting that resembles *in vivo* environments. The 3D structure not only affects the spatial organization of the cell surface receptors involved in interactions with cells milieu, but also induce the physical constraint to cells. These spatial aspects in 3D results in the stimuli transduction from the outside to the inside of cells, and ultimately influence on gene expression and cellular behaviors. Compared to 2D cell culture, 3D culture replicates more similar the actual microenvironment where cells reside in tissue and therefore the behavior of cells in 3D culture reflects closely the *in vivo* responses. [226].

3 MATERIALS AND METHODS

3.1 Technical equipment

Device	Supplier
Autoclave VB65	Systec
AxioCam Mrm	Carl Zeiss
Axiovert 40 CFL	Carl Zeiss
Centrifuge Fresco	Heraeus
Centrifuge Heraeus Biofuge Fresco	Thermo Scientific
Centrifuge Heraeus Labofuge 200	Thermo Scientific
CO_2-lid PM S1	Carl Zeiss
CO_2-Incubator HeraCell150	Thermo Scientific
Corbett Rotor-Gene—6000	Qiagen
Digital camera	Pentax K-50
Electrophoresis chamber	Thermo Scientific
Filter set 10	Carl Zeiss
Filter set 62 HE	Carl Zeiss
Fine and Precision Balances	Satorius
Freezer Arctiko	Esbjerg (Dänemark)
Imagingsystem vilber Laurmat	Peqlab
Incubator XL S1	Carl Zeiss
Mastercycler® peronal	Eppendorf
Microcomp electrophoresis Supply E452	Consort
Nanodrop 1000	Thermo Scientific
Neubauer cell chamber	Improved LaborOptik
Laser scanning microscope 710	Carl Zeiss
Objective EC Plan-Neofluar 20x/0.50 M27	Carl Zeiss
Objective CP Achromat 10x/0,25	Carl Zeiss
PerfecBlue Semi-Dry Electroblotter	SEDEK M
PerfectBlue Vertical Double Gel System-Twin L	Peqlab
pH-Electrode FE20	Mettler Toledo
Pipette Accurpette	VWR
Pipette Research	Eppendorf
Pipetus®	Hirschmann Laborgeräte
Power supply electrophoresis E844	Consort
Safety cabinet HeraSafe	Thermo Scientific
Scanning electron microscope	Nova NanoSEM 450
Shaker MS3 digital	IKA
Sterile filters (0.22µm)	Carl Roth
Syringes Injekt® 10ml - 50 ml	B. Braun Melsungen AG, Melsungen
Tecan Infinite® M200	Tecan Group
Thermomixer compact Eppendorf	Eppendorf
Ultrasonic baths , Sonorex super RK 102H	Bandelin
Waterbath M20 Lauda	Dr. R. Wobser GmbH & Co.
Zeta-seizer Nano ZS	(Malvern, Malvern Hills, UK)

3.2 Software

AxioVision 4.8.2 (Carl Zeiss); BioCapt Software (Vilber Lourmat), Excel® 2013, Word® 2013 (Microsoft® Corporation, Redmond (USA)); i-control software (Tecan Deutschland GmbH, Crailsheim); Malvern version 7.03 (2002-2013 Malvern Instruments Ltd.); NanoDrop 1000 version 3.8 (Thermo Fisher Scientific); NCBI/ Primer-BLAST online software; Origin 9.1G OriginLab® (Corporation, Northampton (USA)); Rotor-Gene 6000 Series Software 1.7 (Qiagen); STATISTICA 9 (Dell Software); ZEN 2012 black edition System (Carl Zeiss).

3.3 Experimental part

Cell culture

3.3.1 The human hepatoblastoma cell line HepG2 was obtained from Cell Line Service GmbH (CLS Eppelheim, Germany). Cells were maintained in Dulbecco's modified Eagle's medium with low glucose (DMEM) supplemented with 10% (v/v) fetal bovine serum (FBS), 2 mM L-glutamine, 100 µg/ml penicillin and 100 µg/ml streptomycin (complete cell culture medium). All mentioned reagents were purchased from Biowest. The cells were kept at 37°C in a cell incubator under a humidified atmosphere with 5% CO_2. With the exception of cytotoxicity assays, cells were deprived of serum (1% FBS) for at least 24 h prior to the treatment with chemicals.

For longer storage cells were frozen (- 80 ˚C) in complete growth medium supplemented with 10% (v/v) DMSO in 1ml aliquots of approximately 5 x 10^6 cells.

In experiments in which was required to know the cells concentration, Neubauer chamber (Improved LaborOptik) was used to count cells under Microscope Axiovert 40 CFL with objective CP-Achromat 10x/0,25Ph1 (Carl Zeiss) after staining with Trypan Blue 5% (Roth). Number of cells was estimated according to equation:

$$C = \frac{A \times squere\ area\ of\ the\ chamber\ \times depth\ of\ the\ chammber\ \times\ D}{N}$$

C- cells concentration in 1 ml; *A*-number of counted cells (arithmetic mean); *N* – number of squares; *D*- dilution factor;

3D cell culture

Three different hydrogels were developed to generate hepatocytes spheroids: Matrigel depleted growth factors and phenol red (Corning, Netherlands), gelatin type A from porcine skin (Sigma) and collagen type I (Sigma). A stock of Matrigel was prepared in a

3.3.2 concentration of 1 mg/ml in DMEM and diluted in ratio 1:1 with cell culture medium before cell seeding. Gelatin solution (10% w/v in DMEM) was sterilized using a syringe filter with a 0.22 μm pore size (Carl Roth) and prior to use incubated about 30 min. at 37 °C to obtain liquid consistency. The gelatin solution was then cross-linked with 1% v/v transglutaminase (100 u/g, Ajinomoto). Collagen gel was obtained by mixing DMEM and collagen type I solution (10 mg/ml in 0.1% acetic acid). pH was adjusted to 7.4 with 1 M NaOH (Sigma, sterilized by autoclaving). HepG2 cells were mixed with the above mentioned hydrogels and cultured at 37 °C in a cell incubator.

Metabolic activity of HepG2 cells

3.3.3 Albumin and urea in the cells lysates were measured using the BCG Albumin Assay Kit and the Urea Assay Kit (from Sigma). Samples were collected after 3, 5, 7 and 10 days of initial cell seeding from 2D and 3D cultures. Changing the culture media every 2–3 days was essential for optimal growth of spheroids in 3D culture and for cells growing in monolayer. Cells were extracted from the hydrogels directly before the experiment by using collagenase (400 u/ml) and dispase (4 u/ml) (Gibco) with incubation time 5 min for cells in collagen gel and Matrigel and 25 min for cells in gelatin gel. Cells number was estimated at each time point using 5% Trypan Blue (Carl Roth), and the data were normalized to 1×10^6 cells. Cultures were briefly washed with PBS and homogenized with urea assay buffer (urea measurements) or Cellytic M/Protease Inhibitor Coctail (Sigma) (albumin measurements) and analyzed according to protocols provided by the manufacturer. Known quantities of human albumin and urea were used as standards. Standard curve after subtraction blank was plotted (the standard curve was set up in each

3.3.4 time the assay was run) and the amount of urea and albumin in unknown samples were read from standard curves using linear function f(x) =ax + b, where y- measured absorbance, a- slope, x-concentration, b-intercept.

Proliferation assay, growth of spheroids

The colorimetric assay CellTiter 96® Aqueous One Solution (Promega) was used to determine the number of viable cells. The assay based on modified Mosman's method

[227]. 2 x 10^4 cells were seeded on the surface of each well of 96-well plates to obtain 2D cell culture. For 3D cell cultures, cells were first mixed with previously prepared hydrogels and subsequently seeded on well plates. Assay was performed after 1, 3, 7, and 10 days of cultivation cells in 2D and 3D cell culture by adding 20 µl of the CellTiter reagent directly to the culture wells. After 3 h of incubation in a cell culture incubator, absorbance was recorded at 490 nm with a plate reader (Tecan). Known numbers of HepG2 cells were used as standards. Standard curve after subtraction blank was plotted (the standard curve was set up in each time the assay was run) and the cell number in unknown samples were read from standard curves using linear function f(x) =ax + b, where y- measured absorbance, a- slope, x-concentration, b-intercept. The growth of spheroids was estimated by measuring their diameters (over 16 days) on the images obtained with an LSM 710 microscope (Carl Zeiss) in orthogonal view after staining nuclei with DAPI (AppliChem) with excitation 358 nm and emission 461 nm. Objective EC Plan-Neofluar 20x/0.50 M27 (Carl Zeiss) was used. Error bars represent the standard deviation of three independent experiments with 100 images taken per each time point.

3.3.5 Assessment of nanoparticle induced cytotoxicity (Alamar Blue)

Cells viability were determined using the Alamar Blue Assay. 15.000 cells were seeded in each well of 96-well plates in the form of monolayer or spheroids. After 8 days the cells were treated with varying concentrations of nanoparticles: silver nanoparticles (AgNP, 10 nm), zinc oxide nanoparticles (ZnONP, 25 nm, and 14nm), silicon dioxide nanoparticles (SiO_2NP, 10 nm and 20 nm), titanium dioxide nanoparticles (TiO_2 4-8 nm and 16-26 nm) all obtained from PlasmaChem or heavy metals cadmium chloride ($CdCl_2$, Sigma) and nickelsulfat hexahydrat ($NiSO_4 \cdot 6\ H_2O$, Sigma). All NP were sonicated (Bandelin, Sonorex super RK 102H) for 15 min at room temperature directly before use to resuspend formed agglomerates. After 24 h or 72 h of incubation all wells were washed 3 times with PBS and Alamar Blue (50 µM, Alfa Aesar) was added. Absorbance was recorded at 540 nm with reference at 630 nm by using a plate reader. Cytotoxicity (in percent) was expressed by dividing the absorbance recorded for treated cells with the absorbance obtained for untreated control samples (after subtraction of blank: cell culture medium in polystyrene well-plate). To visualize toxic effect of NP, cells were stained with propidium iodide (4 µM) and calcein AM (4µM) (Sigma) in Hanks' Balanced Slats (Sigma). After 10 min of incubation in darkness, images were recorded using the LSM

710 microscope. The respective excitation and emission wavelengths were 490 nm and 540 nm for calcein AM, and 560 nm and 690 nm for propidium iodide. An EC Plan-Neofluar 20x/0.50 M27 objective was used.

Dynamic light scattering measurements

3.3.6 The size distribution of nanoparticles was estimated by dynamic light scattering (DLS). Measurements were performed at 25 °C using the Zeta-seizer Nano ZS (Malvern, Malvern Hills, UK). Stock solutions were diluted in ratio 1:5 in complete cell culture media (see section ***3.3.1***) or 1:5 in deionized water. Samples were measured in triplicate.

Contact angle measurements

3.3.7 For measuring the contact angle (CA) the samples were placed on a horizontal surface and a 5 µl water droplet was deposited on the surface using a micropipette. The samples were photographed using a digital camera (Pentax K-50) with 18-135 Pentax lens at right angle to the surface of the sample. The images were analyzed using the DropSnake plugging for the free program ImageJ [228]. CA<90°- hydrophilic surface, CA>90°- hydrophobic surface (Figure 4).

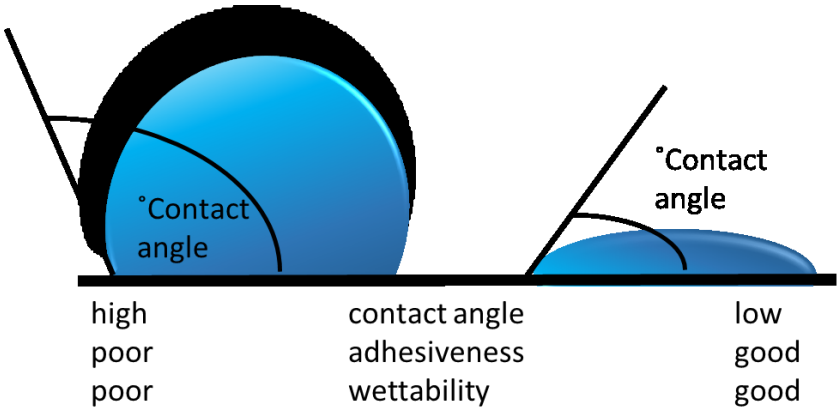

3.3.8

Figure 4. Schematic overview of contact angle properties

Sample preparation for SEM analysis

To characterize the scaffolds architecture, scanning electron microscopy (SEM) was performed using a Nova NanoSEM 450 instrument. Hydrogels were prepared on indium tin oxide (ITO) coated glass (surface resistivity 8-12 Ω per square) obtained from Delta Technologies Ltd., USA. Samples were fixed with 3 % glutaraldehyde in 0.1 M phosphate buffered saline (PBS) pH 7.2 (Sigma) and post-fixed with 2 % osmium tetroxide (Sigma). Afterwards, samples were washed three times with PBS and

dehydrated with an ethanol series (50%, 70%, 80%, 90%, 95%, 100%, Sigma). After the dehydration step, samples were dried with hexamethyldisilazane (HMDS, Sigma) evaporated and then air-dried overnight at a room temperature. Dried samples were mounted on aluminum specimen holders. SEM imaging was performed under low vacuum conditions with uncoated samples and under high vacuum with samples coated with 1 nm sputtered gold.

	Chemicals	**Temperature**	**Time**	**Repetitions**
fixation	2%-4% glutaraldehyde in phosphate buffer	Room temp or 0-4˚C	2h	1
washing	0,1 M (pH 7.2) Phosphate buffer	Room temp or 0-4˚C	30min	3
Post-fixation	1%-2% osmium tetroxide in phosphate buffer	Room temp or 0-4˚C	2h	1
washing	0,1 M (pH 7.2) Phosphate buffer	Room temp or 0-4˚C	30min	3
dehydration	30%ethanol 50% 70% 80% 90% 95% 100%	Room temp or 0-4˚C	10min 10min 10min 10min 10min 10min 30min	1 1 1 1 1 1 2
HMDS	ethanol 100%:HMDS 100% 2:1 ethanol 100%:HMDS 100% 1:1 ethanol 100%:HMDS 100% 1:2 HMDS 100%	Room temp or 0-4˚C	10min 10min 10min 10min	1 1 1 2
Air drying		25˚C 37˚C 45˚C	overnight 4h 4h	1 1 1
Coating with gold (1nm)				

3.3.9

Plasmid amplification

pNiFty2-SEAP lyophilized plasmid (InvivoGen, Figure 5) was resuspend in Milli-Q water to obtain a 1 µg/µl solution. 25 µl of competent cells E. coli strain DH5α (Thermo Fisher) were transformed with 1 µl of plasmid using heat shock method. Firstly, mixture was kept 20 minutes on ice, than 45 seconds in 42 ˚C and again 2 minutes on ice. Next,

500 µl of S.O.C. medium (Invitrogen) was mixed with cells and shaked 30 minutes in 37 ˚C. Afterwards, cells were seeded on agar LB medium (5g tryptone, 2.5g NaCl, 2.5g yeast, 7.5g agar/0.5 L deionized water; (Roth) autoclaved) with 25 µg/ml zeocin (InvivoGen) as a selective antibiotic, and incubated overnight at 37 ˚C. Next, one colony of cells was pick up and placed into 5 ml liquid LB medium (5g tryptone, 2.5g NaCl, 2.5g yeast/0.5 L deionized water; autoclaved) with 25 µg/ml zeocin and incubated overnight at 37 ˚C. Next, plasmid DNA was isolated from cell pellet using QIAprep Spin (Qiagen) following the manufacturer's protocol. Concentration and quality of extracted plasmid DNA was analyzed using Nanodrop 1000 (Thermo Scientific).

$$\frac{Absorbance_{260\,nm}}{Absorbance\ _{280\,nm}} > 1.8 \text{ acceptable purity of sample}$$

$$\frac{Absorbance_{260\,nm}}{Absorbance\ _{230\,nm}} > 1.8 \text{ acceptable purity of sample}$$

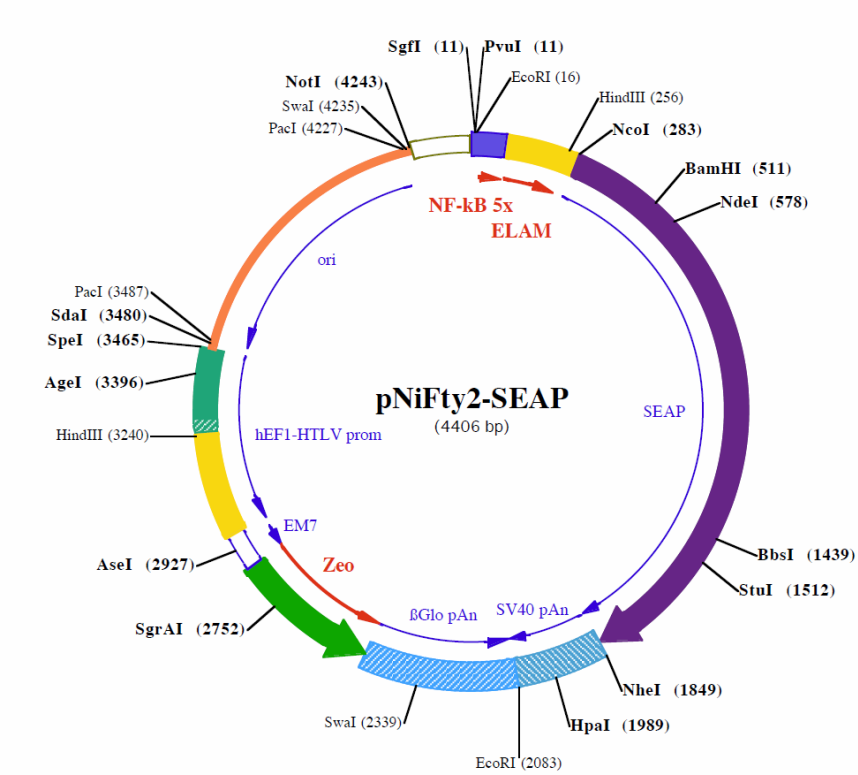

Figure 5. Map of pNiFty2-SEAP plasmid

NF-κB5-eLAM is an engineered ELAM promoter combining five NF-κB sites (ggggactttcc) with the proximal ELAM promoter. SEAP is a secreted form of human embryonic alkaline phosphatase. sV40 pAn is the Simian Virus 40 late polyadenylation

signal enables efficient cleavage and polyadenylation reactions resulting in high levels of steady-state mRNA. Ori is a minimal E. coli origin of replication. hEF1/HTLV promoter exhibits a strong activity and yields long lasting expression of a transgene *in vivo*. EM7 is a bacterial promoter that enables the constitutive expression of the antibiotic resistance gene in E. coli. Zeo represent resistance to the antibiotic Zeocin and is conferred by the *Sh ble* gene from *Streptoalloteichus hindustanus*. The *Sh ble* gene is driven by the hEF1-HTLV promoter in tandem with the bacterial EM7 promoter allowing selection in both mammalian cells and E. coli. βGlo pAn is the human beta-globin 3'UTR and polyadenylationsequence allows efficient arrest of the transgene transcription.

Transient transfection

3.3.10 Twenty four hours before the transfection cells were seeded on 24-well cell culture plates at a density of 4 x 10^4 cells per well in 0.5 ml of complete growth medium. The transfection was performed using 2 µl of Lipofectamine 2000 reagent (Life Technologies) and 500 ng of pNiFty2-SEAP plasmid according to the manufacturer's protocol. 24 h after transfection complete cell culture medium was replaced with selective medium (300 µg/ml zeocin, DMEM, 10 % FBS) containing zeocin as a selective antibiotic. Five days later, the transiently transfected cells were used for experiments.

3.3.11

Stable transfection and single colony screening

Twenty four hours before the transfection cells were seeded on 24-well cell culture plates at a density of 4 x 10^4 cells per well in 0.5 ml of complete growth medium. The transfection was performed using 2 µl of Lipofectamine 2000 reagent (Life Technologies) and 500 ng of pNiFty2-SEAP plasmid according to the manufacturer's protocol. 24 h after transfection complete cell culture medium was replaced with selective medium (300 µg/ml zeocin, DMEM, 10 % FBS) containing zeocin as a selective antibiotic. The optimal dose of zeocin was determined using Alamar Blue assay. 300µg/ml of antibiotic was lethal for HepG2 cells after 1 week of exposure. Because, zeocin in solution is not stable, therefore selective medium was renewed every two - three days. Transfected and reproduced cells (confluent monolayer) were then subcultivated and highly diluted (~ 50 cells / well on 12 well plate) to perform single clones selection. Single clone selection enables to obtain 100% clonal purity. Clones were isolated and reproduced using soaked with trypsin paper disks (Ø~6 mm; Whatman filter paper; sterilized by autoclaving). After reproduction of single colonies (scaled up to T75 flask), 20 of them (with the highest

growth rate and vitality) were induced with TNF-α (diluted in deionized water; Sigma**)** and LPS (diluted in cell culture medium; Sigma) and screened using NF-κB_HepG2 cells assay (***3.3.12***) to find the most sensitive one. Clone 13 stood out with the lowest background, linearity and smallest standard deviation. Therefore, this clone, was considered as a *SuperClone* and implemented for further experiments. Developed sensor cell line was named NF-κB_HepG2.

NF-κB_hepG2 cells assay

3.3.12 NF-κB_HepG2 cells and transiently transfected HepG2 cells were stimulated with chemicals t=1-24 h (kept in 37˚C, 5% CO2 and humidified atmosphere). Then cell culture supernatants were placed into fresh Eppendorf tubes and centrifuged 10 min, 13.000 rpm to clarified solutions (after centrifugation samples may be stored in -80 ˚C). To continue assay cell culture supernatants were transferred (20 µl) to fresh 96-well plate. First inactivation step of endogenous alkaline phosphatase was done by heating samples in 65 ˚C for 10 min (SEAP is heat stable). Later samples were mixed with (46 µl) *Assay Buffer* (20 mM L-Homoarginine (Sigma), 1mM $MgCl_2$ (Roth), Tris base (Roth) pH 9.0) and incubated 15 min in cell culture incubator. L-Homoarginine is a second inhibitor of endogenous alkaline phosphatase. Divalent ions (Mg^{2+}) are cofactors of SEAP and pH 9.0 is optimum for enzyme activity [229]. In the last step 120 mM (34µl) *p*-nitrophenyl phosphate (*p*NPP; fresh prepared; Sigma) was added and incubated t=1h with samples in 37˚C. In preliminary experiments optimum concentration of *p*-nitrophenyl phosphate and incubation time was estimated. Secreted alkaline phosphatase (reporter protein) catalyzes the hydrolysis of *p*-Nitrophenyl phosphate producing a yellow product under alkaline conditions which was conveniently measured at 405 nm on a plate reader (Figure 6; Tecan Infinite® M200 Tecan Group). SEAP activity revealed in cell culture medium is directly proportional to changes in intracellular amount of SEAP mRNA and protein. Results were presented as relative values of absorbance calculated according to equation below. In this calculation method control (unstimulated cells) = 1.

$$RA = \frac{A - A_B}{A_C - A_B}$$

RA- relative absorbance; *A*- absorbance of analyzed sample (supernatant from stimulated cells); A_B-absorbance of blank (cell culture medium); A_C- absorbance of control (supernatant from unstimulated cells)

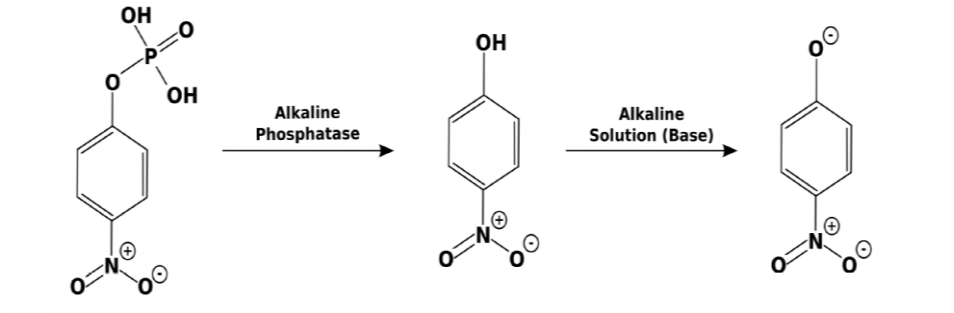

p-nitrophenyl phosphate(pNPP) *p*-nitrophenol *p*-nitrophenolate

Colorless Colorless Yellow

Figure 6. Secreted alkaline phosphatase catalysis the hydrolysis of *p*-Nitrophenyl phosphate producing a yellow product under alkaline conditions.

Western Blot

3.3.13 Cell preparation: Stimulated HepG2 cells (t=24h) with ZnONP 80 µg/ml, AgNP 15µg/ml, SiO_2NP 250µg/ml, staurosporine (positive control)10µM and unstimulated cells (negative control) were harvested using tripsin with EDTA, counted using Neubauer chamber and lysed in an appropriate volume of ice-cold lysis buffer for 30 minutes on ice. Samples (contained $2x10^7$cells) were spin down for 30 minutes at 13 000 g, 4°C. The supernatant was transferred to a fresh tube. Next, samples were mixed with 2 x Laemmli sample buffer, incubated at 95 °C for 5 minutes (Thermomixer compact Eppendorfand) and stored in -80 °C for further use.

Gel-Electrophoresis: The glass plates used for sample separation were cleaned with detergent and ethanol. The resolving gel was prepared as indicated below and poured into glass plates. Isopropanol was added on top of the resolving gel to remove air bubbles. The gel was allowed to polymerise for up to 10 minutes. Once gel polymerized, the isopropanol was washed from the top of the gel using deionised distilled water. The stacking gel and comb was placed cautiously. The gel was allowed to polymerise for 15 minutes. As an electrophoresis chamber PerfectBlue Vertical Double Gel System- Twin L (Peqlab) was used. SDS/polyacrylamide gel electrophoresis of whole-cell extract proteins and blotting were done. Samples were electrophoresed through the stacking gel at 110 V and trough the resolving gel 160 V using microcomp electrophoresis supply E452 (Consort). As a standard PageRuler Prestained Protein Ladder (Fermentas) was

used. Electrophoresis was stopped once the bromophenol front approached the end of the gel plates.

Western-Blot: The blot sandwich was prepared:

Cathode → 4 filter papers (Whatman-Paper 3 mm CHR, Amersham) soaked with cathode buffer → gel → nitrocellulose blotting membrane (Protranns 0,45 µm) and 2 filter papers soaked with anode buffer 1 → 4 filter papers soaked with anode buffer → Anode

The transfer was carried out with 110 mA for t= 90 minutes using PerfecBlue Semi-Dry Electroblotter SEDEK M (Peqlab). Next, nitrocellulose membrane was blocked t= 60 minutes in nonfat dry 5% w/v milk (Roth) in TBST. Then, membrane was incubated with diluted (1:1000) primary antibody (Anti-human PARP antibody; source - rabbit, Cell Signaling; Cat. No #9542) in 5% w/v nonfat dry milk in TBST at 4°C with gentle shaking, overnight. After washing step with 1 x TBS, 0.1% Tween 20 (x 3, t= 5 minutes) membrane was blocked again t= 30 minutes in nonfat dry 5% w/v milk in TBST. Then secondary anti- rabbit antibody HRP-linked (source – goat, Cell Signaling; Cat. No #7074S) were applied (diluted 1:2000 in nonfat dry 5% w/v milk in TBST) and incubated with gentle shaking in room temperature t= 60 minutes. After final washing step with 1 x TBST (3x, t= 5 minutes) a commercially available enhanced chemiluminescence (ECL) solution (Amersham) was breafly prepared to facilitate the visualization of the bonds. The ECL mixture was added to the membrane and incubated under dark conditions at room temperature for 10 minutes before developing (Kodak-developer and replenisher; Fixation Solution - Carestream Kodak from Sigma-Aldrich) the blots with imaging films (CL-Exposure Film Thermo Scientific).

Lysis - Buffer

750 mM NaCl; detergents mix (Nonidet P-40 5% (Substitute Amresco); sodium deoxycholate 2.5 % (Berlin Chemie)); 0.5 % SDS (Roth); Protease Inhibitor Cocktail (Sigma) in atio 1:100 (inhibitor:buffer); 250 mM Tris-buffer (Roth) pH 7.5; Mili-Q water

Laemmli Buffer

60 mM Tris-HCl pH 6.8 (Roth); 2 % (v/v) SDS (Roth); 10 % (v/v) glycerol (Roth); 5% (v/v) β- mercaptoethanol (Sigma); 0.01% (w/v) bromophenol blue (Sigma)

1L 10x TBS

24.2 g Tris (Roth); 87.66 g NaCl; pH 7.6; H_2O

5L TBST

500 ml 10x TBS; 5 ml Tween 20 (Roth); H_2O

Stacking gel

1.3 ml Bis-Acrylamide (AppliChem); 1 ml of 1M Tris pH 6.8; H_2O 7.7 ml; TEMED 15 µl (Roth); 30 µl of 10% APS (Sigma)

10 % resolving gel

7 ml 1.5 M Tris pH 8.8; Bis-Acrylamide 9.3 ml; H2O 11.6 ml; TEMED 30 µl; 90 µl of 10% APS

Cathode buffer 0.5 L

1.51 g Tris (Roth); 2.6 g 6-aminohexanoic acid (Roth); 100 ml Methanol (VWR); H_2O

Anode buffer-1 0.5 L

18.17 g Tris; 100 ml Methanol; H_2O

Anode buffer-2 0.5 L

1.51 g Tris; 100 ml Methanol; H_2O

RNA isolation and cDNA synthesis

3.3.14

Total RNA was extracted from cell pellets (1 x 10^6 cells) using the RNeasy MiniKit (Qiagen) according to the manufacturer's protocol. RNA concentration and purity were assessed photometrically using A_{260}/A_{280} ratio (Tecan). 2 µg of total RNA was converted to cDNA in a 20 µl reaction volume using First Strand cDNA synthesis Kit (Thermo Scientific). All reagents were mixed in followed order:

Template- total RNA	2 µg
Primer Oligo$(dT)_{18}$ 100 µM	1µl
Water, nuclease-free	to 11µl
5 x reaction buffer	4 µl
RiboLock RNase Inhibitor (20 u/µl)	1 µl
dNTP Mix 10 mM	2 µl
M-MuLV reverse Transcriptase (20 u/µl)	2 µl
Total volume 20µl	
Incubation 60 min at 37 ˚C. Termination of the reaction by heating samples at 70 ˚C for 5 min. Products stored at -80 ˚C.	

3.3.15

Real-Time PCR

Primers were designed using online software NCBI/ Primer-BLAST and were purchased from Eurofins Genomics.

GAPDH fwd	5'-GAAGGTGAAGGTCGGAGTC-3'	226bp
GAPDH rev	5'-GAAGATGGTGATGGGATTTC-3'	
IκB-alpha fwd	5'-GGCAGCAACGACACAGAAAC-3'	128bp
IκB-alpha rev	5'-GCGGTGGGTAATGGAGACAT-3'	

Specificity of designed primers and length of their products was firstly examined on electrophoresis gel after PCR reaction with genomic DNA of HepG2 cells as a template (chapter: ***3.3.16*** and ***3.3.17***) and further by performing melting curve analysis (, appendix). Real-Time PCR analysis was done on Rotor-Gene 6000 (Corbett) system using the GoTaq qPCR Master Mix (Promega):

GoTaq qPCR Master Mix	12,5 µl
Upstream PCR primer 0.2 µM	1 µl
Downstream PCR primer 0.2 µM	1 µl
Template (cDNA)	2 µl
Nuclease-free water	To final volume of 25µl

Program:

Hot-Start activation	95 ˚C, 3 minutes	
Denaturation	95 ˚C, 15 seconds	} 40 cycles
Annealing/ Extension	60 ˚C, 60 seconds	
Melting curve analysis / Termination	65 ˚C -95 ˚C	

Data were analyzed with the Pfaffl quantification model [230] using GAPDH (glyceraldehyde-3-phosphate dehydrogenase) as reference gene. Real-Time PCR efficiencies were calculated, according to equation:

$$E = 10^{-1/slope} - 1$$

E- efficiency of Real-Time PCR; *slope* (*a*): f(x) = *a*x +b –slope of standard curve of serial dilutions of DNA

Relative expression ratio in real-time PCR was calculated according to equation:

$$R = (E_{\text{target gene}})^{\Delta C_T \text{ target gene (control –stimulated sample)}} / (E_{\text{ref: gene}})^{\Delta C_T \text{ reference gene (control –stimulated sample)}}$$

R- relative expression ratio; $E_{target\ gene}$- is the real-time PCR efficiency of target gene transcript; $E_{ref\ \text{gene}}$- is the real-time PCR efficiency of a reference gene transcript; C_T – cycle threshold.

Genomic DNA isolation

3.3.16 1x 10^6 (HepG2) cells were used to isolate genomic DNA. Both the isolation, and purification was carried out with the Flexi Gene DNA Kit (Qiagen, Hilden) following the manufacturer's protocol.

Polymerase chain reaction (PCR) and Agarose gel electrophoresis

3.3.17 Specificity of designed primers and length of their products was examined on electrophoresis gel after PCR reaction. PCR analysis was done on Mastercycler personal (Eppendorf) using Taq PCR Kit (New England Biolabs) and genomic DNA as a template. In PCR reaction all reagents were mixed in followed order:

Taq reaction buffer (with $MgCl_2$ 25mM)	10 µl
dNTP 10 mM	1µl
Upstream Primer 0.2 µM	2 µl
Downstream Primer 0.2 µM	2 µl
Template DNA	1 µg
Taq DNA Polimerase 1.25 u/ 50 µl PCR	0.25 µl
Nuclease free water	To final volume of 50 µl

Program:

Initial denaturation	95 ˚C, 30 seconds	
Denaturation	95 ˚C, 30 seconds	40 cycles
Annealing	60 ˚C, 45 seconds	
Extension	68 ˚C, 60 seconds	
Final extension	72 ˚C, 5 minutes	
Hold	4 ˚C	

Agarose gel electrophoresis was performed in 1.8 % (w / v) agarose (Roth) in 1x TAE-Puffer (2M Tris-base (Roth), 1M acetic acid (Merck), 0.05M sodium EDTA

(Applichem)). The DNA samples were mixed with 6 x Orange DNA Loading Dye (Fermentas) and loaded into the gel. Separation was done on power supply Electrophoresis E844 Consort at a constant voltage of 100 V. As a size standard 100 bp DNA Ladder Plus (Fermentas) was used. Separated DNA fragments were stained for 20 minutes in ethidium bromide solution (Roth; 2 µg/ml in 1x TAE) and analyzed using Imaging system vilber Laurmat (Peqlab).

NF-κB activation

3.3.18 To confirm the desirability of considered biomarker, activation of NF-κB pathway after nanoparticles exposure was analyzed using NF-κB p65 ELISA Kit (eBioscience). Cells were stimulated t=6h with ZnONP 80 µg/ml, AgNP 15µg/ml, SiO_2NP 250µg/ml and 20 ng/ml TNF-α. Then cells were harvested, counted using Neubauer chamber (Improved LaborOptik), 1 x10^6 cells were lysed and followed steeps of the assay were performed according to manufacturer's protocol. Negative control represents lysate from unstimulated HepG2 cells; positive control represents lysate from cells which continuously had activated NF-κB (subunit p65) pathway (provided by supplier). Results were presented as relative value calculated according to equation below. In this calculation method control (unstimulated cells) = 1.

$$RA = \frac{A - A_B}{A_C - A_B}$$

3.3.19 *RA*- relative absorbance; *A*- absorbance of analyzed sample; A_B-absorbance of blank (cell culture medium in a polystyrene well plate); A_C- absorbance of control (supernatant from unstimulated cells)

Statistics

Quantitative data were expressed as arithmetic mean ± standard deviation. Student´s t-test was used to analyze the statistical significance of the data ($p < 0, 05$ vs. control; STATISTICA 9). All measurements were made in at least three independent experiments.

4 RESULTS

4.1 Development of whole cell-based biosensor

Currently used methods of testing chemicals and assessing their risks haven't followed with recent progress in science, which point to completely new factors that need to be examined, such as the importance of the timing of exposure, the effects of low-dose exposures and the scope of variability in the human population, or interactions of hazardous agents with assay components [231], [232], [233], [234], [235]. Moreover, conventional methods rarely predict toxicity in physiological concentration range and how chemicals act and interact with biological systems. Current medical application give NP access to tissues that may be usually fetched up via the skin, by inhalation or the gastrointestinal tract [236]. Better understanding and proper risk assessments of NP is therefore required in response to the rapid increase in development, production and utilization of NP in the industry. ZnONP, SiO_2NP and AgNP were chosen as NP-models because of their universal features, wide applications, different size, tendency of agglomeration and chemical composition. Since nanoparticle safety issues are not entirely settled, continued research is required to characterize the effects of nanoparticles on human health and the environment. Therefore, the purpose of presented project was to create system which can be applied to a wide variety of potentially hostile nanoparticles in basic screening to ensure initial caution of adverse effects and trigger subsequent analysis and remedial actions without the exact analysis of the interaction mechanism between nanoparticles and living systems. To meet these challenges, sensor cells have been developed. Furthermore, created biosensor with an absorbance readout allows monitoring the metabolic activity in a hepatocyte cells under a broad range of conditions in a real time with superior chemical range and sensitivity. These approaches allow testing of more chemicals at lower cost, can also help characterize the underlying mechanisms by which chemicals interact with human cells and provide physiologically relevant data in response to the analyte.

Properties of nanoparticles

The stability of NP in various aqueous suspension is the major challenge in nanotoxicology [130]. The magnitude of the cytotoxicity endpoints depends on the agglomeration state of nanoparticles [130]. Therefore, the tendency of NP agglomeration in complete cell culture medium was examined by DLS measurements. ZnONP have a larger mean hydrodynamic size in a cell culture medium compared to exactly the same NP in deionized water (Table 4). Thus, clustered nanoparticles rather than individual particles were observed. High standard deviations suggest that the NP create clusters of various sizes. In contrast, SiO_2NP and AgNP did not show high tendency to agglomerate.

4.1.1

NP	Nominal size[1] (nm)	Average hydrodynamic diameter in deionized water (nm)	Average hydrodynamic diameter in cell culture medium (nm)
Ag	10	6.873 ± 3.330	6.887 ± 4.176
SiO_2	10	30.99±20.01	41.65 ±22.09
ZnO	25	43.58 ±9.113 292 ±42.50	134.7 ±108.2 3902.0 ±1119.0

Table 4. Hydrodynamic size of NP in a deionized water and complete cell culture medium (size distribution by intensity of scattered light). All presented data as mean of triplicate ± SD measurements of DLS. [1]Data obtained from PlasmaChem providing NP.

Furthermore, the reagglomeration state of nanoparticles was examined in the context of their cytotoxicity (Figure 7). A higher toxic effect of nanoparticles with sonication step included was observed. Stimulation with sonicated 80 µg/ml ZnONP reveals higher cytotoxicity up to 22% compared to the same concentration of ZnONP without sonication step. Consequently, to keep exactly the same experimental conditions, nanoparticles were always sonicated directly before incubation with cells.

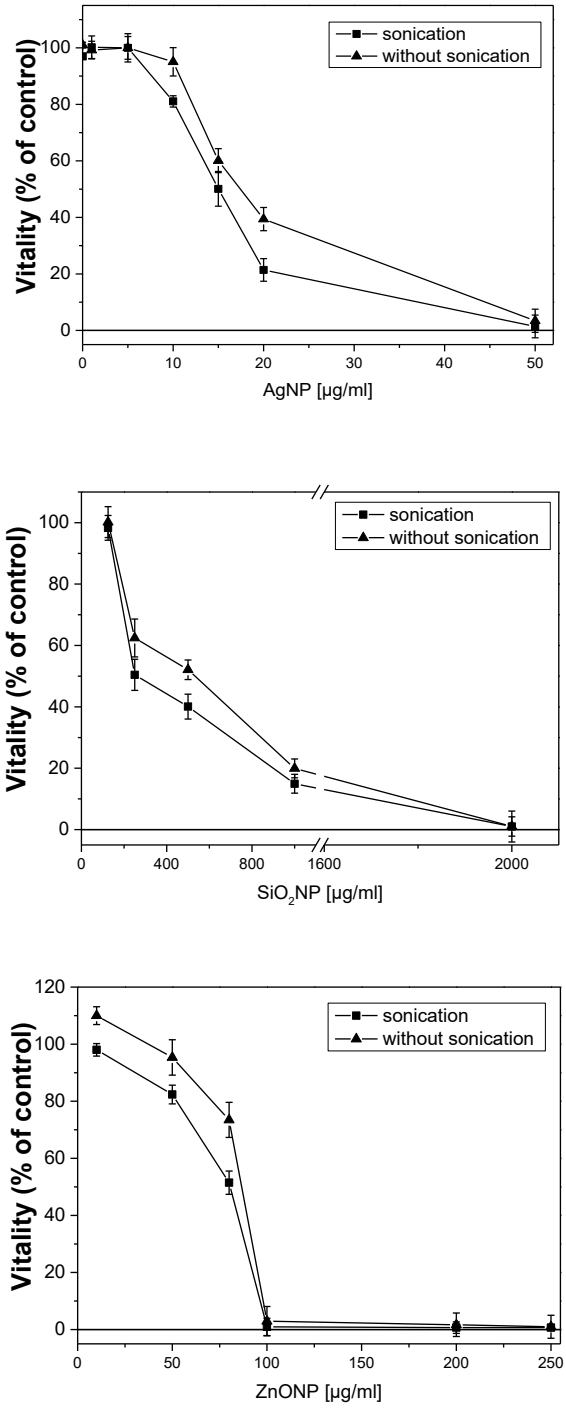

Figure 7. Dose-response analysis of AgNP, SiO_2NP and ZnONP on HepG2 viability in a monolayer with and without sonication step; (t= 24h); (n=6 ± SD).

It is known that serum albumin binds and thereby reduces toxic effects of chemicals [237], [238]. Therefore, to optimize the dosimetry of NP for *in vitro* toxicity assessments, the cytotoxic effect of the NP on HepG2 cells (after 24h incubation time) was measured under normal (10% FBS) and serum-deprived (1% FBS) conditions using

the Aalmar Blue endpoint cytotoxicity assay (Figure 8, Table 5). As expected the toxic effect of AgNP (EC_{50}=34 ± 7.58 µg/ml), ZnONP (EC_{50}=95 ± 5.19 µg/ml) and SiO_2NP (EC_{50}=400 ± 9.19 µg/ml) using 10% FBS was lower than with 1% FBS. There was no difference in cell survival between unstimulated control with 1% FBS and 10% FBS, which eliminates the influence of the FBS on cell viability. Therefore, the toxicity assays were carried out under serum-deprived conditions.

	ZnONP EC_{50} [µg/ml] ± SD	SiO_2NP EC_{50} [µg/ml] ± SD	AgNP EC_{50} [µg/ml] ± SD
1% FBS	80 ± 3.74	250 ± 1.75	15 ± 2.99
10% FBS	95 ± 5.19	400 ± 9.19	34 ± 7.58

Table 5. The EC_{50} values were obtained by fitting the dose response function to the experimental data using nonlinear regression analysis.

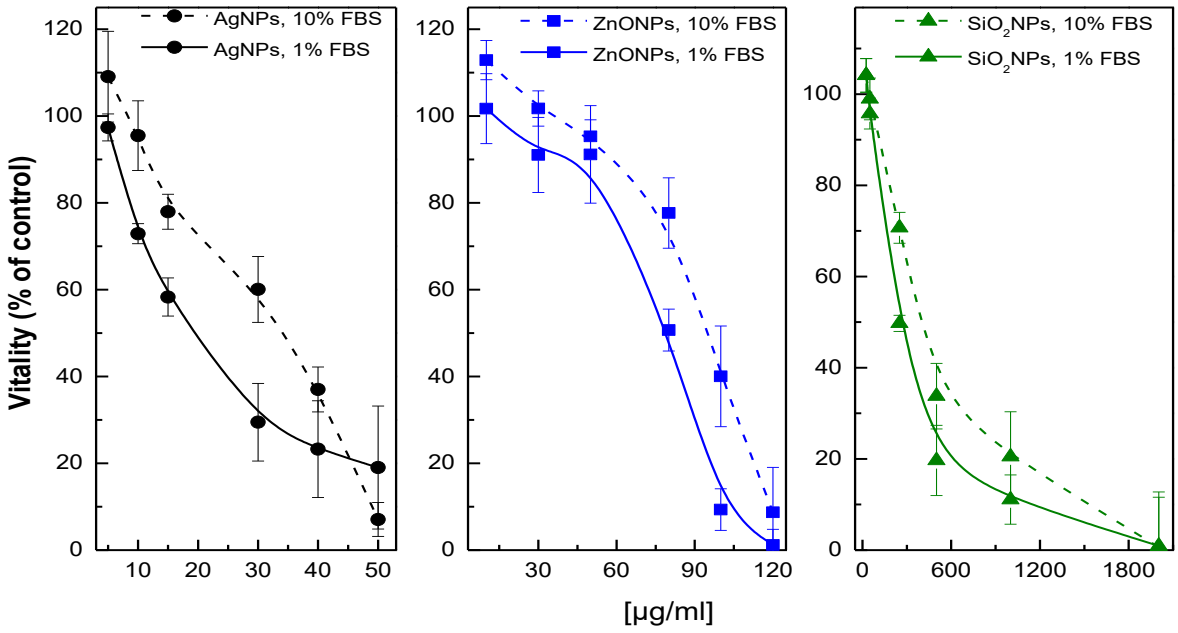

4.1.2

Figure 8. Dose-response analysis of AgNP, ZnONP and SiO_2NP using 10% FBS or 1% FBS on HepG2 vitality in a monolayer; (t= 24h); (n=6 ± SD).

Screening pathway examination

In order to select stress response pathway for later development of sensor cells, activation of NF-κB signaling after exposure of HepG2 cells with nanoparticles was analyzed. Cells were stimulated for 6 h with ZnONP 80 µg/ml, AgNP 15µg/ml, or SiO_2NP 250µg/ml. These concentrations corresponded to toxicity EC_{50} values observed in monolayer after 24 h of incubation (compare Table 5). In the ELISA assay,

discrimination between activated and inactivated NF-κB molecules (subunit p65) was feasible because inactivated NF-κB molecules are in complex with their inhibitors (IκB) and the antibody used for detection can bind only to dissociated NF-κB molecules with available epitopes. As expected, cell treatment with nanoparticles resulted in activation of the NF-κB pathway (Figure 9). Exposure of cells to ZnONP resulted in 6-fold induction in comparison to unstimulated cells (negative control), whereas AgNP and SiO_2NP provoked a 5-fold and 3-fold induction, respectively. As expected, the strong activation was observed after stimulation of HepG2 cells with the cytokine TNF-α, which is well known activator of NF-κB pathway [239], [240], [241].

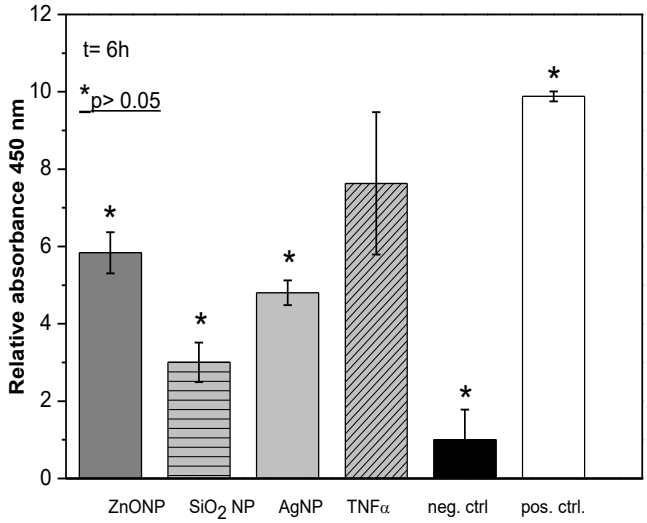

Figure 9. Activation of NF-κB (subunit p65) after stimulation HepG2 cells (t=6h) with 80 µg/ml ZnONP, 250 µg/ml SiO_2NP, 15 µg/ml AgNP and 20 ng/ml TNFα. Negative control (neg. ctrl.) represents HepG2 cells without stimulation; positive control (pos. ctrl.) represents lysate from cells with constantly activated molecules NF-κB (subunit p65, provided by supplier); (n=4 ± SD).

4.1.3

Generation NF-κB_HepG2 sensor cells

After having confirmed that the NF-κB pathway is activated in response to the exposure of HepG2 cells to NP, the next step was to generate a sensor cell line that would allow for the rapid determination of NP effects based on reporter gene activation. To this end, a commercially available reporter plasmid (pNiFty2-SEAP) was chosen to construct transgenic HepG2 cells.

In first experiments HepG2 cells were transiently transfected to examine the usefulness of pNiFty2-SEAP plasmid (map and description of plasmid in chapter ***3.3.9***) for screening of nanoparticles toxicity. Five days after transfection the cells were treated

with 15 µg/ml AgNP, 250 µg/ml SiO_2NP and 80 µg/ml ZnONP (t=8h). Obtained data showed that the level of SEAP reporter enzyme increased after stimulation of cells with nanoparticles with the highest induction represented by more than 6-fold after treatment with 80 µg/ml ZnONP (Figure 10).

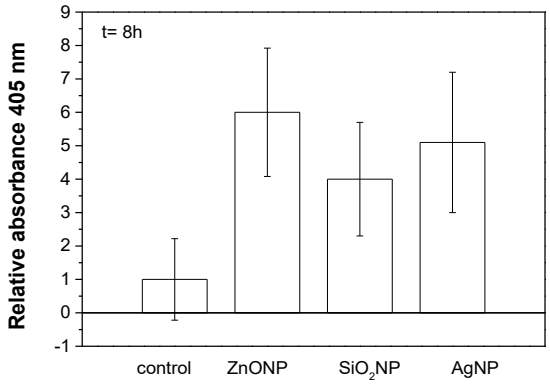

Figure 10. Induction of transiently transfected HepG2 cells with pNiFty2-SEAP vector with 15 µg/ml AgNP, 250 µg/ml SiO_2NP and 80 µg/ml ZnONP (t=8h), control represent unstimulated transiently transfected cells; (n=4 ± SD).

Based on this result, HepG2 cells were stably transfected (chapter: ***3.3.11***) with a reporter vector (pNiFty2-SEAP plasmid) derived from an ELAM promoter combining with five NF-κB binding sites (ggggactttcc) to amplify signal. In the absence of NF-κB pathway activation the reporter displays low activity. Induction of NF-κB activates the promoter resulting in expression of the reporter gene (SEAP) and enables monitoring toxic effect of chemicals (Figure 11).

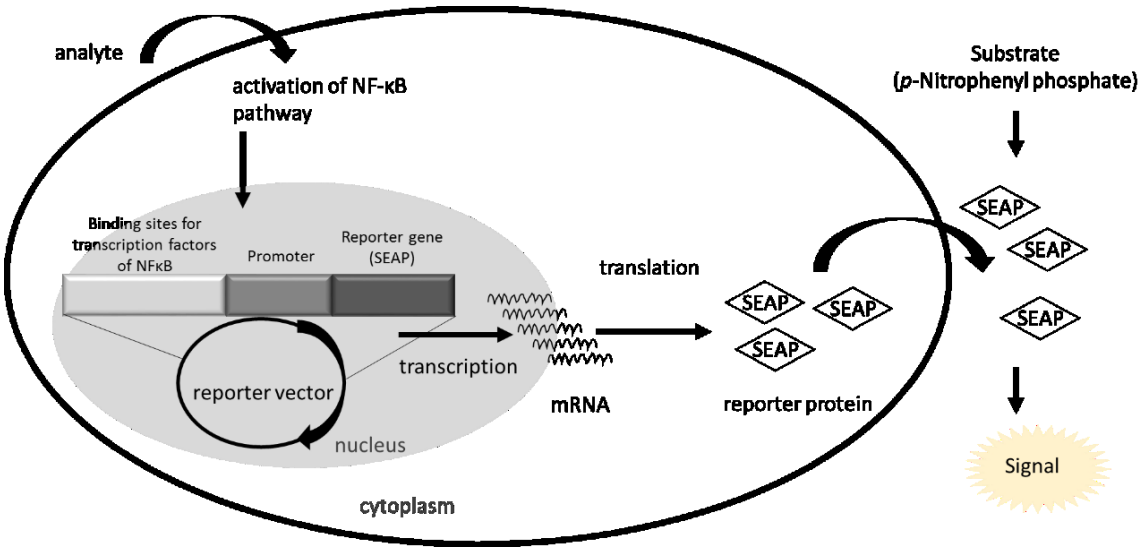

Figure 11. Schematic representation of working cell-based biosensor. After bioavailable analyte passes across the cellular membrane, activates a regulatory protein, which is a transcription factor, therefore, initiating transcription and translation of the reporter gene. Further addition of an external substrate provide measurable signal results.

After stable transfection single colony selection was performed (schematic overview of experiment is presented on Figure A. 1, appendix and described in above mentioned chapter). Aim of single clone selection was to obtain 100% clonal purity. To screen clones and establish, optimize and validate the sensor cell-based assay, stimulation with TNF-α and LPS has been performed as proof-of-concept setup. LPS next to TNF-α is second well known activator of NF-κB pathway [242]. After reproduction of single colonies, 20 of them (with the highest growth rate and viability) were induced with TNF-α (30 ng/ml – 200 ng/ml), LPS (0.01 µg/ml - 60 µg/ml) and screened to find colones with linear output. Clone 13 stood out with the lowest background, linearity and relatively small standard deviation (Figure 12). Therefore, this clone, was considered as a *SuperClone* and implemented for further experiments. Additionally, clone 2; 15, 16 and 19 were initially considered and tested as possiblle sensor cells parallel to clone 13 due to their dose-depended response in linear manner (Figure A. 2, appendix). Hovewer, all of them displayed lower sesnitivity for nanoparticles toxicity detection compared to clone 13 in subsequent experiments.

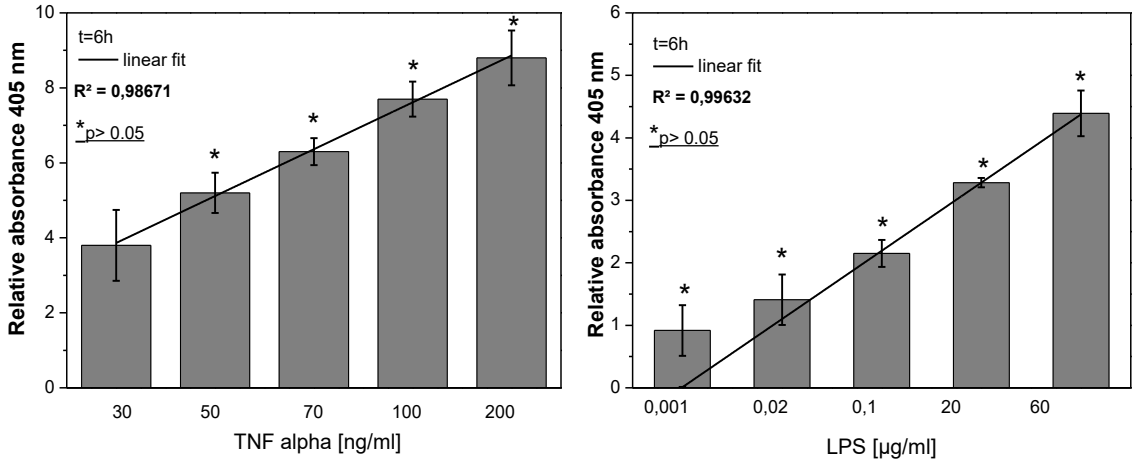

4.1.4

Figure 12. Response of stable transfected HepG2 cells with pNiFty2-SEAP vector, clone 13 (clone 13- later named as sensor cells or NF-κB_HepG2 cells) after stimulation with TNF-α and LPS (t=6h) with linear fitting, (ctrl=1, unstimulated cells, n=3 ± SD).

Evaluation of the NF-κB_HepG2 cells

Firstly, the growth rate of the transfected cells was analyzed using Neubauer cell chamber. Both, genetically modified and non-modified cell lines require a similar time of 36 h to double the population with initial density $5x10^5$ cells / well in a 6-well plate. Growth curves indicate that both HepG2 cells and NF-κB_HepG2 cells require > 160 h to stabilize their growth and reach plateau Figure 13.

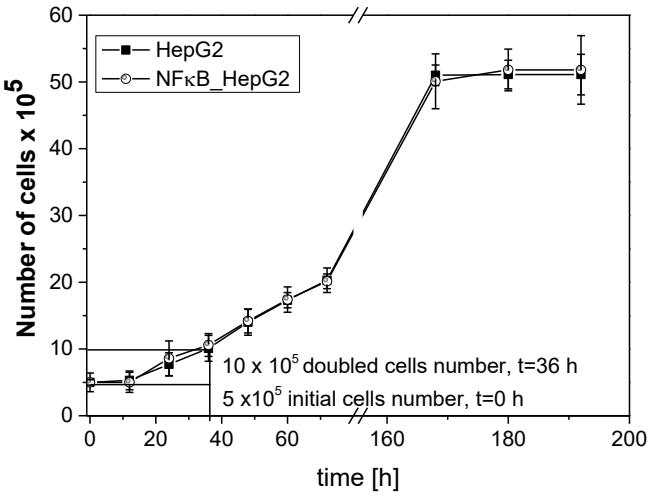

Figure 13. Growth rate of HepG2 (non-modified cell line) and NF-κB_HepG2 (modified cell line). Initial cell seeding 5 x 10^5 cells/ well; observation over t=192h; (n=4 ± SD).

The established stable sensor cell line was compared with untransfected cells to examine if genetic modifications had an impact on the properties of the cells. Known inducers of cell death (DMSO and ethanol) were used to compare cells viability. After incubation cells (t=24h) with DMSO (1 % - 10% (v/v)), both, modified and non-modified cell lines showed similar half maximal effective concentration EC_{50}= 4% (Figure 14). Similar results were observed after incubation of cells with ethanol (2%-16% (v/v)) EC_{50}= 8% for both HepG2 and NF-κB_HepG2 cells (Figure 14).

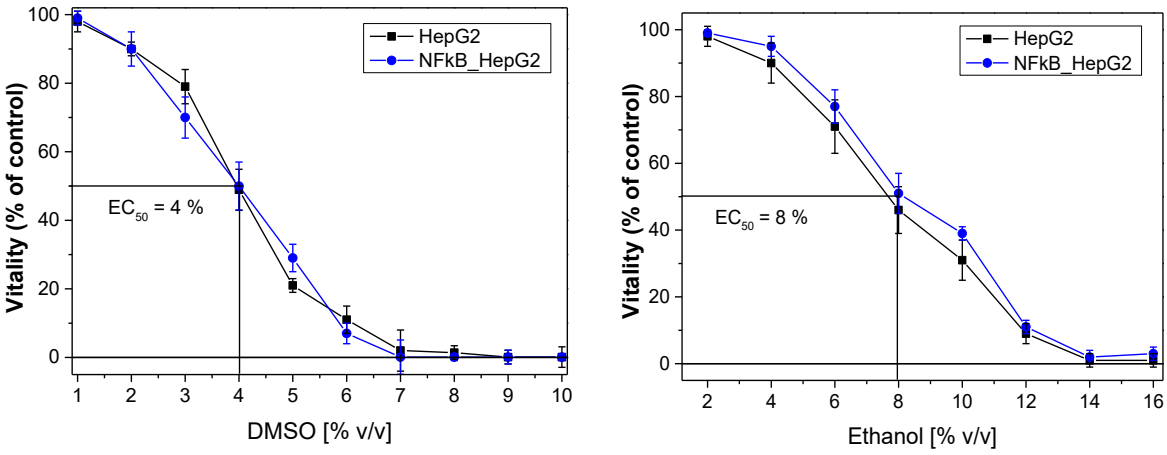

Figure 14. Dose response comparison of sensitivity between modified and non-modified cell lines. Exposure time t=24h, stimulation with DMSO (1-10 % v/v) and ethanol (2-16 % v/v), (n=3 ± SD)

Moreover, the stability of the sensor cell response upon storage of cells was verified after 3, 25 and 35 subcultivations. NF-κB_HepG2 cells were stimulated with TNF-α 30 ng/ml and LPS 0.02 µg/ml (t=8h) and it was found that even after one year of storage and repeated re-activation transfected cells are characterized by producing stable reporter signals (Figure 15).

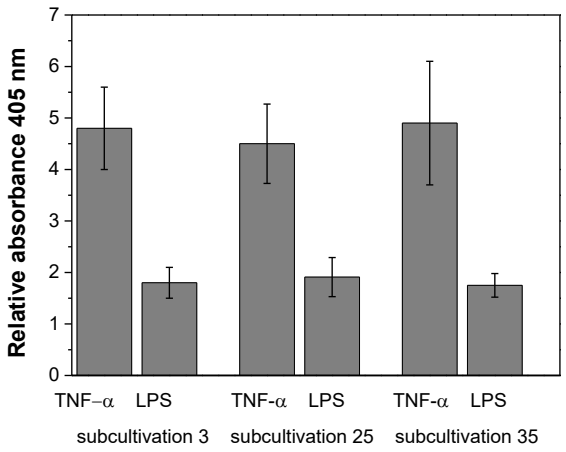

Figure 15. Investigation of the sensor cells stability after 3, 25 and 35 subcultivations. NF-κB_HepG2 cells exposed to 30 ng/ml TNF-α and 0.02 µg/ml LPS, t= 8h., (n=3 ± SD)

The reporter protein is secreted by the sensor cell into the cell culture medium. Therefore, it was examined whether cell culture media of stimulated cells could be stored for further use. One week storage of samples in -80 ˚C did not significantly change signal compared to fresh samples; however, longer storage (t=1month) resulted in considerable degradation of the reporter enzyme (Figure 16). Consequently, all data presented in this study result from measurements of fresh samples.

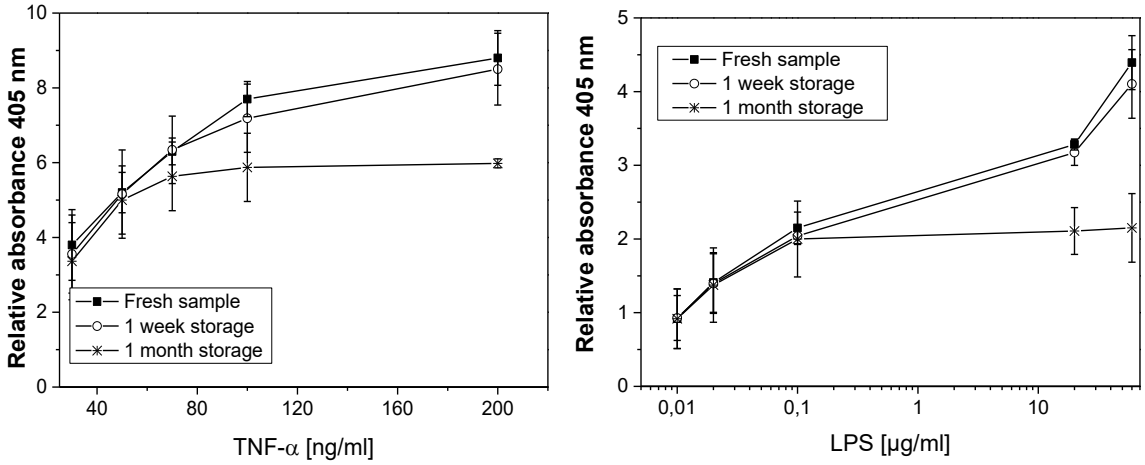

Figure 16. Examination of storage conditions of cell culture supernatants on final signal. NF-κB_HepG2 cells were stimulated with TNF-α and LPS, t=8 h, then samples were collected and stored (1 week or 1 month) in -80 ˚C before endpoint measurement; (n=4 ± SD)

The correlation between SEAP activity and NFκB_HepG2 cell number was examined next (Figure 17). As shown, the more cells present, the higher the SEAP activity detected in the culture medium. Therefore, to compare results between experiments is indispensable design assays with exactly the same number of cells. The minimum cell number needed for detectable SEAP activity at 8 h post-plating was > 250.

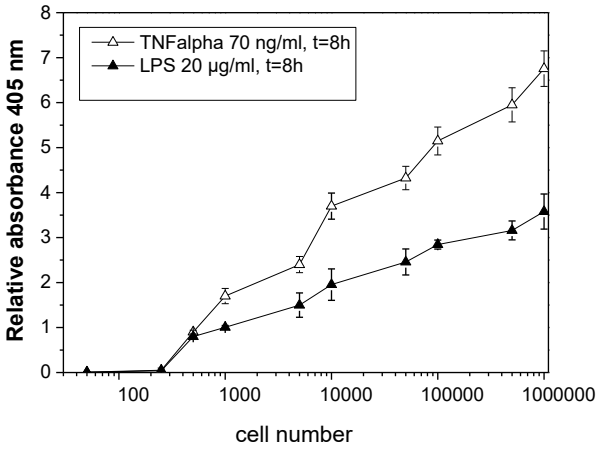

Figure 17. The correlation between SEAP activity and NFkB_HepG2 cell number after stimulation with 70 ng/ml TNF-α and 20 µg/ml LPS, t= 8h., (n=5 ± SD).

4.1.5 Summary

DLS measurement revealed a tendency of ZnO nanoparticles agglomeration in cell culture medium. Both sonication and FBS concentration influenced nanoparticle cytotoxicity. Therefore, all experiments were performed in exactly the same condition using 1% FBS medium and sonicated NP directly before their application. Moreover, sensor cells based on an inducible gene expression system were developed. The validation and optimization of the sensor cell line was carried out with activators (TNF-α, LPS) of NF-κB pathway. Genetic modifications display any influence on cells viability and growth rate. One year observation of sensor cells exhibit stable signal. Nevertheless, analysis of the supernatant storage warns against work with outdated samples, theretofore, all experiments were carried on fresh samples.

4.2 Application of cell based biosensor

4.2.1 Application of NF-κB_HepG2 cells for nanoparticle toxicity assessment

In the next step of the project, the established stable NFκB_HepG2 reporter cell line (clone 13) was used to determine the safety of nanomaterials. With increasing concentration of nanoparticles and incubation time signal in sensor cells increased, thus revealing an NFκB-mediated stress response (Figure 18). Developed system based on sensor cells requires 2 h of incubation time with nanomaterials to display measurable signal. Furthermore, selected threshold concentrations (for AgNP 3.75 µg/ml; for SiO_2NP 125 µg/ml and for ZnONP 20 µg/ml) are the lowest concentrations detectable in monolayer cell culture with developed system after t=2h stimulation. Application of lower doses require longer incubation time to observe significant response of NFκB_HepG2 cells. Assessment NP toxicity with developed cell-based biosensor is more sensitive method than applying widely used commercial cytotoxicity assay Alamar Blue (Figure 8). Threshold concentrations AgNP 3.75 µg/ml; SiO_2NP 125 µg/ml and ZnONP 20 µg/ml detectable with sensor cells after 2 h of incubation are not detectable with above mentioned commercial assay even after 24 h of time exposure cells to nanomaterials. The highest activation of NFκB pathway and thus the highest expression of reporter protein provide ZnONP among tested nanomaterials. High concentrations of examined analytes (AgNP > 30µg/ml; ZnONP >160µg/ml; SiO_2NP > 500 µg/ml) or extended incubation time (> t=12h) resulted in lower signals, which is a measure of damage of the sensor cells. Nevertheless, in the working range of the biosensor a linear signal was observed (Figure 18).

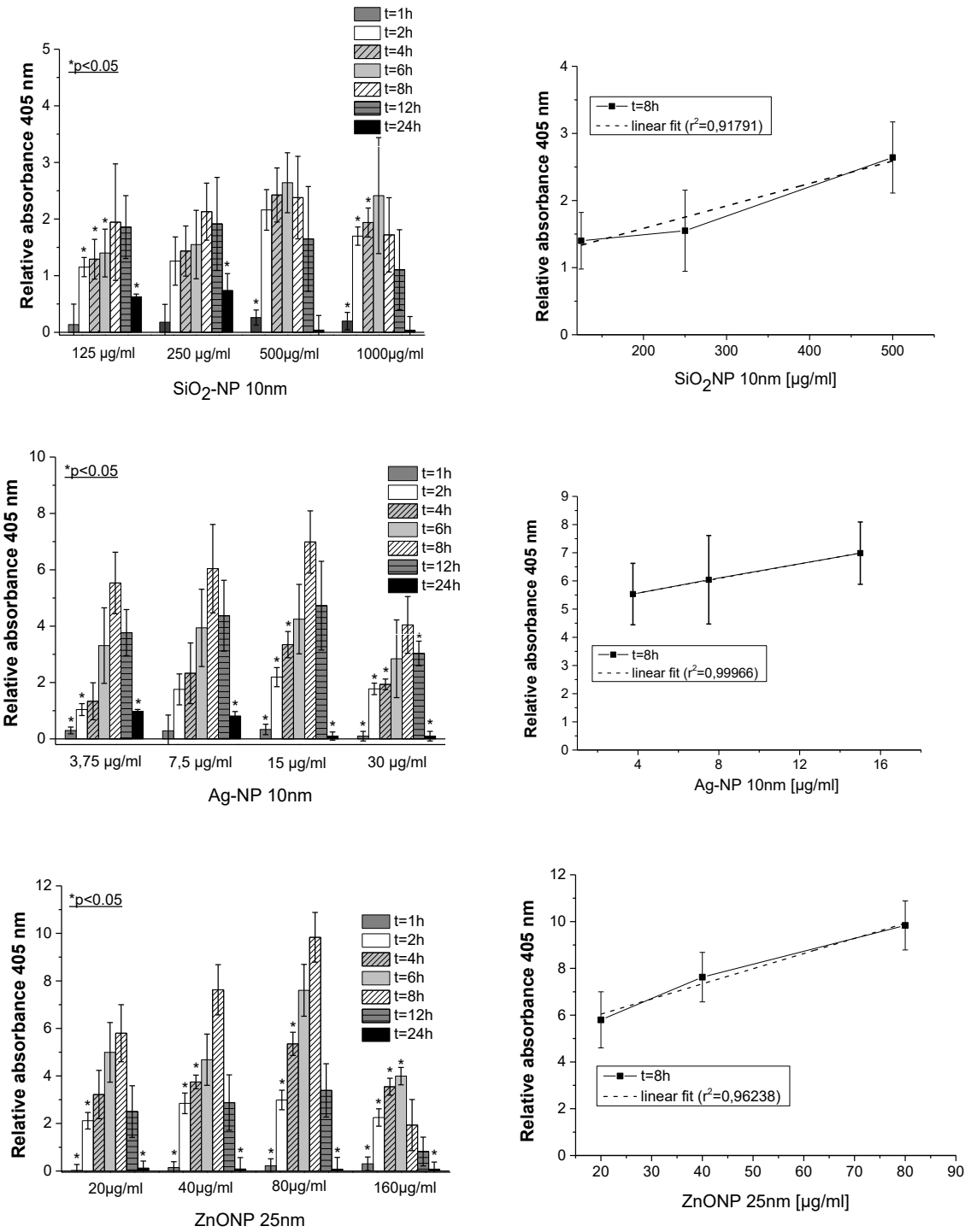

Figure 18. Relative response of sensor cells after stimulation with AgNP, SiO_2NP and ZnONP in monolayer; (ctrl=1, unstimulated cells; n=10 ± SD).

To further characterize the NF-κB-mediated stress response to NP exposure, investigation of the NF-κB transactivation potential via quantitative RT-PCR (RT-qPCR) of IκB-α expression was performed to verify correlation between mRNA levels of activated NF-κB elements with levels of expressed reporter protein. As was explained in chapter

2.2.5.1, termination of NF-κB transcription is mediated through the NF-κB-dependent synthesis of the IκB-α inhibitory subunit. Therefore, to quantify NF-κB activation by RT-qPCR, the expression of IκB-α mRNA was examined (Figure 19). After t=2h stimulation NF-κB_HepG2 cells with nanoparticles mRNA level of IκB-α was the highest for AgNP (30μg/ml), ZnONP (160 μg/ml) and SiO_2NP (500 μg/ml). Longer time exposure resulted in decreasing of mRNA levels and after ca 6h reached plateau. Obtained results coincide with SEAP (reporter protein) expression. Maximum expression of IκB-α mRNA was recorded after 2h stimulation with examined NP whereas, maximum abundance of reporter protein was noticed after 6h after stimulation for SiO_2NP and 8h for AgNP and ZnONP. Naturally, cells needs more time for translation and post-translations modification in compare to transcription what may explain shift in the observed time. Additionally, it was observed the highest mRNA level after stimulation with ZnONP among tested nanomaterials what correspond as well to protein abundance after stimulation with this kind of nanoparticles.

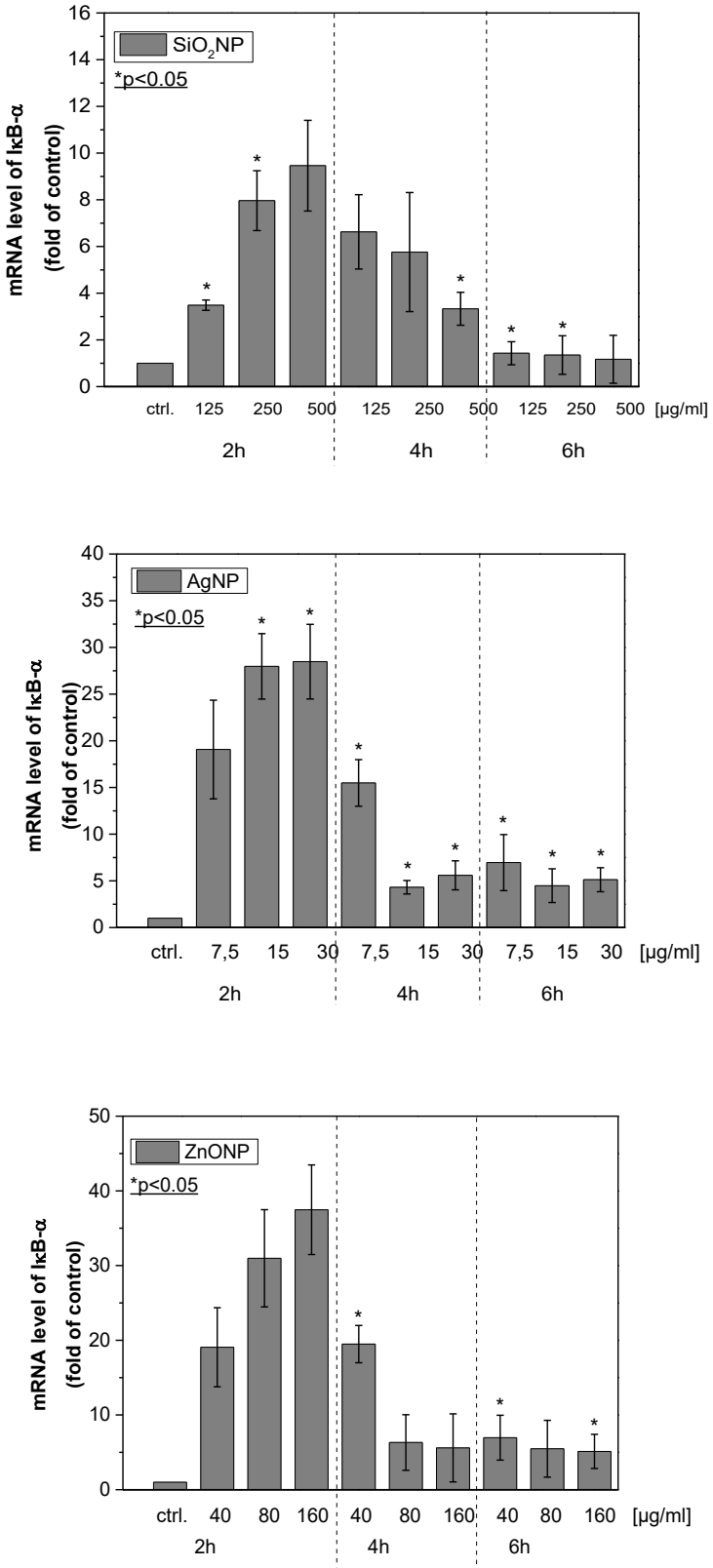

Figure 19. mRNA level of IκB-α in NF-κB_HepG2 cells after stimulation with AgNP, SiO_2NP and ZnONP as a fold of control (ctrl=1, unstimulated cells; n=6 ± SD).

Moreover, to have more detail information how analyzed nanoparticles interact with HepG2 cells Western Blot analysis was performed (Figure 20). Cleaved form of PARP protein is known marker of apoptic cells [243], [244], therefore apoptosis was examined using anti-human PARP antibody. As negative control was used cell lysate from unstimulated HepG2 cells and as positive control was used cell lysate from cells stymulated with 10 µM staurosporine, which is known as a toxic compound activating apoptosis. Obtained results indicate that nanomaterials activate pro-apoptotic cascades in HepG2 cells.

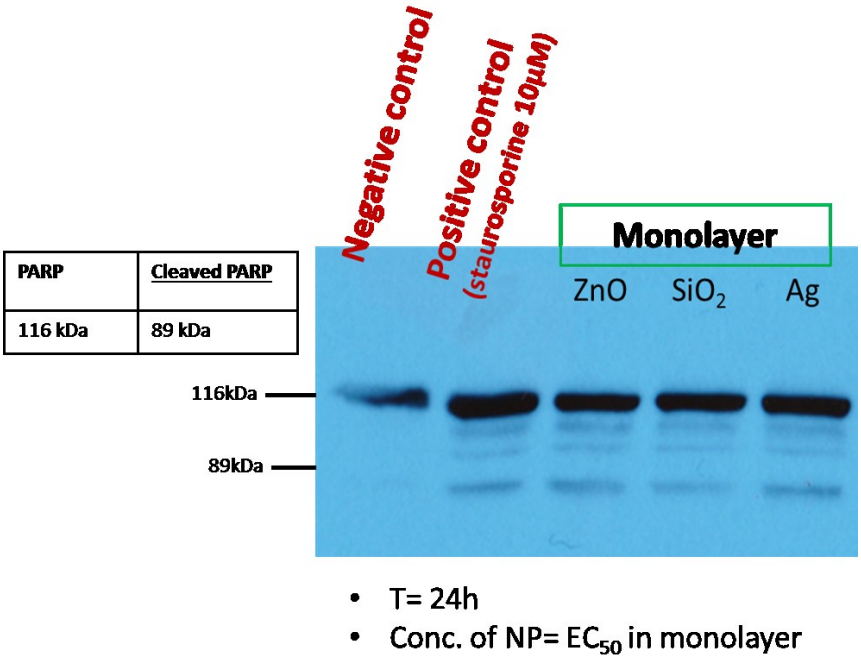

Figure 20. Western Blot analysis of pro-apoptic action of nanoparticles on HepG2 cells. As a primary antibody, anti-human PARP antibody (source - rabbit, Cell Signaling; Cat. No #9542 were used.) HepG2 cells were stimulated (t=24h) with ZnONP 80 µg/ml, AgNP 15µg/ml, SiO_2NP 250µg/ml and staurosporine 10 µM (positive control), as negative control unstimulated cells were used. Cleaved PARP is marker of apoptic cells.

4.2.2

Summary

Genetic modification of the human hepatoblastoma cell line (HepG2) involving the coupling of a cellular signaling system with a reporter gene was successfully conducted. Therefore, developed sensor cells produced measurable reporter gene products encoded in transfected vector after exposure of cells to activators of the NF-κB pathway. Three different kinds of nanoparticles were used as a model nanoparticles (ZnONP 20 nm, AgNP 10nm and SiO_2NP 10nm) because of their universal properties and application. With increasing concentrations of nanoparticles and incubation times, responses of sensor cells increased, suggesting activiation of the NF-κB-mediated stress response. High

concentration of analyte or long incubation time provided decrease of the signal due to the damage of sensor cells. Investigation of the NF-κB-mediated transactivation of IκB-α expression in the sensor cells confirmed the activiation of the NF-κB pathway, indicating that NF-κB_HepG2 cells are perfect indicators of toxicity in very early stages of exposure to stressors.

4.3 Development of the three dimensional environment for cell-based biosensor

Cell culture in two dimensions is a widely used method of cultivation of cells in thousands of laboratories worldwide for the past decades. However, the culture of cells in two dimensions is limited in that it does not reproduce the anatomy and physiology of a tissue. Work with third dimension in cell culture is more relevant to human and animal physiology. Moreover, two-dimensional cell cultures do not properly represent the functions of the tissues that have specific cell-cell and cell-matrix interactions and completely different transport conditions. Oxygen, nutrient or waste gradients are not present in a monolayer. Coating surfaces with poly-L-lysine, collagen [245], albumin, fibronectin [246], [247] and many others biocompatible materials can mediate more natural basal adhesion; however, cells are still forced into monolayer morphology. Although establishing co-cultures can increase contact between cells [248] [249], 2D surfaces still inhibit the ability of cells to form multidimensional structures. Models for the estimation of cell toxicity must reflect the *in vivo* situation as closely as possible. There is a broad spectrum of three dimensional cell cultures models that vary widely due to the diverse requirements of different cell lines and applications [250],[163]. Spheroids are self-assembled agglomerates of cell colonies that naturally resemble avascular environments with gradients of nutrients, O_2, CO_2 and water soluble wastes [164], [160]. Unlike conventional 2D cell cultures, multicellular spheroids readily mimic a real tissue better. The chemical and physical properties of the cell environment such as wettability, roughness, stiffness, softness [251], or microstructure (pore size, pore shape) [252] have been shown to have a crucial effect on cells behavior. Hydrogels with a high water content imitate a natural soft tissue more than any other type of polymeric biomaterials. With this objective, three dimensional environments for cells using three different types of hydrogels were developed and tested including transglutaminase-crosslinked gelatin, collagen type I and growth-factor depleted Matrigel. Even though a variety of research

on 3D cultures has recently been published, the results were mostly compared with conventional 2D cultures and not with different conditions of 3D cultures. Therefore, in presented thesis to bridge this gap different environments created from hydrogels were examined.

Hydrogels characterization

4.3.1

Hydrogel materials generally exhibit good biocompatibility and high permeability for oxygen, nutrients and other water-soluble metabolites, making them an attractive scaffold for cells [189]. A variety of hydrogels has been developed as microenvironment for cells [253], [188], [254]. Moreover, a slight distinction in concentration of natural polymers, crosslinking agents, and size of porous can make a huge differences in cell behavior. Cross- linking of gelatin was necessary due to gelatins properties: in concentration lower than 10 % in 37 ˚C is liquid and higher concentration of gelatin resulted in inhibition of HepG2 cells growth. In a first step, highly recommended acetic acid and glutaraldehyde as cross-linking agents were examined. However, both of them were problematic due to difficulties to remove their excess, which resulted in cell cytotoxicity (workflow of experiment is presented on Figure A. 4, appendix). To circumvent this problem, transglutaminase (EC 2.3.2.13) as a cross-linking agent was used which catalyzes the formation of isopeptide bonds between glutamine and lysine residues in proteins. Optimum pH of this enzyme is pH = 7 and temperature around 37 ˚C, which make it perfect for the use in cell culture research. Additionally, cytotoxicity of transglutaminase was examined prior development it as a crosslinking agent and obtained results indicate any toxic effect on cells (Figure 21).

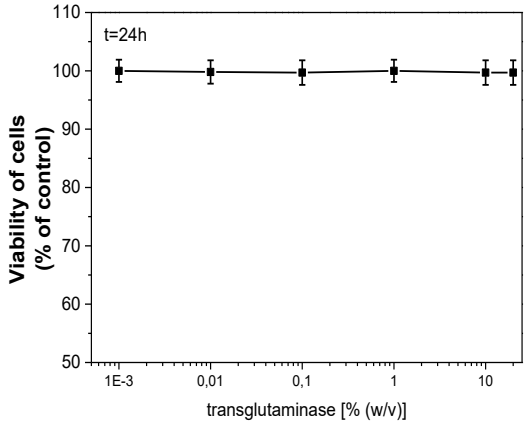

Figure 21. Cytotoxic effect of transglutaminase (0,001% - 20% (w/v)) on HepG2 cells grown in monolayer, t=24h. Alamar blue assay; (n=5 ± SD).

Both Matrigel and collagen type I solution have gel-like consistency at 37 ˚C, therefore they do not require cross-linking. Scanning electron microscopy was used to compare the morphologies of hydrogels created by gelatin cross-linked with transglutaminase, Matrigel, and collagen type I (Figure 23 and Figure 24). All materials showed different pore sizes and different architectures. These observations suggest that the nanometer-scale architecture of the ECM (Extra Cellular Matrix) has an impact on the structure, functions and composition of the integrin-mediated adhesions. In all hydrogels generation of HepG2-spheroids was performed successfully (Figure 22).

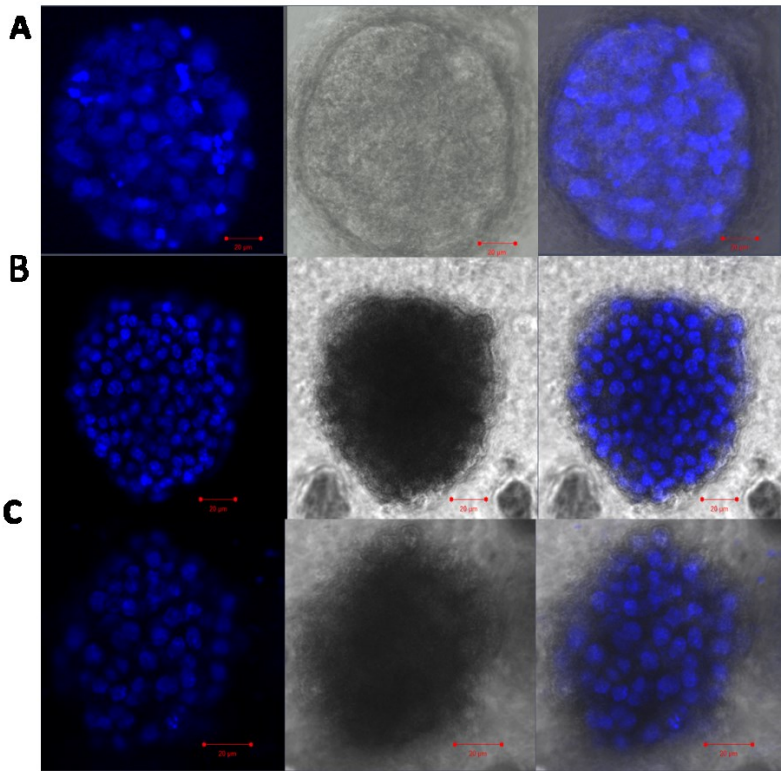

Figure 22. Morphology of spheroids created in gelatin gel (A) collagen I gel (B) and Matrigel (A). From the left: nuclei stained with DAPI, phase contrast image and merge; scale bars 20μm.

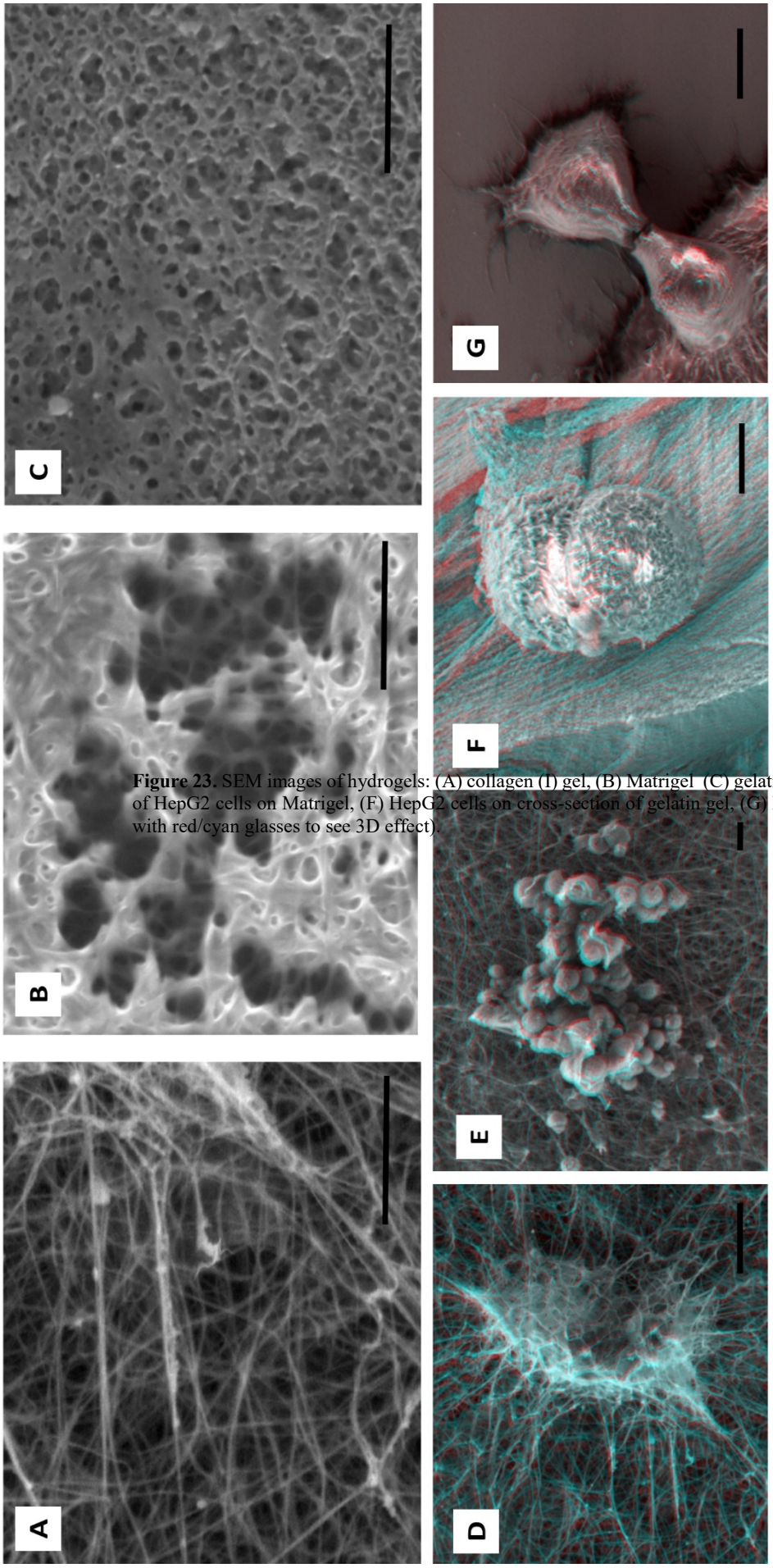

Figure 23. SEM images of hydrogels: (A) collagen (I) gel, (B) Matrigel (C) gelatin gel 10%(v/v) cross-linked with trans
of HepG2 cells on Matrigel, (F) HepG2 cells on cross-section of gelatin gel, (G) HepG2 cell on ITO glass (2D); all ima
with red/cyan glasses to see 3D effect).

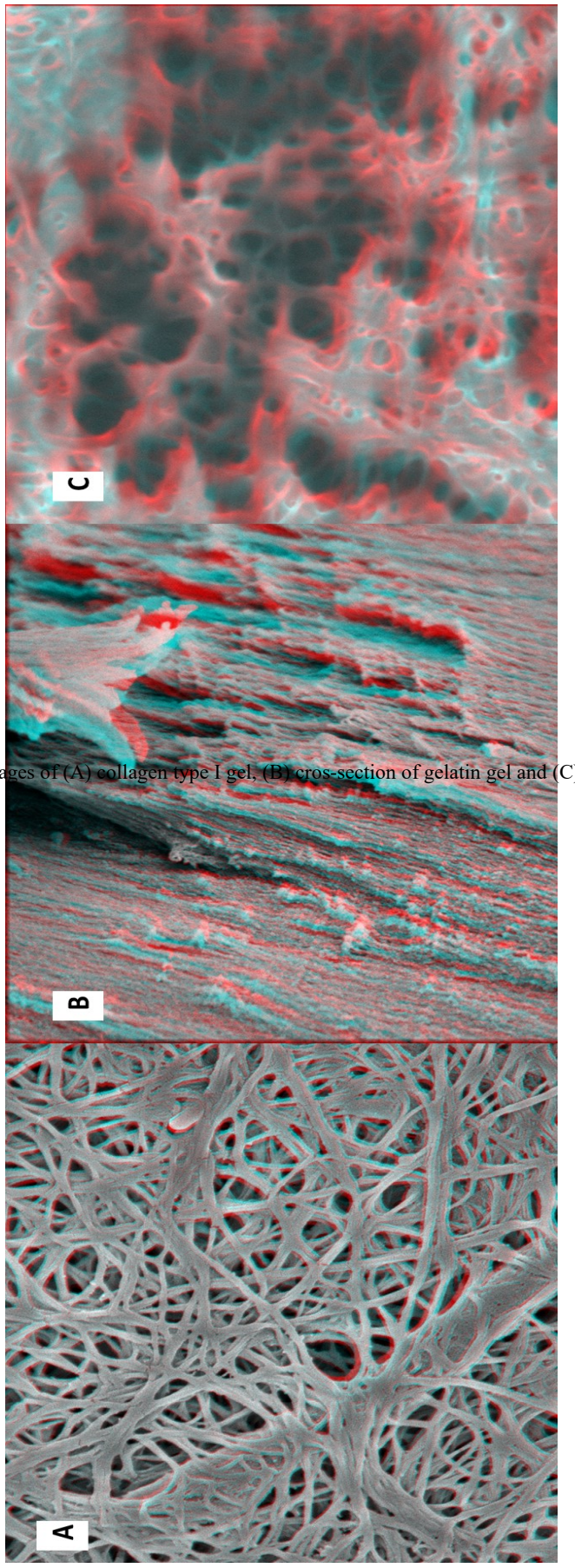

Figure 24. Images of (A) collagen type I gel, (B) cross-section of gelatin gel and (C) Matrigel. Anaglyph 3D images (please look at

The surface hydrophobicity is well known to be a key factor in a cell response and can be assessed by contact angle (CA) measurements. The lower the contact angle, the more hydrophilic the surface is. Results show that gelatin gel has the most hydrophobic surface (CA_{left} 109.773 ± 9.28 ˚ and CA_{right} 132.759 ± 14.19˚) and Matrigel possess the lowest hydrophobic properties (CA_{left} 11.529 ± 3.91 ˚ and CA_{right} 11.377 ± 2.35˚) (Table 6). Surface wettability is related to the rate of cell adhesion, proliferation and differentiation [255], [256]. As described in the literature, liver cells prefer to settle on hydrophilic areas [257].

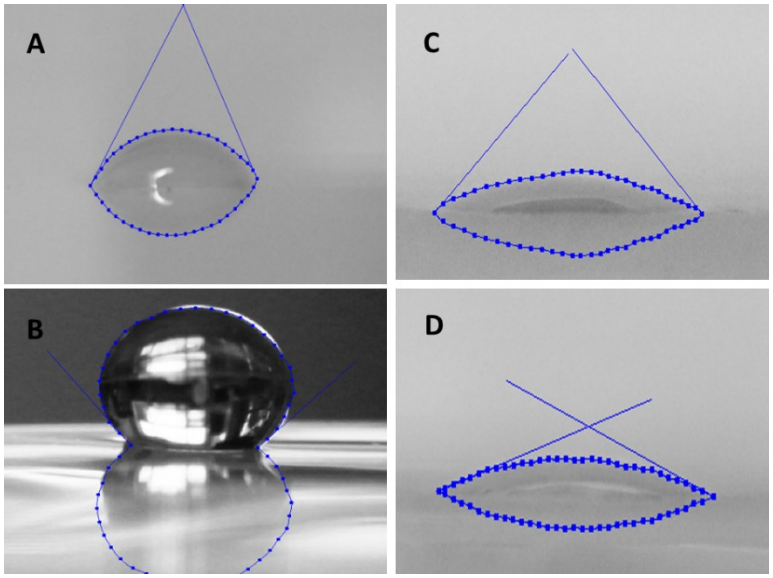

	Polystyrene well plate	Collagen type I	Gelatin	Matrigel
Contact Angle (degrees)	$_{Left}$ 56.823 ± 8.13 $_{Right}$ 72.849 ± 12.2	$_{Left}$ 41.717 ± 5.413 $_{Right}$ 41.573 ± 4.770	$_{Left}$ 109.773 ± 9.28 $_{Right}$ 132.759 ±14.19	$_{Left}$ 11.529 ± 3.91 $_{Right}$ 11.377 ± 2.35

Table 6. Values of contact angle of 5µl of water droplet spreaded on the surfaces of collagen type I gel, gelatin 10% gel, Matrigel and polystyrene well plate. Data present mean of n=10 ± SD. Image shows selected examples of water droplets on polystyrene well-plate (used for 2D cell culture) –A, on gelatin gel –B, on collagen I gel –C, on Matrigel – D. CA<90°- hydrophilic, CA>90°- hydrophobic.

Growth of HepG2 cells in 2D and 3D environments

4.3.2

The dynamics of spheroids growth was analyzed as the function of the increasing number of viable cells over time. Up to 7 days of cultivation, a similar cell number was observed on a monolayer and in gels with different final concentration of gelatin (3.5%, 6.5%, 10% v/v) whereas a somewhat higher cell number was observed in collagen and in Matrigel. After longer time of liver spheroids cultivation (>1 week) the number of viable cells stabilized. This could be assigned to the balance between an outer layer of highly proliferative cells and the growth over time of necrotic space inside the spheroids, due to insufficient distribution of O_2, CO_2 and nutrients. On the other hand, cells in a monolayer can proliferate as long they have space on the dish; at the last day of the experiment; on day 10, the cells were approximately 95% confluent (Figure 25).

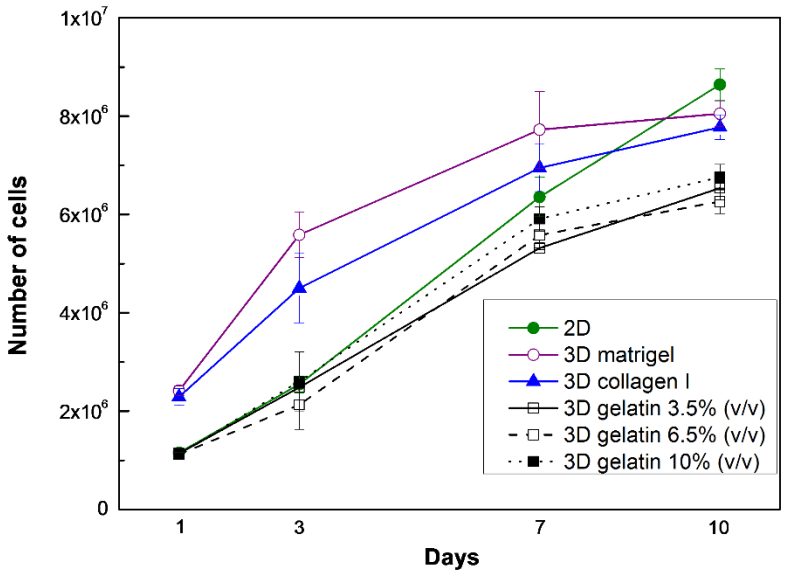

Figure 25. Proliferation of HepG2 cells after 1, 3, 7 and 10 days of cultivation in a monolayer, embeeded in Matrigel, collagen (I) gel and gelatin gel with different final concentrations (3.5%; 6.5%; 10%); (n=8 ± SD).

As a consequence of the highly proliferative activity of cells in the outer layer of the spheroids, an increase of their size was observed continuously over time (Figure 26). After 16 days of cultivation, spheroids reached an average size of 258 ± 54 µm in Matrigel, 214 ± 52 µm in collagen (I) gel and 201 ± 41 µm in gelatin gel.

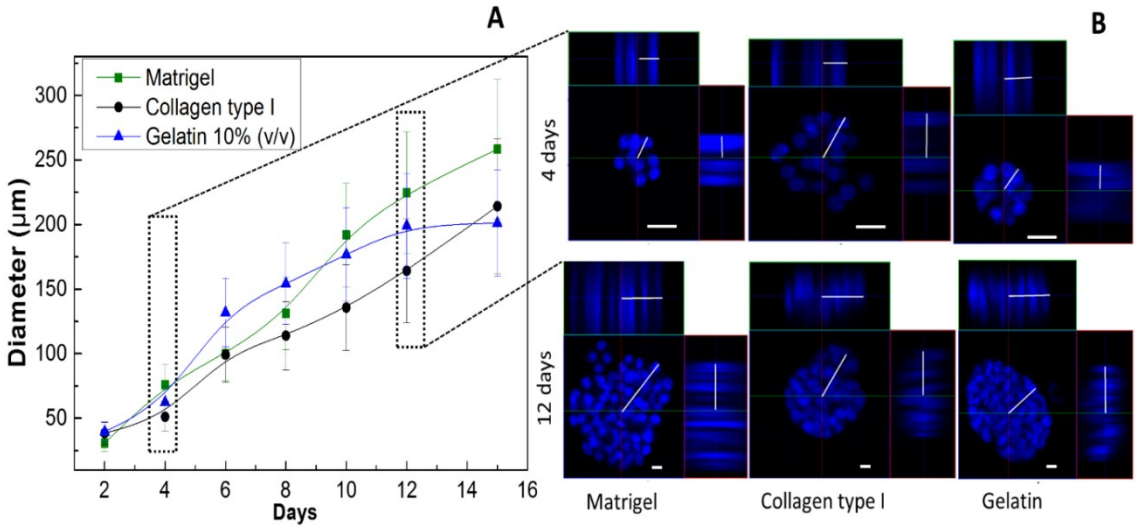

Figure 26. (A) Spheroid diameter as function of time in culture. HepG2 cells were cultivated over 16 days embeeded in Matrigel, collagen (I) gel and gelatin gel. Data represent mean ± SD of three independent experiments with 100 images taken per each time point. (B) Example images of HepG2 in Matrigel after staining with DAPI, scale bars 20µm. Ortho view allows to measure distances in three dimensions.

4.3.3 Functionality of HepG2 cells in 2D and 3D environments

One of the critical function of liver cells is the synthesis of albumin, a molecule of 585 amino acids known to be important for maintenance of colloid osmotic pressure [258], the scavenging of free radicals [259], and the binding and transport of compunds [260]. Therefore, albumin production is recognized as a marker of hepatocyte metabolic activity *in vitro* and is generally identified as an indicator of liver-specific functions. Albumin secretion after 3 and 5 days of cultivation was not detectable in samples from 2D and 3D cultures. However, after 7 days of cultivation albumin output in monolayer was 5.47 ± 0.027 µM/ 10^6 cells compared to 4.43 ± 0.042 µM/ 10^6 cells in the collagen (I) gel. In contrast, albumin production was about 30-fold higher in gelatin gel (115.97 ± 0.054 µM/10^6cells) and Matrigel (141.83 ±0.07 µM/10^6cells) (Figure 27 A). Urea production is the second biomarker of hepatocyte function. It was considerably higher when cells were cultivated in 3D environment in comparison to cells in 2D (Figure 27 B). Urea production gradually increased with time and cells in Matrigel exhibited the highest output of urea (0.017 ± 0.007 nM/10^6 cells).

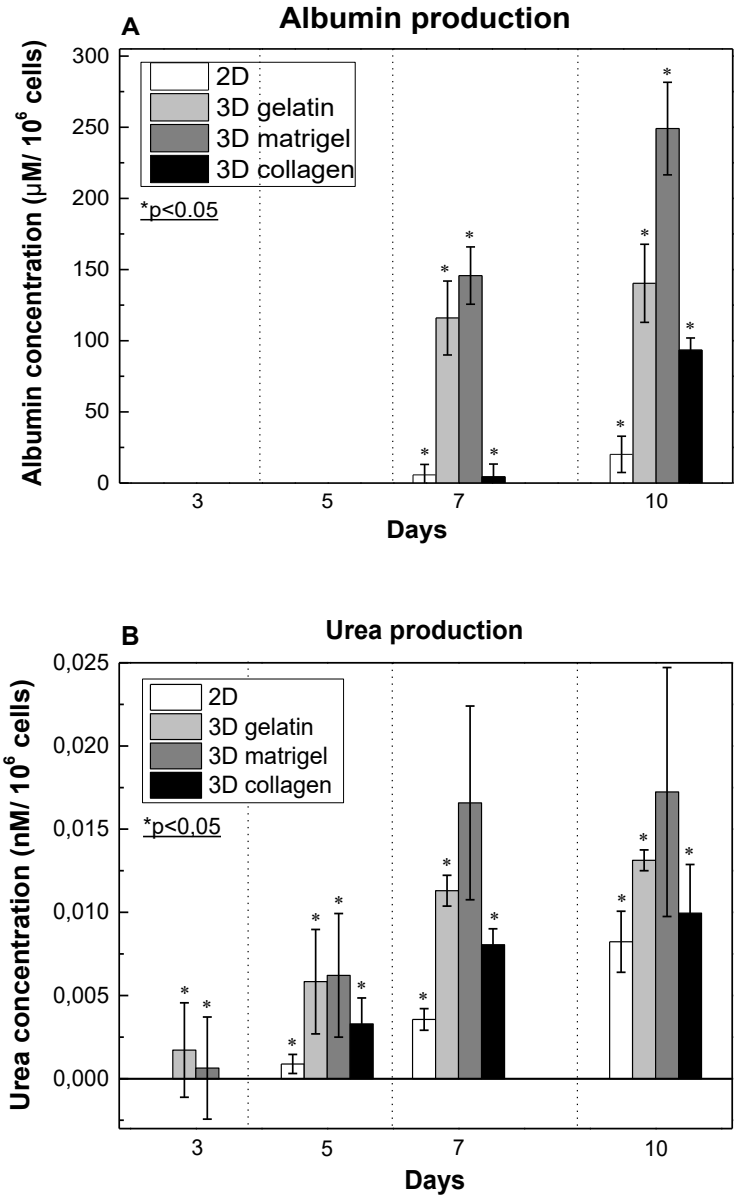

4.3.4

Figure 27. Albumin (B) and Urea (A) production in HepG2 cells after 3, 5, 7 and 10 days of cultivation. Albumin production was not detectable at days 3 and 5. Data were normalized to 10^6 cells, (n=4 ± SD).

Summary

Hydrogel properties strongly depend on the macromolecular structure, methods of preparation, and degrees of crosslinking. Because cells can feel and respond to the physical properties of their environment, selecting the right material and corresponding properties is essential in cell biology research. The choice of environment in presented PhD-thesis was preceded by experiments that allow for the identification of suitable conditions to grow the selected cell line. Obtained results demonstrates different architecture, size of pores, network construction and wettability of examined hydrogels.

Moreover, spheroid formation in all analyzed artificially created microenvironment was successfully performed. Among tested microenvironments Matrigel turned out to be a suitable three-dimensional substrate for HepG2 cells, allowing these cells to re-establish hepatocyte - like properties that are not observed under the conditions of conventional cell culture. Cells in Matrigel exhibited a high growth rate and biosynthesis of albumin and urea. The presented 3D cell culture models improve the predictive outcome of toxicity assessments *in vitro* and are a step forward for a better understanding and characterization of these systems.

4.4 Assessing nanoparticle toxicity in a 3D cell environment

Firstly, application of widely used MTT assay as a basic cytotoxicity test in 3D cell culture was considered. MTT is a colorimetric assay in which colorless tetrazolium salt (3-(4, 5-dimethylthiazol-2-yl)-2, 5-diphenyl-tetrazolium bromide) is converted into dark blue formazan under activity of mitochondrial dehydrogenases in viable, metabolic active cells. The amount of formazan is proportional to number of living cells [261], [227]. However, transfer MTT assay from monolayer cell culture to 3D cell culture was unsuccessful due to difficulties in dissolution of formazan crystals in hydrogels. Longer incubation of samples with organic solvent (DMSO) did not solve this issue. Therefore, Alamar Blue assay was implemented as an alternative cytotoxicity test. Here, resazurin is reduced by viable cells into resorufin (maximum absorbance at 573 nm). So far there is no conclusive studies proving in which compartment of the cell the reduction of resazurin process takes place. Resorufin does not form crystals and is soluble in cell culture medium, which is an obvious advantage over the MTT assay [262], [263].

HepG2 cells were exposed to different concentrations of NP for 24h and 72h in 2D and 3D cell environments. Dose-response curves are presented in Figure 28. The toxic effect of nanomaterials was lower when cell were embedded in hydrogels than when cells were grown as monolayer cultures. This difference in cell survival is especially visible after 72 h of nanoparticle exposure. To highlight evidence that cell environment has significant influence on cell response to toxic compounds Figure 28 A2-C2 shows comparison of toxic effects after 24h of NP incubation in concentration equal half maximal effective concentration (EC_{50}) on cells in monolayer. As Figure 28 A2-C2 shows

exactly the same concentration is significant less toxic for cells embedded in Matrigel, collagen type I or gelatin. To visualize toxic effect of examined nanomaterials HepG2 cells after 24h of incubation with 15 µg/ml AgNP; 80 µg/ml ZnONP and 250 µg/ml SiO_2NP were stained with propidium iodide (dead cells; red color) and calcein-AM (viable cells; green color). Although the spheroid culture did not undergo distinct morphological changes, dead cells were observed (example images Figure 28 C2).

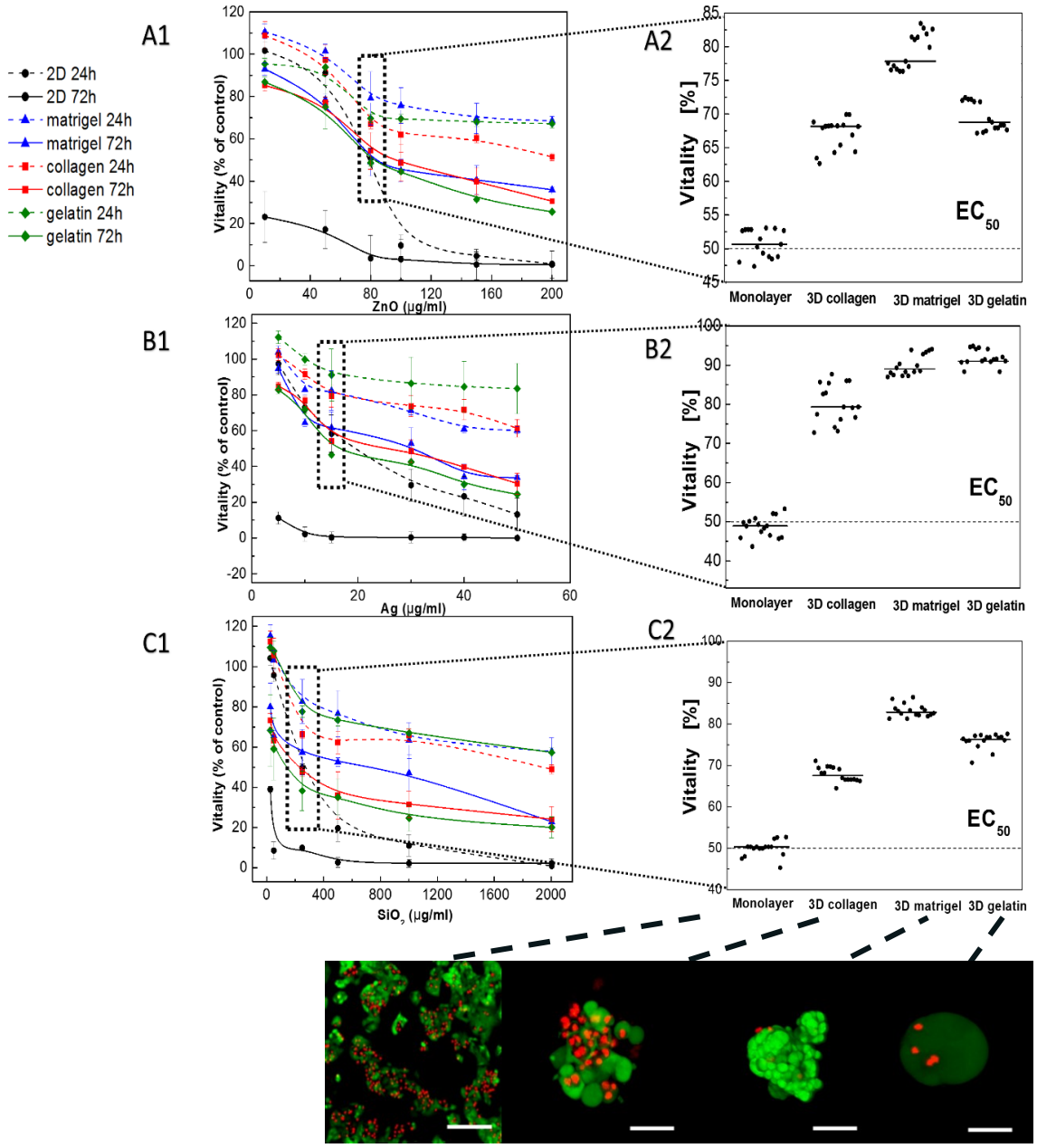

Figure 28. Viability of HepG2 cells after exposure to ZnONP (A1), AgNP(B1) and SiO_2NP (C1) for 24h or 72h; (n=10 ± SD). Graphs (A2,B2,C2) show comparison of toxic effect after 24h of NP incubation in concentration equal EC_{50} for cells in monolayer (single dot reflects single result, horizontal line shows average value). Optical visualization of dead cells:-propidium iodide and viable cells - calcein AM was performed under microscope; scale bar: spheroids 100 µm and 200 µm in monolayer.

Changes in cellular morphology observed under the phase-contrast microscope are an obvious initial sign of toxic effects. In monolayer HepG2 cells usually appear flat and densely packed. However, their shape changed after 24 h of NP exposure. A significant number of cells were round and partially detached (Figure 29). Similarly, spheroids exposed to NP for 24 h were observed under microscope and any substantial alteration in their morphology was noticed in comparison to untreated control, only a decrease in their size was recognized (this observation was exploit in next experiment).

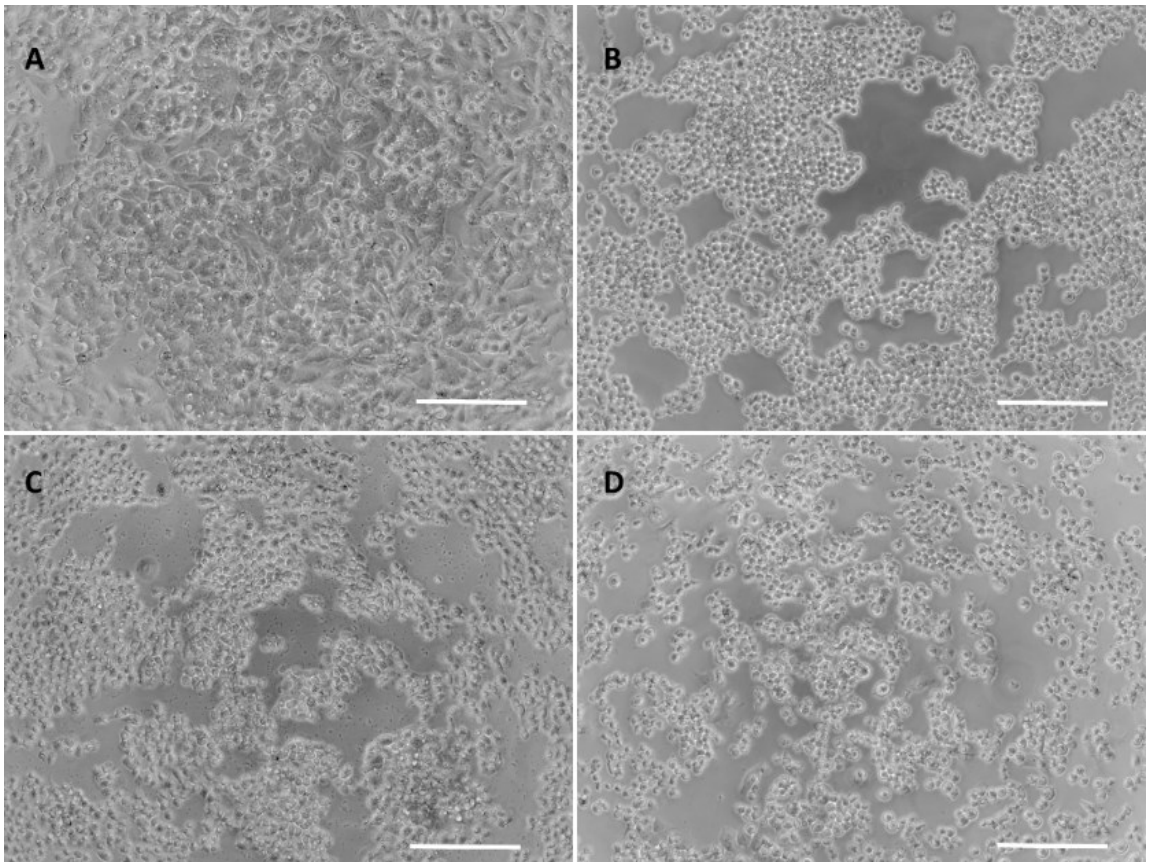

Figure 29. Morphology of HepG2 cells grown as monolayer after nanoparticles exposure (t=24h); (A) control, (B) AgNP 15µg/ml, (c) SiO_2NP 250µg/ml, (D) ZnONP 80µg/ml. Scale bar 200µm.

Moreover, the influence of the frequency of dosing of nanoparticles was analyzed. AgNP were dosed with different frequency (every 12 h or every 24 h) and with different concentration (2.5 µg/ml or 5 µg/ml), while the final concentration was exactly the same (15 µg/ml) for both dosings. The results (Figure 30) indicated that a higher frequency of dosing the lower concentration of NP resulted in higher disintegration of spheroids and stronger toxic effect than the less periodicity dosing with higher concentrations of the NP.

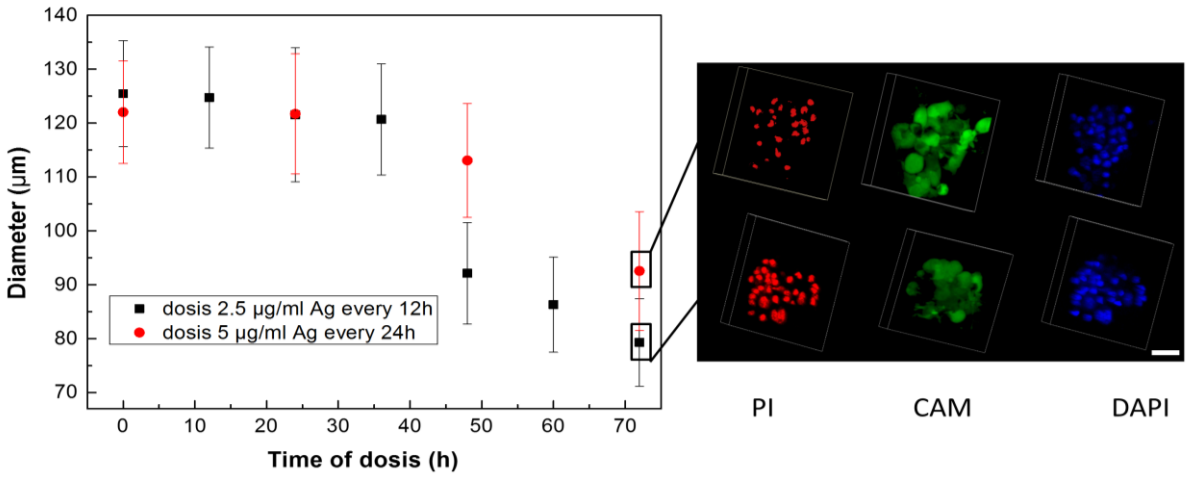

Figure 30. Dosage effect of AgNP (10 nm) on spheroids size. Cells HepG2 were cultivated in a Matrigel and over 72 h AgNP were dosed with different frequency (every 12 h or every 24 h) and with different concentration (2.5 µg/ml or 5 µg/ml), with equal final concentration (15 µg/ml). Data represent mean ± SD of three independent experiments with 100 images taken per each time point. Cell staining performed at the endpoints of the experiments, (dead cells (PI)-propidium iodide; viable cells (C AM) - calcein AM; nuclei –DAPI. Scale bar 40 µm.

4.4.1 Summary

HepG2 cells cultivated in three dimension display higher resistance to toxic effects of examined nanomaterials then in 2D cell culture. The data suggest that measurements of the toxicity of nanoparticles in 2D and 3D cultures of the same cells differ significantly, suggesting that conclusions drawn from 3D cell culture models may more reliably reflect the *in situ* situation since cells in native tissue create even more complex structures. Therefore, hepatocytes cultivated as spheroids structures embedded in artificial environments provides an excellent experimental tool for toxicity assessments as an intermediate between simple cell culture and animal models and enable analysis of dosing effect even in *in vitro* conditions.

4.5 Application of NF-κB_HepG2 cells in 3D environment

Matrigel turned out to be the most suitable environment for HepG2 cells and was therefore implemented as a 3D environment for NFκB_HepG2 sensor cells to improve predictive value of cytotoxicity assays (Figure 31). The same experiment was carried out as described in chapter: ***4.2.1***, but cells were cultivated in Matrigel instead in monolayer form. Error bars were much smaller compared to measurements in 2D therefore, application of 3D environment ameliorated precision of sensor cells. However, as

expected, the relative response of NFκB_HepG2 cells in 3D environment was lower compared to monolayer cell culture. This can be explained by lower sensitivity of cells in 3D environment to nanomaterials (what was presented on Figure 28).

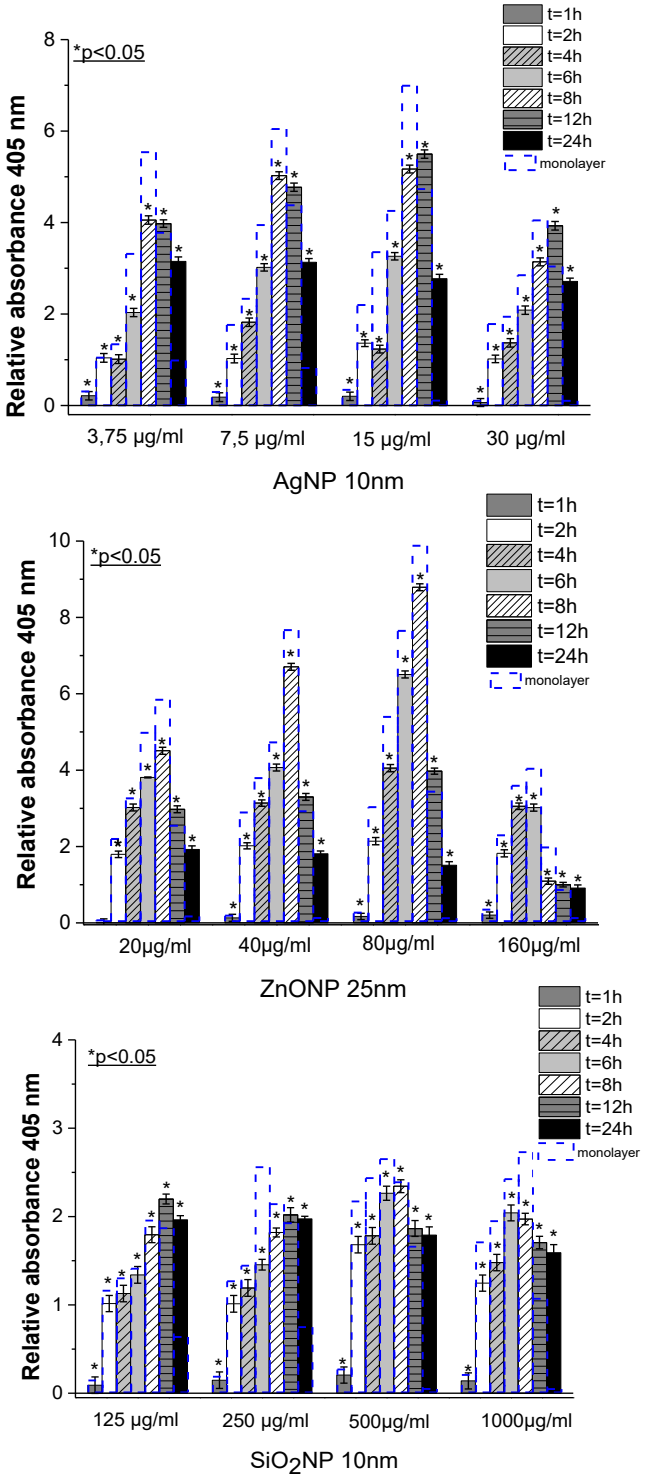

Figure 31. Relative response of sensor cells in Matrigel after stimulation with AgNP, SiO_2NP and ZnONP; (ctrl=1, unstimulated cells; n=7 ± SD).

One of the major advantages of the developed system is the possibility of implementation it in the basic screening. Therefore, in order to ascertain the feasibility of detecting cytotoxicity by sensor cells, a series of experiments with another kind of nanomolecules (ZnONP 14 nm, TiO_2NP 16-26 nm, TiO_2NP 4-8 nm and SiO_2NP 20 nm) were performed (Figure 32). Firstly, working ranges and cytotoxic effects of nanoparticles were tested using Alamar Blue assay. Maximum examined concentration was 300 µg/ml for TiO_2NP 4-8 nm, 600 µg/ml for SiO_2NP 20nm, 400 µg/ml for ZnONP 14nm and 500 µg/ml for TiO_2NP 16-26 nm. Higher concentration of analyzed nanomaterials provided precipitation and the disappearance of clarity of cell culture medium. The response of NFκB_HepG2 cells increased with increasing concentration of analytes. Moreover, all examined nanomaterials provided response of sensor cells in dose- depended manner. It is also important, that the most toxic were TiO_2NP 4-8 nm and the lowest toxicity was observed after stimulation sensor cells with SiO_2NP 20 nm and these data coincide for both types of measurements Alamar Blue and developed NFκB_HepG2 cells. Furthermore, sensor cells detected toxic effects of nanoparticles at lower concentration (10µg/ml is already detectable) and shorter incubation time.

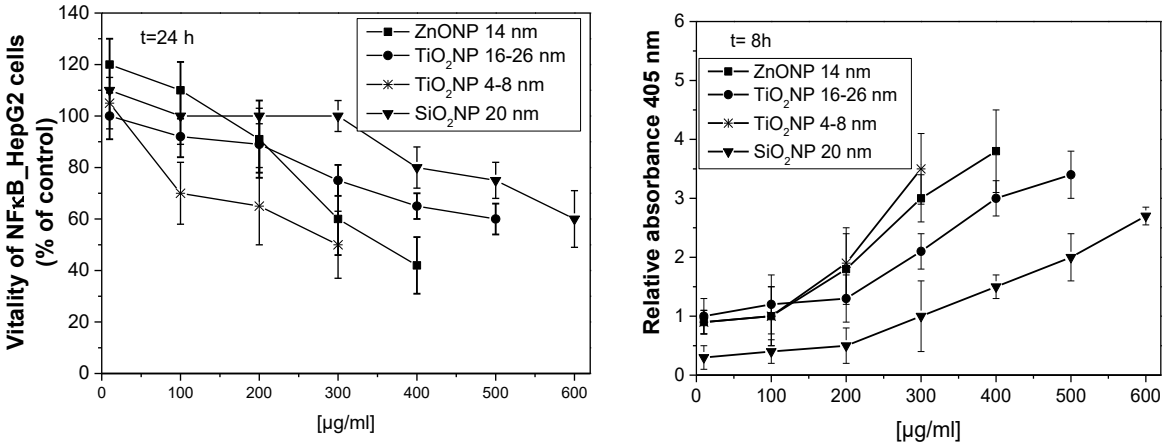

Figure 32. Dose-response analysis (left) after incubation NF-κB_HepG2 cells in Matrigel t=24h with ZnONP 14nm, TiO_2NP 16-26 nm, TiO_2NO 4-8 nm and SiO_2NP 20 nm using Amar Blue assay; (n=4 ± SD). And response of sensor cells (right) cultivated in Matrigel after incubation t=8 h with the same nanomaterials; (ctrl=1, unstimulated cells; n=5 ± SD).

Since the developed NFκB_HerpG2 cells showed promise to detect cytotoxicity through NF-κB pathway activation caused by nanomaterials, the sensor cells were applied to assess cytotoxicity of heavy metals as well. Both, $NiSO_4$ (Figure 33) and $CdCl_2$ (Figure 34) induced response of the biosensor; at 0.4 mM of $NiSO_4$ and 8 µM of $CdCl_2$ after t=6h a maximum response of the NFκB_HepG2 cells was observed. Higher concentrations resulted in decrease of the signal due to damage of sensor cells.

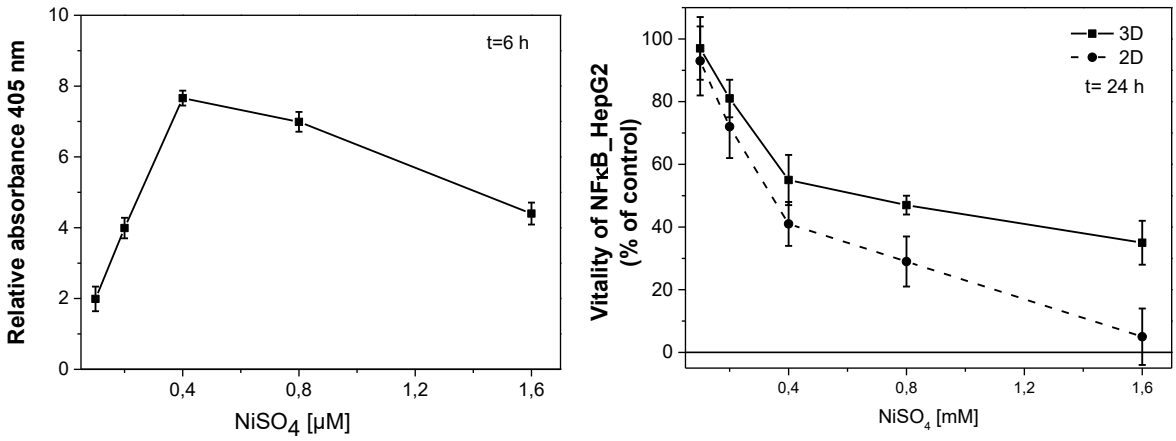

Figure 33. Response of sensor cells (left) cultivated in Matrigel after incubation t=6 h with $NiSO_4$; (ctrl=1, unstimulated cells, (n=4 ± SD). And dose-response analysis (right) after incubation NFκB_HepG2 cells in Matrigel and monolayer (t=24h) with above mentioned heavy metal using Amar Blue assay; (ctrl=1, unstimulated cells; n=4 ± SD).

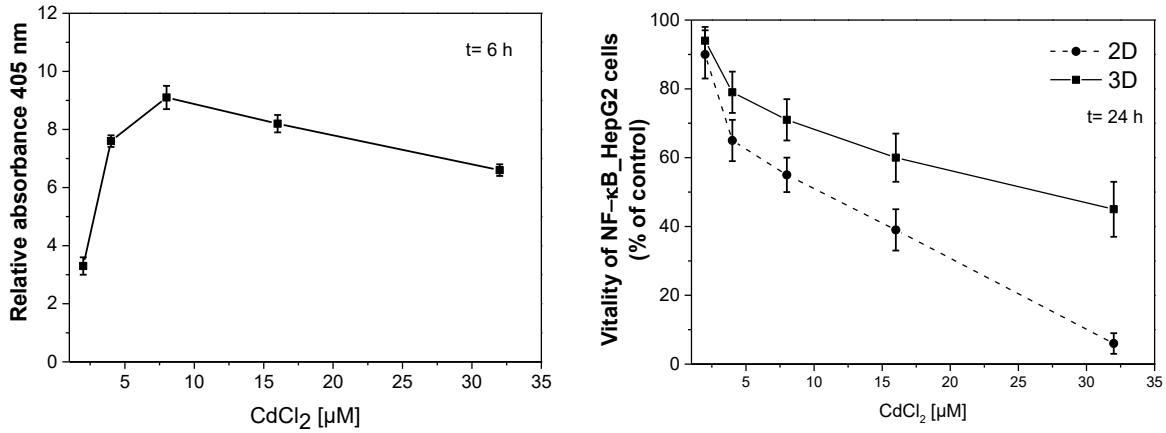

Figure 34. Response of sensor cells (left) cultivated in Matrigel after incubation t=6 h with $CdCl_2$; (ctrl=1, unstimulated cells (n=4 ± SD). And dose-response analysis (right) after incubation NFkB_HepG2 cells in Matrigel and monolayer (t=24h) with above mentioned heavy metal using Amar Blue assay; (ctrl=1, unstimulated cells; n=4 ± SD).

Next, detection of DMSO by sensor cells was examined, since DMSO is described as a compound which induce cell stress without activating of NF-κB signaling (Figure 35) [264], [265]. Over t=12 h of monitored time relative response of sensor cells stayed on a constant level, thus toxic effect of DMSO was not detectable. Dimethyl sulfoxide may be used as a negative control in further investigations with developed sensor cells and as a solvent of compounds that must be dissolved in DMSO.

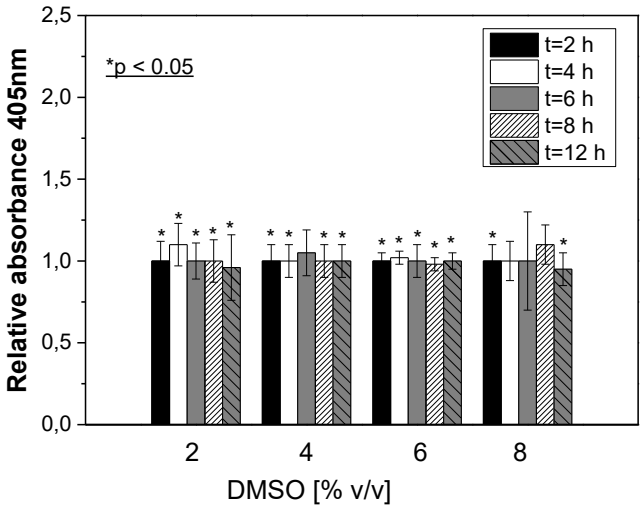

Figure 35. Response of sensor cells cultivated as monolayer form after incubation t=2-12 h with DMSO; (ctrl=1, unstimulated cells; n=3 ± SD).

Summary

4.5.1 The featured cell-based biosensor in 3D cell culture (Figure 36) model provides a platform for an in-depth analysis of NP toxicity. NF-κB_HepG2 cells detect toxic effect of agents which activate NF-κB pathway even after 2h of exposure time what is impossible to detect performing commercially available Alamar Blue assay. Comparison of the dose and time depended detection of the nanomaterials toxicity between sensor cells in 2D and 3D environment showed higher precision of NF-κB_HepG2 cells in Matrigel. Exactly the same sensor cells were applied for screening toxic effect of heavy metals. Obtained results indicate that developed CBB may take advantage as a screening tool of activators of NF-κB signaling in general and use in high throughput applications.

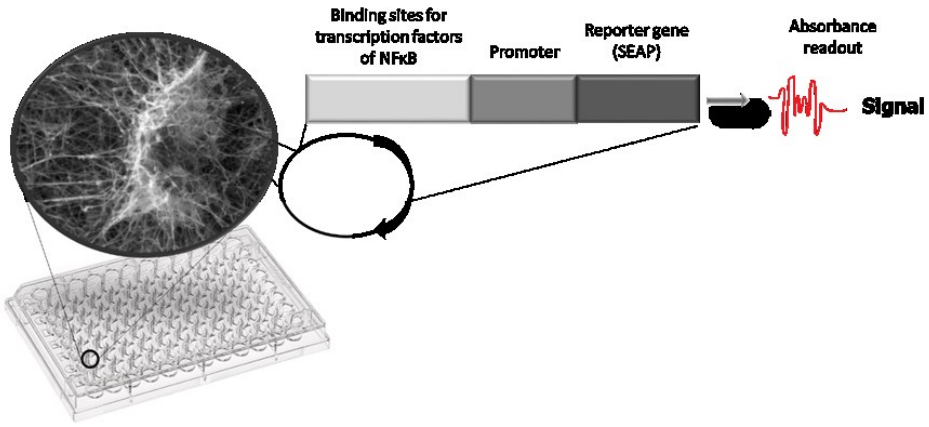

Figure 36. Schematic of NF-kB_HepG2 cells in 3D milieu created on 96-well plate for high throughput applications.

5 DISCUSSION

5.1 Development of whole-cell based biosensor

The recombinant HepG2-based biosensor cell line seems to be a perfect hepatotoxicity model. Firstly, immortalized cells are easy to transfect and do not have limited life time like primary cells, this make them advantageous in cell-based bioengineering. Nevertheless, realizing that HepG2 cells differ from hepatocytes which can be found in native tissue [266], [267], [268], adoption of three dimensional environment was a balanced solution. Implementation of biosensor and 3D cell culture is anticipated to ensure more predictive results for *in vivo* studies, as 3D models come closer to *in vivo* conditions than conventional 2D monolayer culture [269], [270], [271], [272], [273], [274] (an in-depth discussion concerining the development of 3D environment for CBB is continued in the chapter ***5.3***). The advantages of using cell based sensors include rapid growth and ease of culturing cells compared to complex experiments on tissues slices or animals. The mammalian cells can report information such as bioavailability, cellular metabolism, and physiological responses relevant to human and animals. This type of information is important for the development of functional biosensing. The opportunity of mammalian cells to imitate how the organism interacts with toxicants has become a fundamental tool for screening, sensing, and evaluating environment, food, or clinical hazards. Moreover, the implemented extracellular reporter system (SEAP) is advantageous considering 3D cell culture because preparation of cell lysates and thus extraction cells from hydrogels is not required. Aditionally, the kinetics of reporter gene expression can be easily studied by repeated collection of medium from the same cultures; analysed cells are not disturbed during measurement of SEAP activity and remain intact for further investigations, also background from endogenous alkaline phosphatase can be eliminated; and assay may be readily automated using multi-well plates. In turn, to confirm the desirability of considered molecular recognition, activation of the NF-κB pathway after exposure of cells to nanoparticles was analyzed using ELISA assay. Review of the literature [110], [275], [112] and obtained results presented on Figure 9 complement each other, confirming that nanoparticles activate the NF-κB pathway. Additionally, usefulness of the designed reporter construct for nanoparticles cytotoxicity screening was examined initially on transiently transfected HepG2 cells with pNiFty2-SEAP vector. Results presented on Figure 10 indicate increase of SEAP activity in

transiently transfected cells after incubation with ZnONP, SiO_2NP and AgNP compared to untreated control. Moreover, analysis of the results on the Figure 10 point out high background and standard deviation. Therefore, unquestionably essential was selection of single clones to establish, optimize, validate sensor cell-based assay. 100% clonal purity allows conduction of the study using a defined and homogenous cell system. Furthermore, stimulation of sensor cells with TNF-α and LPS has been performed as a proof-of-concept setup. Clone 13 (Figure 12) stood out with the lowest background, linearity and with relatively small standard deviation. Therefore, this clone, was considered as a SuperClone and implemented for further experiments. Depending on, in which place of genomic DNA vector was inserted and in how many copies, transfected cells may display different expression levels of proteins coded in inserted plasmid. This statement may explain response with different sensitivity of analyzed clones after stimulation with LPS and TNF-α (presented on Figure A. 2, appendix). Moreover, mentioned above linearity of the signals is an essential feature of sensors because it indicates that an output is directly proportional to input over its entire range while, standard deviation emphasize precision of developed system. Because some reports warn that genetic modification of cells may have influence on cells basic functionality [276], it was important to examine the influence of cell transfection on cell proliferation and both modified and non-modified cell lines are characterized by similar growth rate with t=36 h needed for doubling their population (Figure 13), this value does not differ obtained from the supplier data. Similarly, cells sensitivity stayed unaltered (Figure 14). Both, modified and non-modified cell lines were stimulated with known inducers of cell death DMSO and ethanol. 4% (v/v) of DMSO and 8% (v/v) of ethanol provide 50% of cell death (t=24 h). Correlation between SEAP activity and number of NF-κB_HepG2 cells was also examined. As shown on Figure 17 the more cells present in the sample, the higher SEAP activity was detected. Therefore, to compare results between different experiments necessary was to design assays with exactly the same number of cells. Additionally, the minimum number of cells with implemented reporter system was determined and to detect stimuli ~250 cells is required (examined with strong activators NF-κB pathway), this density is relatively low in comparison to widespread used commercially available assays like MTT, LDH, where detectable signal is represented by ~1000 of cells. Furthermore, one year monitoring of NF-κB_HepG2 cells (Figure 15) indicate that transfected cells are characterized by a stable signal (in the meantime cells were frozen and thawed). Nonetheless, accomplished examination of storage conditions of cell culture supernatant (Figure 16) warns against

work with outdated samples (older than 1 week, -80˚C). Keeping this in mind all presented experiments were carried out on fresh samples.

5.2 Application of whole cell-based biosensor in 2D environment

The created biosensor responds optimally to bioactive analytes, is characterized by fast response time, label-free experimentation and simple protocol. Therefore, developed HepG2-based biosensor is a useful tool to study the physiological effects of analytes. As (Figure 18) display NF-κB_HepG2 cells detect toxic effect of NP even after 2h of exposure time, NF-κB signaling belongs *to rapid acting*, therefore, NF-κB pathway seems to be perfect screening signaling of cytotoxicity in very early stage. This can be explained by NFκB-transcription factors, which are present in cytoplasm in an inactive form and do not require new protein synthesis in order to be activated. This allows NF-κB to be fast responder to harmful cellular stimuli. Whole cell-based biosensors measure bioavailable rather than total quantities of chemicals. Furthermore, in adopted inducible promoter; the reporter signal level increases with stressor concentration/ incubation time and after reach a maximum value signal decreases due to the toxic effect on the cell (damage of biosensor; Figure 37). The critical concentration value will depend on the degree of cellular resistance to the stimuli (for AgNP 15 μg/ml t=8 h; for SiO_2NP 500 μg/ml t=6 h and for ZnONP 80 μg/ml t=8 h in monolayer). Furthermore, selected threshold concentrations (for AgNP 3.75 μg/ml; for SiO_2NP 125 μg/ml and for ZnONP 20 μg/ml) are the lowest concentrations detectable in monolayer cell culture with developed system after t= 2h stimulation. Application of lower doses require longer incubation time to observe significant response of NFkB_HepG2 cells. Comparison of the data obtained from nanomaterials toxicity assessment applying sensor cells (Figure 18) and commercially available assay (Alamar Blue; Figure 8) display higher sensitivity of developed system. All commercial assays based on the reduction of tetrazolium salts differentiate cells into death and viable. Even in the terminal phase of the toxicity (late apoptosis) cells still are able reduce tetrazolium salts and are counted as a viable cells. This explain long incubation time of toxic compounds with this kind of assays. Therefore, NFκB_HepG2 cells seems to be attractive alternative for assessment toxicity of pro-inflammatory agents in early stage and short time.

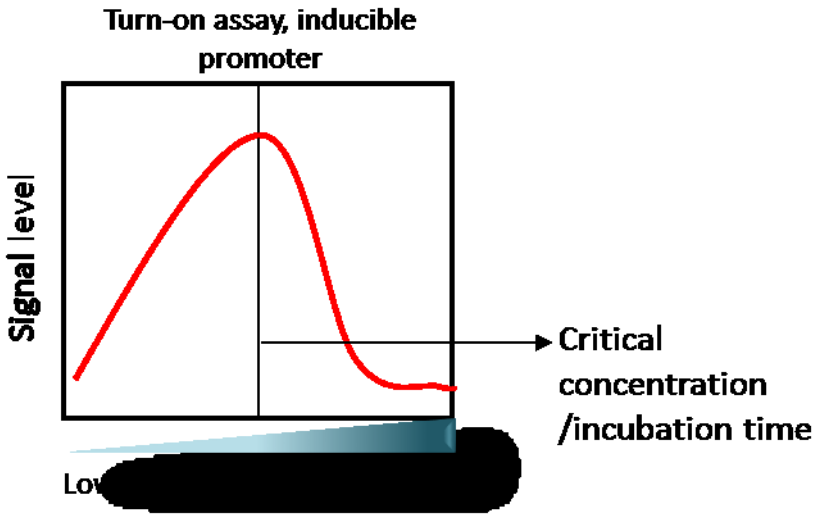

Figure 37. *Turn on* assays use inducible promoters; the reporter signal level increases with increasing concentration of analyte or incubation time. This reporter signal may reach a maximum value, after which decreases due to the toxic effect on the cell.

Measurements taken from mRNA and protein levels are complementary and both are indispensable for a complete comprehension of how the NFκB_hepG2 cell works. To quantify NF-κB activation by real-time PCR the expression of IκB-α mRNA was analyzed (according to explanation in chapter: ***2.2.5.1***) Maximum expression of ikB-α mRNA (Figure 19) was recorded after 2h stimulation with examined NP whereas, maximum abundance of reporter protein was noticed after 6h after stimulation for SiO_2NP and 8h for AgNP and ZnONP. Naturally, cells needs more time for translation and post-translations modification in compare to transcription what may explain shift in the observed time. Moreover, mRNA levels after 4 h stimulation with all kind analyzed NP decreased and reached a plateau what can be assumed to relatively short half-life time of the transcript and switching pro-inflammatory pathways into pro-apoptotic pathways what results in inhibition of expression reporter gene. Now, highly stressed cells direct the metabolism into death, instead of expressing redundant reporter protein. Additionally, it was observed the highest mRNA level after stimulation with ZnONP among tested nanomaterials what correspond as well to protein abundance after stimulation with this kind of nanoparticles.

Still challenging is the issue of establishing a nominal and effective dosimetry of nanoparticles in cytotoxicity assays. Teeguarden et al. [277] estimated that only a small fraction of nanoparticles in the lower part of the suspension would reach cells by sedimentation and predicted problems in determining the nominal dose of NP in *in vitro* experiments. Another hypothesis put forward by Lison et al. [278] states that the most of

NP will interfere with adherent cells and impose biological effects (because of convection forces). Furthermore, the pH, protein/electrolyte content and viscosity of cell culture medium firmly influence on the agglomeration process [279], [280] and may cause significant differences in the estimation of toxic doses. Considering the above mentioned aspects the state of agglomeration was verified by DLS measurements (Table 4). Size of ZnONP, AgNP and SiO_2NP examined by DLS was higher than this obtained from the supplier (based on TEM measurements). This is attributed to not only the intrinsic features of DLS analyses based on light scattering measurements but to the agglomeration of particles in the culture media as well. As a rule, image analysis based on the TEM micrographs gives the 'true radius' of the particles, and DLS assures the hydrodynamic radius on an ensemble mean, resulting in that the particle size observed using DLS is bigger than the actual single particle size [281]. According to obtained results ZnONP have a high susceptibility to agglomerate in cell culture media, such that the noticed toxic effect is provided not by single ZnONP but also by their agglomerates which may accomplish sizes of about 150 times larger than single nanoparticles. In contrast, AgNP and SiO_2NP do not have a substantial tendency to agglomerate in cell culture media. Dispersion and stability of tested nanoparticles are relevant in biological application. Therefore, nanoparticles were sonicated directly before toxicity assays to examine toxic effect of the NP agglomeration state. Results (Figure 7) showed higher cytotoxicity of sonicated NP. This observation may be explained that for cells is easier uptake smaller molecules, thus, noticed higher toxic effect. Sonication is commonly used to break up agglomerated NP which usually performed in a solvent. The size of dispersed agglomerates of NP depends on the suspension milieu such as volume of suspension solution, solvent type and concentration. In sonication, oscillation of liquid induce nucleation and collapse of solvent bubbles; bubble assembling and collapse at the surface of solids can be very efficient in chopping solids. In this technique, breaking the agglomerates is usually regulated by power, time and dispersion volume. However, sonication couldn't prevent long term agglomeration of nanoparticles [282], [283], [284]. Due to the extremely high surface-to-volume ratio of NP, nanomolecules have a very active surface chemistry in comparison to bulk biomaterials. Therefore, in biological applications, they aim to reduce their large surface energy by interacting with the medium components in which they are dispersed. Obtained results confirm that FBS which contains proteins can bind NP and reduce their toxic potential (Table 5). Significant lower cytotoxicity was observed when cells were cultivated in medium with 10% FBS.

According to this observation, it is recommended to perform all toxicity measurements under serum-deprived conditions (1 % FBS). To be able to compare the results between different experiments, the validation of an analytical procedures was necessary. In presented study were maintained always exactly the same experimental conditions. It means NP were always sonicated directly before experiments and cells were deprived FBS for toxicity assays. Furthermore, the optical properties of some NP may interfere with the endpoint measurement of absorbance in a biochemical assay. Possible interference effects (such as surface plasmon resonance and quantum confinement) that can initially from varying size, shape, surface modality, inter-particle interaction and composition make optical characterization of each NP species essential. Higher concentrations of NP have greater probability of interfering with assay function, and the use of high concentrations is not rare in toxicological research based on cells metabolic activity assays [233], [285]. Therefore, NP concentration should be limited in the final sample, this rise next advantage of developed in this study reporter assay, where in final step analyzed supernatant is centrifuged to get rid of NP unabsorbed by cells and toxicity of analyte may be analysed in lower concentration, since sensor NF-κB_hepG2 cells are characterized by greater detection limit than above mentioned cell-based assay.

5.3 Implementation of 3D cell culture as an environment for CBB

The presented methods of hydrogel preparation ensure successful, rapid and simple protocols for large-scale generation of spheroids with hepatocytes. Despite, primary hepatocytes taken directly from a living tissue are still recognized as the most dependable model in a toxicity tests, some reports show that immortal hepatocytes can recover liver-like functionality when cultivated in three dimensions [286], [287]. This assumption was verified in this study, showing that HepG2 cells achieved liver-like cell functionality in 3D environments as deduced from light-level production of albumin and urea by the HepG2 cells that was not observed with the same cells in conventional 2D culture (Figure 27). Interestingly, HepG2 cells growing in Matrigel 3D matrix were able to recover hepatocyte-typical activity as judged by the production of albumin and urea, but the cells required at least 7 days to recognize the 3D shape of their environment. It is to be expected that the 3D environment requires adaptation for individual cell lines, but it may be predicted that other cell lines, including cancer cells, may acquire *in situ*-like properties

not observed in conventional cell culture and thus provide ,more predictable and representative experimental results for *in vivo* cytotoxicity assessments. All presented hydrogels have three-dimensional geometry, are highly porous (Figure 23 and Figure 24) and allow to exchange medium, water-soluble waste, and gases. Additionally, they are based on the natural polymers that normally build the surroundings of cells in tissues *in vivo*. The highest proliferation activity of HepG2 cells was observed in Matrigel (Figure 25), which could be assigned to the surface properties of this material. Contact angle measurements showed that Matrigel provided the highest wettability of tested hydrogels (Table 6) that is in a good agreement with the literature and the observation that liver cells prefer to settle and proliferate on hydrophilic substrates [257]. Moreover, a high growth rate may be assigned to residual growth factors which are reduced but usually cannot be fully eliminated from Matrigel. Similarly, the highest diameter size of spheroids was observed when HepG2 cells were embedded in Matrigel (Figure 26). Nevertheless, high error bars indicate that cells form spheroids with various sizes. Even after the most accurate initial reagglomeration cells (by pipetting) and their mixing with the hydrogel, standardization of spheroids size was not fully solved. An interesting phenomenon is the issue of long-term plateau phase: spheroid stopped growing, but all the time (over 26 days observation) cells in the outer part were viable. High viability was confirmed by live/dead staining performed in 26 day of culture (Figure A. 5, appendix). This phenomenon is not common in classical culture system *in vitro*, where space limitations result in degeneration of the culture and its gradual dieback. However, the condition of maintaining a constant number of viable cells is a characteristic feature of the environment *in vivo* homeostasis. Homeostatic mechanisms are not fully understood in 3D cell culture. Nevertheless, the observation of growth arrest of the spheroids in hydrogels may be a result of signaling pathways that inhibit cell growth analogously to the *in vivo* situation. Based on the available results it is not possible to place bolder hypothesis, however, the developed system proved to be a good model for future studies of this phenomenon. Obtained results indicate that Matrigel is the most suitable environment for HepG2 cells in this study and obtained data emphasize the importance of proper selection of the three dimensional environment and demonstrates how slight distinctions in concentrations of natural polymers, sizes of pores, wettability, and morphological differences in the structure of hydrogels can make a difference in cell physiology, which is the basis for their use as sensor cells to generate suitable predictions of cytotoxicity of test compounds. In 2D culture, cells adhere and grow on a flat surface.

Monolayer framework allows all of the cultivated cells to obtain a homogenous amount of nutrients from the medium during growth. Since death cells are usually detached from the surfaces and easily removed during medium change therefore, the monolayer is mostly composed of viable cells. Cells grown in 2D culture are usually more flat and stretched than they would appear *in vivo*. When cells grown in 3D environment are in contact with matrix and other cells, so that the cell morphology closer resembles its natural shape in the body. Furthermore, spheroids are comprised of cells in different stages (including proliferating, semi sleeping - *quiescent*, necrotic, apoptotic and hypoxic cells). The outer layers of a spheroid represent proliferating cells, which are highly exposed to the medium. The core cells receive less oxygen, growth factors, and nutrients therefore tend to be in a semi sleeping- *quiescent* or in a hypoxic state. Described cellular heterogeneity is more similar to native tissues and because the morphology and the interactions of cells grown in 3D environment is more similar to what occurs *in vivo*, the cellular processes of these cells also closely emulate what is seen in native tissue.

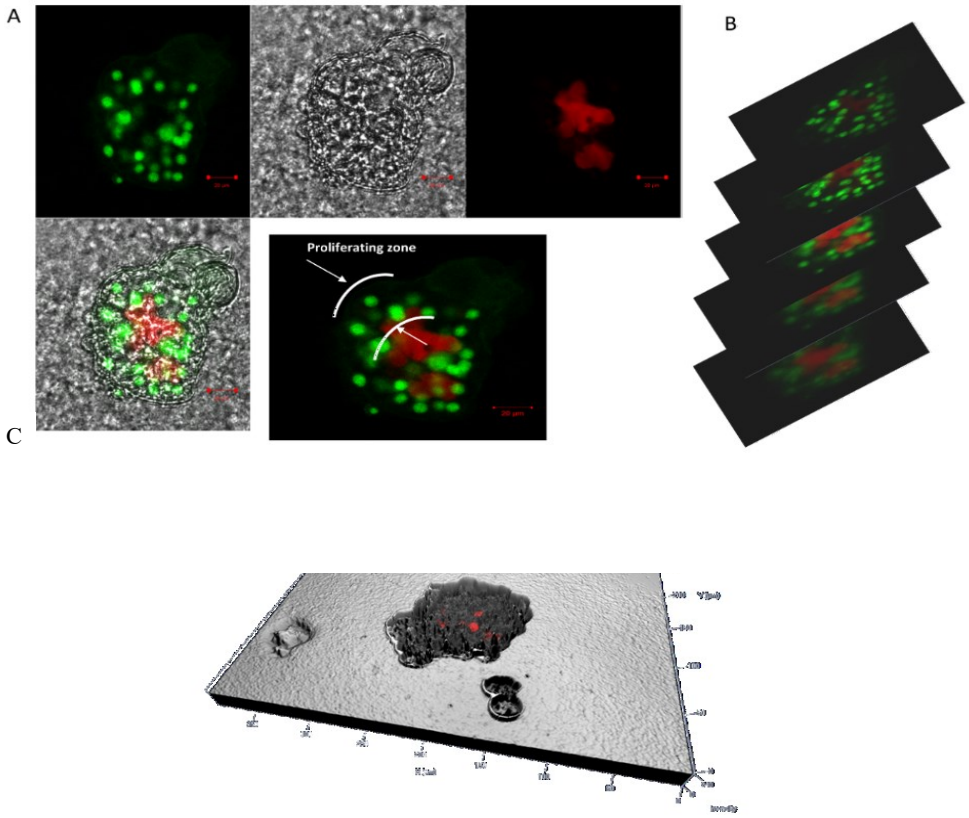

Figure 38. The structure of the 10 days old spheroid, (A) view of the individual channels of a multi-channel image; (B) recording images of spheroid at different focal planes of the entire sample volume. This "Z stacks" was generated by incrementally stepping through a sample using a focal drive, (spheroid stained with calcein AM (green, viable cells) and propidium iodide (red, dead cells)). Scale bar 20 μm. (C) 2.5D view of HepG2 cells with display of the two-dimensional intensity distribution of cells in a pseudo 3D mode.

Wrzesinski et al. [288] showed that cells are much more sensitive to toxins shortly after trypsinization. Typically a 4 days old 80% confluent cell culture is not the same as a 1 day old 80% confluent cell culture: cell will have metabolic activity and reactivity at different levels. On that account, all the presented toxicity assays were conducted after 8 days of cultivation cell in monolayer (~90% of confluence) and with 8 days old spheroids in 3D environments. Assessment of NP-induced cytotoxicity in 3D cell cultures shows lower toxic effects in comparison to the same exposure time and dose in monolayers (Figure 28). In the monolayer culture, cells are in contact with about 50% of their surface with a solution of NP, what results in high mortality of cells. Additionally, cells grown on flat surfaces possess an abnormal architecture and are typically under mechanical stress which results in lower tolerance to negative external environmental stimuli, whereas cells in 3D (representing their native shape) are less susceptible to environmental pressures. Moreover, the most straightforward explanation for increased resistance in 3D cultures to NP-mediated toxicity is that the cells inside the spheroids may be protected from NP penetration by the cells in the outer layer of the spheroid. In addition, the lower toxicity of NP in the 3D cultures may be due to the hindered diffusion through the hydrogels and therefore, decreased NP uptake and penetration into the inner layers of the spheroids [289]. Furthermore, after exposure spheroids to xenobiotics a most of well oxygenated external cells die. Subsequently, *quiescent* cells that become situated at the periphery of the spheroids have better access to nutrients. These *quiescent* cells thus return to the cell cycle and resume growth. Putting forward broader finding, spheroid heterogeneity it could be valuable model of tumors heterogenity and their response to anticancer drugs [290].

Another aspect worth mentioning concerns cell viability and the influence of the frequency of dosing with NP, what is usually ignored in the basic research. The entire system including time point of application should be considered to be a step closer to the natural conditions. Therefore, the dosage effect of nanoparticles on the dynamics of disintegration of spheroids was investigated (Figure 30). Here, two models of dispense dosage were applied: frequent dosage of small concentrations and less frequent dosage of higher concentrations. The first regime turned out to be more toxic, indicating that the influence of NP dosing on their toxicity can be determined even at the level of *in vitro* studies in 3D models. Moreover, microscopic observation of decreasing spheroid dimensions is low-cost, easy to conduct and is suitable for long-term observation of

exactly the same spheroids as opposed to other viability assays requiring termination of a cell culture. Complexity of cell culture model determines toxic effect of xenobiotics. To be able transfer results from *in vitro* to *in vivo* level many aspects should be considered like mentioned dosage effect, long time exposure, therefore possible cytotoxicity of metabolites of analyzed compounds. Nevertheless, cells surrounding, have prominent influence on their resistance and functionality in general.

5.4 Application of whole cell based biosensor in 3D environment

Because, Matrigel proved to be the most proper environment for HepG2 cells, therefore, Matrigel was implemented as a 3D milieu for sensor cells to improve predictive value of cytotoxicity assays. Comparison of the dose and time depended detection of the nanomaterials toxicity between sensor cells in 2D and 3D environment showed higher precision of NF-κB_HepG2 cells in Matrigel. Demonstrated data on Figure 31 indicate lower standard deviation compared to exactly the same experiment performed using monolayer cell culture (Figure 18). As expected relative response of sensor cells in 3D environment was lower compared to monolayer cell culture. This may be explained by higher resistance to nanomaterials of cells in 3D environment. Since, cells in native tissue create multilayer structures with hindered diffusion of chemicals and uneven exposure of cells to external stimuli, developed 3D system seems mimic native tissue more closely. Moreover, Figure 32 demonstrates successful application NFκB_HepG2 cells in basic screening of nanomaterials with different sizes and chemical composition. Moreover, sensor cells exhibit detection of NP toxicity at lower concentration and shorter incubation time compared to commercially available assays based on metabolism activity of cells. There are many efforts in understanding the effects of various nanoparticles on cell viability and metabolism, however, not much is known regarding the distinct molecular mechanisms of inflammation and cellular stress using low exposure concentrations. Therefore, developed NF-κB_HepG2 cells address perfectly this gap in the literature. Developed biosensor may be used in a basic screening of all components which activate NF-κB pathway and since, heavy metals are inducers of pro-inflammatory pathways [291], [292]. Therefore, to verify this concept NF-κB_HepG2 cells were stimulated with $NiSO_4$ and $CdCl_2$. Data shown on Figure 33 and Figure 34 dose-depended response of sensor cells and similarly, like in the case of nanomaterials, high concentration of heavy

metals provide decrease in signal due to their damage. Created biosensor can be applied in basic screening without the exact analysis of the interaction mechanism between NP and living systems. Nonetheless, already application of NF-κB_HepG2 cells gives information whether the analyzed analyte is characterized by pro-inflammatory action. Taking into account the use of described system in technology, NF-κB_HepG2 cells may be an advance screening system with simple procedure for companies which produce nanomaterials for accessing the risks posed by chemicals and providing proper safety information to their users.

Nevertheless, CBB have some feature that might limit their application. Unlike to nucleic acid- or antibody-based methods, CBBs are unsuitable for the identification of the analyte. Activation of cell signaling pathways or cell death may be the results of exposure to multiple stimuli. Therefore, cell-based biosensors may give rather an answer if analyte is toxic in physiological range to the cells than what kind of components contain examined sample. Undoubtedly interaction of chemicals with living cells are complex and involved many intracellular pathways. Until now CBB which are specific to exactly one type of analyte were not described. Therefore, to improve specificity of cell-based biosensor, reporter expression should be regulated by multiple response elements or bioengineered cells should express artificial receptor which is selective to particular analyte and linked with intracellular signaling cascade.

6 SUMMARY

The emergence of human-based models is incontestably required for the study of complex physiological pathways and validation of reliable *in vitro* methods as alternative for *in vivo* studies in experimental animals for toxicity assessment. With this objective, three dimensional environments for human cells were developed and tested using three different types of hydrogels including transglutaminase-crosslinked gelatin, collagen type I and growth-factor depleted Matrigel. Cells grown in Matrigel exhibited the greatest cell proliferation and spheroid diameter. Moreover, urea and albumin analysis indicated that the created system allows the immortalized liver cell line (HepG2) to re-establish normal hepatocyte-like properties which are not observed under the conditions of conventional cell cultures. This study presents a reproducible technology for production of complex-shaped liver multicellular spheroids as a system which improves the predictive value of cell-based assays for safety and risk assessment. The time- and dose-dependent toxicity of nanoparticles demonstrates higher cytotoxic effects when HepG2 cells grown as monolayer than embedded in hydrogels. The experimental setup provided evidence that cell environment has significant influence on cell sensitivity and that liver spheroids are useful and novel tools to examine NP dosing effect even at the level of *in vitro* studies.

Moreover, the created cell-based biosensor responds optimally to bioactive analytes, has a fast response time, offers label-free experimentation and simple procedures. Besides, the developed NF-κB_HepG2 cells enable detect cytotoxicity of variety nanoparticles with different chemical composition, size, tendency of agglomeration or cytotoxic potential and other stimuli which activate NF-κB signaling (e.g. heavy metals), in very early stage, before cell death, in short time even after 2 h time exposure as opposed to widely used commercially available cell-based assays like MTT, XTT Alamar Blue or LDH. Successful modification of HepG2 cells resulted in generation of novel NF-κB_HepG2 sensor cells with extracellular reporter protein (human secreted alkaline phosphatase) and its application in cytotoxicity of nanomaterials detection has not been investigated before. The developed NF-κB_hepG2 cells may also provide a useful tool to study distinct molecular mechanisms of inflammation and cellular stress using low exposure concentrations of cell irritants. The presented sensor based on human cells in three dimensional milieu provides a novel application for nanoparticles screening that joins the complex *in vitro* model imitating living tissue with high throughput analytical

methods. This system can be applied to a wide diversity of potentially hostile compounds in basic screening to provide initial warning of adverse effects and trigger subsequent analysis and remedial actions.

7 ZUSAMMENFASSUNG

Die Entwicklung von Zellmodellen basierend auf humanen Zellen ist eine unbestrittene Voraussetzung zur Untersuchung komplexer physiologischer Stoffwechselwege und die Validierung zuverlässiger *in vitro* Methoden als Alternative zu *in vivo* Studien im experimentellen Tierversuch zur Toxizitätsbeurteilung. Mit diesem Ziel wurden dreidimensionale Umgebungsstrukturen unter Verwendung drei verschiedener Typen von Hydrogelen, darunter Transglutaminase-vernetzte Gelatine, Collagen Typ I und Wachstumsfaktor-freies Matrigel, für humane Zellen entwickelt und getestet. Die in Matrigel kultivierten Zellen zeigten die größten Proliferationsraten und Spheroid-Durchmesser. Darüber hinaus deuten die Harnstoff- und Albumin-Analyse darauf hin, dass das entwickelte System der immortalisierten Leberzelllinie (HepG2) das Wiederherstellen normaler Hepatozyten-ähnlicher Eigenschaften, die nicht unter den Bedingungen der konventionellen Zellkultur auftreten, ermöglicht. Diese Arbeit präsentiert eine reproduzierbare Technologie zur Herstellung komplex geformter multizellulärer Leberzell-Spheroide als ein System zur Verbesserung des Vorhersagewertes von zellbasierten Assays zur Sicherheits- und Risikobeurteilung. Die zeit- und dosisabhängige Toxizität von Nanopartikeln demonstriert bei Wachstum der HepG2 Zellen als Monolayer höhere zytotoxische Effekte als beim Einbetten der Zellen in Hydrogele. Der experimentelle Aufbau bewies, dass das Umgebungsmilieu einen signifikanten Einfluss auf die Sensitivität der Zellen hat und Leberzell-Spheroide ein nützliches und neues Werkzeug zur Untersuchung von dosisabhängigen Effekten von Nanopartikeln selbst im Dosisbereich der *in vitro* Studien darstellen.

Darüber hinaus reagiert der entwickelte zellbasierte Biosensor optimal auf bioaktive Analyte, zeichnet sich durch eine schnelle Ansprechzeit aus und bietet eine markierungsfreie und einfache experimentelle Prozedur. Zudem ermöglichen die entwickelten NF-κB_HepG2 Zellen die Detektion der Zytotoxizität einer Vielzahl von Nanopartikeln mit unterschiedlicher chemischer Zusammensetzung, Größe, Tendenz zur Agglomeration oder zytotoxischen Potential und anderen Stimuli, die den NF-κB Signalweg in einem sehr frühen Stadium vor dem Zelltod auslösen (z.B. Schwermetalle). Im Gegensatz zu weit verbreiteten kommerziellen zellbasierten Assays wie dem MTT-, XTT-, Alamar Blue oder LDH-Test erfolgt die Detektion in sehr kurzer Zeit bereits nach zwei Stunden. Die entwickelten NF-κB_HepG2 Zellen könnten ein nützliches Werkzeug

zur Untersuchung bestimmter molekularer Mechanismen der Entzündungsreaktion und des zellulären Stresses unter Verwendung geringer Konzentrationen der reizenden Substanzen darstellen. Der auf humanen Zellen in einem dreidimensionalen Milieu basierende präsentierte Sensor liefert eine neue Applikation zum Nanopartikel-Screening, die ein komplexes, lebendes Gewebe imitierendes *in vitro* Modell mit Hochdurchsatz-Analytikmethoden verbindet. Dieses System kann für die grundlegende Überprüfung vieler potentiell gefährlicher Substanzen verwendet werden, um frühe Hinweise auf schädliche Effekte zu geben und weiterführende Analysen und Gegenmaßnahmen zu veranlassen.

8 REFERENCES

1. McNaught, A.D., et al., *Compendium of chemical terminology IUPAC recommendations*. 2006, International Union of Pure and Applied Chemistry: Oxford.
2. Chambers, J.P., et al., *Biosensor recognition elements.* Curr Issues Mol Biol, 2008. **10**(1467-3037 (Print)).
3. Thevenot, D., et al., *Electrochemical biosensors: recommended definitions and classification.* Biosensors \& Bioelectronics, 2001. **16**: p. 121-131.
4. Pearson, J.E., A. Gill, and P. Vadgama, *Analytical aspects of biosensors.* Ann Clin Biochem, 2000. **37 (Pt 2)**: p. 119-45.
5. Wang, B. and M. Buck, *Customizing cell signaling using engineered genetic logic circuits.* Trends Microbiol, 2012. **20**(8): p. 376-84.
6. Bradley, R.W. and B. Wang, *Designer cell signal processing circuits for biotechnology.* N Biotechnol, 2015.
7. Brophy, J.A.N. and C.A. Voigt, *Principles of genetic circuit design.* Nat Meth, 2014. **11**(5): p. 508-520.
8. Morris, M.K., et al., *Logic-based models for the analysis of cell signaling networks.* Biochemistry, 2010. **49**(15): p. 3216-24.
9. Taniguchi, A., *Live cell-based sensor cells.* Biomaterials, 2010. **31**(23): p. 5911-5915.
10. Stenger, D.A., et al., *Detection of physiologically active compounds using cell-based biosensors.* Trends in Biotechnology, 2001. **19**(8): p. 304-309.
11. Finkbeiner, S., M. Frumkin, and Paul D. Kassner, *Cell-Based Screening: Extracting Meaning from Complex Data.* Neuron, 2015. **86**(1): p. 160-174.
12. Bulich AA, I.D., *Use of the luminescent bacterial system for the rapid assessment of aquatic toxicity.* ISA Trans., 1981. **20**(1): p. 29-33.
13. Vopálenská, I., L. Váchová, and Z. Palková, *New biosensor for detection of copper ions in water based on immobilized genetically modified yeast cells.* Biosensors and Bioelectronics, 2015. **72**: p. 160-167.
14. Chouteau, C., et al., *Development of novel conductometric biosensors based on immobilised whole cell Chlorella vulgaris microalgae.* Biosensors and Bioelectronics, 2004. **19**(9): p. 1089-1096.
15. Chouteau, C., et al., *A bi-enzymatic whole cell conductometric biosensor for heavy metal ions and pesticides detection in water samples.* Biosensors and Bioelectronics, 2005. **21**(2): p. 273-281.
16. Shing, W.L., L.Y. Heng, and S. Surif, *Performance of a cyanobacteria whole cell-based fluorescence biosensor for heavy metal and pesticide detection.* Sensors (Basel), 2013. **13**(5): p. 6394-404.
17. Singh, J. and S.K. Mittal, *Chlorella sp. based biosensor for selective determination of mercury in presence of silver ions.* Sensors and Actuators B: Chemical, 2012. **165**(1): p. 48-52.
18. Banerjee, P. and A.K. Bhunia, *Mammalian cell-based biosensors for pathogens and toxins.* Trends Biotechnol, 2009. **27**(3): p. 179-88.
19. Liu, F., et al., *A lab-on-chip cell-based biosensor for label-free sensing of water toxicants.* Lab on a Chip, 2014. **14**(7): p. 1270-1280.

20. Wang, T.-H., G.-H. Hui, and S.-P. Deng, *A novel sweet taste cell-based sensor.* Biosensors and Bioelectronics, 2010. **26**(2): p. 929-934.
21. Xing, J.Z., et al., *Microelectronic cell sensor assay for detection of cytotoxicity and prediction of acute toxicity.* Toxicology in Vitro, 2006. **20**(6): p. 995-1004.
22. Hofmann, U., et al., *A sensitive sensor cell line for the detection of oxidative stress responses in cultured human keratinocytes.* Sensors (Basel), 2014. **14**(7): p. 11293-307.
23. Chen, P., *Detection of DNA Damage Response Caused by Different Forms of Titanium Dioxide Nanoparticles using Sensor Cells.* Journal of Biosensors & Bioelectronics, 2012. **03**(05).
24. Hofmann, U., et al., *A whole-cell biosensor as in vitro alternative to skin irritation tests.* Biosens Bioelectron, 2013. **39**(1): p. 156-62.
25. Banerjee, P., et al., *A novel and simple cell-based detection system with a collagen-encapsulated B-lymphocyte cell line as a biosensor for rapid detection of pathogens and toxins.* Lab Invest, 2007. **88**(2): p. 196-206.
26. Bouaziz, C., et al., *The in vitro effects of zearalenone and T-2 toxins on Vero cells.* Exp Toxicol Pathol, 2013. **65**(5): p. 497-501.
27. Corbisier, P., et al., *Whole cell- and protein-based biosensors for the detection of bioavailable heavy metals in environmental samples.* Analytica Chimica Acta, 1999. **387**(3): p. 235-244.
28. May, K.M.L., et al., *Development of a Whole-Cell-Based Biosensor for Detecting Histamine as a Model Toxin.* Analytical Chemistry, 2004. **76**(14): p. 4156-4161.
29. Xu, G., et al., *Cell-based biosensors based on light-addressable potentiometric sensors for single cell monitoring.* Biosensors and Bioelectronics, 2005. **20**(9): p. 1757-1763.
30. McElwee, M.K., M.O. Song, and J.H. Freedman, *Copper activation of NF-kappaB signaling in HepG2 cells.* J Mol Biol, 2009. **393**(5): p. 1013-21.
31. Védrine, C., et al., *Optical whole-cell biosensor using Chlorella vulgaris designed for monitoring herbicides.* Biosensors and Bioelectronics, 2003. **18**(4): p. 457-463.
32. Aruoja, V., et al., *Toxicity of nanoparticles of CuO, ZnO and TiO2 to microalgae Pseudokirchneriella subcapitata.* Science of The Total Environment, 2009. **407**(4): p. 1461-1468.
33. Chen, P., et al., *Development of sensor cells using NF-kappaB pathway activation for detection of nanoparticle-induced inflammation.* Sensors (Basel), 2011. **11**(7): p. 7219-30.
34. Lewis, J.C., et al., *Peer Reviewed: Applications of Reporter Genes.* Analytical Chemistry, 1998. **70**(17): p. 579A-585A.
35. Munsky, B., G. Neuert, and A. van Oudenaarden, *Using gene expression noise to understand gene regulation.* Science, 2012. **336**(6078): p. 183-7.
36. Gu, M.B., R.J. Mitchell, and B.C. Kim, *Whole-cell-based biosensors for environmental biomonitoring and application.* Adv Biochem Eng Biotechnol, 2004. **87**: p. 269-305.
37. Belkin, S., *Microbial whole-cell sensing systems of environmental pollutants.* Current Opinion in Microbiology, 2003. **6**(3): p. 206-212.
38. Ahmed, A., et al., *Biosensors for whole-cell bacterial detection.* Clin Microbiol Rev, 2014. **27**(3): p. 631-46.

39. Gutierrez, J.-C., F. Amaro, and A. Martin-Gonzalez, *Heavy metal whole-cell biosensors using eukaryotic microorganisms: an updated critical review*. Frontiers in Microbiology, 2015. **6**.
40. Sorensen, S.J., M. Burmolle, and L.H. Hansen, *Making bio-sense of toxicity: new developments in whole-cell biosensors*. Curr Opin Biotechnol, 2006. **17**(1): p. 11-6.
41. Luckow, B. and G. Schütz, *CAT constructions with multiple unique restriction sites for the functional analysis of eukaryotic promoters and regulatory elements*. Nucleic Acids Research, 1987. **15**(13): p. 5490.
42. Pobjecky, N., et al., *Expression of the ß-glucuronidase gene under the control of the CaMV 35S promoter in Schizosaccharomyces pombe*. Molecular and General Genetics MGG, 1990. **220**(2): p. 314-316.
43. Bennett, M., J. Shern, and R. Kahn, *Reverse Two-Hybrid Techniques in the Yeast Saccharomyces cerevisiae*, in *Protein-Protein Interactions*, C.L. Meyerkord and H. Fu, Editors. 2015, Springer New York. p. 433-446.
44. Fang, Z., et al., *A novel HAC1-based dual-luciferase reporter vector for detecting endoplasmic reticulum stress and unfolded protein response in yeast Saccharomyces cerevisiae*. Plasmid, 2015. **79**: p. 48-53.
45. Vriend, L.E.M., M. Jasin, and P.M. Krawczyk, *Assaying break and nick-induced homologous recombination in mammalian cells using the DR-GFP reporter and Cas9 nucleases*. Methods in enzymology, 2014. **546**: p. 175-191.
46. Soboleski, M.R., J. Oaks, and W.P. Halford, *Green fluorescent protein is a quantitative reporter of gene expression in individual eukaryotic cells*. The FASEB Journal, 2005. **19**(3): p. 440-442.
47. Berger, J., et al., *Secreted placental alkaline phosphatase: a powerful new quantitative indicator of gene expression in eukaryotic cells*. Gene, 1988. **66**(1): p. 1-10.
48. Millan, J.L., *Molecular cloning and sequence analysis of human placental alkaline phosphatase*. 1986(0021-9258 (Print)).
49. Nakashima, K., et al., *Production of human secreted alkaline phosphatase in suspension and immobilization cultures of tobacco NT1 cell*. Biochemical Engineering Journal, 2013. **77**: p. 177-182.
50. B.R. Cullen, M.H.M., *Secreted Placental Alkaline Phosphatase as a Eukaryotic Reporter Gene*. Methods Enzymology, 1992. **216**: p. 362-368.
51. Serrvice, R.F., *Nanotechnology Grows Up*. Science 2004. **304**: p. 1732-1734.
52. Hoyt, V.W. and E. Mason, *Nanotechnology: Emerging health issues*. Journal of Chemical Health and Safety, 2008. **15**(2): p. 10-15.
53. McEuen, P.L., *Nanotechnology: Carbon-based electronics*. Nature, 1998. **393**(6680): p. 15-17.
54. Pardeike, J., A. Hommoss, and R.H. Müller, *Lipid nanoparticles (SLN, NLC) in cosmetic and pharmaceutical dermal products*. International Journal of Pharmaceutics, 2009. **366**(1–2): p. 170-184.
55. Zhou, H., et al., *Robust, Self-Healing Superamphiphobic Fabrics Prepared by Two-Step Coating of Fluoro-Containing Polymer, Fluoroalkyl Silane, and Modified Silica Nanoparticles*. Advanced Functional Materials, 2013. **23**(13): p. 1664-1670.

56. Melo, M.A.S., et al., *Novel dental adhesives containing nanoparticles of silver and amorphous calcium phosphate*. Dental Materials, 2013. **29**(2): p. 199-210.
57. Capolla, S., et al., *Targeted tumor imaging of anti-CD20-polymeric nanoparticles developed for the diagnosis of B-cell malignancies*. International Journal of Nanomedicine, 2015. **10**: p. 4099-4109.
58. Weiss, R., *For science, nanotech poses big unknowns*. Washington Post, 2004. **A01**.
59. Kim, S., et al., *Oxidative stress-dependent toxicity of silver nanoparticles in human hepatoma cells*. Toxicology in Vitro, 2009. **23**(6): p. 1076-1084.
60. Park, M.V.D.Z., et al., *The effect of particle size on the cytotoxicity, inflammation, developmental toxicity and genotoxicity of silver nanoparticles*. Biomaterials, 2011. **32**(36): p. 9810-9817.
61. Liu, W., et al., *Impact of silver nanoparticles on human cells: Effect of particle size*. Nanotoxicology, 2010. **4**(3): p. 319-330.
62. Sharma, V., et al., *DNA damaging potential of zinc oxide nanoparticles in human epidermal cells*. Toxicology Letters, 2009. **185**(3): p. 211-218.
63. Sharma, V., D. Anderson, and A. Dhawan, *Zinc oxide nanoparticles induce oxidative DNA damage and ROS-triggered mitochondria mediated apoptosis in human liver cells (HepG2)*. Apoptosis, 2012. **17**(8): p. 852-870.
64. Heng, B.C., et al., *Toxicity of zinc oxide (ZnO) nanoparticles on human bronchial epithelial cells (BEAS-2B) is accentuated by oxidative stress*. Food and Chemical Toxicology, 2010. **48**(6): p. 1762-1766.
65. Schaeublin, N.M., et al., *Surface charge of gold nanoparticles mediates mechanism of toxicity*. Nanoscale, 2011. **3**(2): p. 410-20.
66. Punnoose, A., et al., *Cytotoxicity of ZnO Nanoparticles Can Be Tailored by Modifying Their Surface Structure: A Green Chemistry Approach for Safer Nanomaterials*. ACS Sustainable Chemistry & Engineering, 2014. **2**(7): p. 1666-1673.
67. Huk, A., et al., *Impact of nanosilver on various DNA lesions and HPRT gene mutations - effects of charge and surface coating*. Particle and Fibre Toxicology, 2015. **12**(1): p. 25.
68. Albanese, A., P.S. Tang, and W.C.W. Chan, *The Effect of Nanoparticle Size, Shape, and Surface Chemistry on Biological Systems*. Annual Review of Biomedical Engineering, 2012. **14**(1): p. 1-16.
69. Gualtieri, M., et al., *Importance of agglomeration state and exposure conditions for uptake and pro-inflammatory responses to amorphous silica nanoparticles in bronchial epithelial cells*. Nanotoxicology, 2011. **6**(7): p. 700-712.
70. Magdolenova, Z., et al., *Impact of agglomeration and different dispersions of titanium dioxide nanoparticles on the human related in vitro cytotoxicity and genotoxicity*. J Environ Monit, 2012. **14**(2): p. 455-64.
71. Orlando, A., et al., *Iron oxide nanoparticles surface coating and cell uptake affect biocompatibility and inflammatory responses of endothelial cells and macrophages*. Journal of Nanoparticle Research, 2015. **17**(9): p. 1-13.

72. Wang, X., et al., *Use of Coated Silver Nanoparticles to Understand the Relationship of Particle Dissolution and Bioavailability to Cell and Lung Toxicological Potential.* Small, 2014. **10**(2): p. 385-398.
73. Yah, C.S., G.S. Simate, and S.E. Iyuke, *Nanoparticles toxicity and their routes of exposures.* Pak J Pharm Sci, 2012. **25**(2): p. 477-91.
74. Wang, Z. and A.B. Malik, *Nanoparticles squeezing across the blood-endothelial barrier via caveolae.* Therapeutic delivery, 2013. **4**(2): p. 131-133.
75. Fullstone, G., et al., *Modelling the Transport of Nanoparticles under Blood Flow using an Agent-based Approach.* Sci. Rep., 2015. **5**.
76. Bouwstra, J.A. and P.L. Honeywell-Nguyen, *Skin structure and mode of action of vesicles.* Advanced Drug Delivery Reviews, 2002. **54, Supplement**: p. S41-S55.
77. Yacobi, N.R., et al., *Mechanisms of Alveolar Epithelial Translocation of a Defined Population of Nanoparticles.* American Journal of Respiratory Cell and Molecular Biology, 2010. **42**(5): p. 604-614.
78. Yang, W., J.I. Peters, and R.O. Williams Iii, *Inhaled nanoparticles—A current review.* International Journal of Pharmaceutics, 2008. **356**(1–2): p. 239-247.
79. Videira, M.A., et al., *Lymphatic Uptake of Pulmonary Delivered Radiolabelled Solid Lipid Nanoparticles.* Journal of Drug Targeting, 2002. **10**(8): p. 607-613.
80. Maisel, K., et al., *Effect of surface chemistry on nanoparticle interaction with gastrointestinal mucus and distribution in the gastrointestinal tract following oral and rectal administration in the mouse.* Journal of Controlled Release, 2015. **197**: p. 48-57.
81. De Jong, W.H., et al., *Particle size-dependent organ distribution of gold nanoparticles after intravenous administration.* Biomaterials, 2008. **29**(12): p. 1912-9.
82. Dobrovolskaia, M.A., D.R. Germolec, and J.L. Weaver, *Evaluation of nanoparticle immunotoxicity.* Nat Nano, 2009. **4**(7): p. 411-414.
83. Elsabahy, M. and K.L. Wooley, *Cytokines as biomarkers of nanoparticle immunotoxicity.* Chemical Society Reviews, 2013. **42**(12): p. 5552-5576.
84. Peer, D., *Immunotoxicity derived from manipulating leukocytes with lipid-based nanoparticles.* Advanced Drug Delivery Reviews, 2012. **64**(15): p. 1738-1748.
85. Solarska, K., et al., *Effect of nanodiamond powders on the viability and production of reactive oxygen and nitrogen species by human endothelial cells.* Diamond and Related Materials, 2012. **21**: p. 107-113.
86. van Meer, G., D.R. Voelker, and G.W. Feigenson, *Membrane lipids: where they are and how they behave.* Nat Rev Mol Cell Biol, 2008. **9**(2): p. 112-124.
87. Kenneth A. Dawson, A.S., Iseult Lynch, *Nanoparticles reconstruct lipids.* Nature Nanotechnology, 2009. **4**.
88. Shang, L., K. Nienhaus, and G.U. Nienhaus, *Engineered nanoparticles interacting with cells: size matters.* J Nanobiotechnology, 2014. **12**: p. 5.
89. Stark, W.J., *Nanoparticles in Biological Systems.* Angewandte Chemie International Edition, 2011. **50**(6): p. 1242-1258.

90. Gou, N., A. Onnis-Hayden, and A.Z. Gu, *Mechanistic toxicity assessment of nanomaterials by whole-cell-array stress genes expression analysis.* Environ Sci Technol, 2010. **44**(15): p. 5964-70.
91. Pan, Y., et al., *Gold nanoparticles of diameter 1.4 nm trigger necrosis by oxidative stress and mitochondrial damage.* Small, 2009. **5**(18): p. 2067-76.
92. Park, E.-J., et al., *Magnetic iron oxide nanoparticles induce autophagy preceding apoptosis through mitochondrial damage and ER stress in RAW264.7 cells.* Toxicology in Vitro, 2014. **28**(8): p. 1402-1412.
93. Huerta-García, E., et al., *Titanium dioxide nanoparticles induce strong oxidative stress and mitochondrial damage in glial cells.* Free Radical Biology and Medicine, 2014. **73**: p. 84-94.
94. Wang, F., et al., *Time resolved study of cell death mechanisms induced by amine-modified polystyrene nanoparticles.* Nanoscale, 2013. **5**(22): p. 10868-10876.
95. Frohlich, E., et al., *Action of polystyrene nanoparticles of different sizes on lysosomal function and integrity.* Part Fibre Toxicol, 2012. **9**: p. 26.
96. Dam, D.H.M., et al., *Direct Observation of Nanoparticle–Cancer Cell Nucleus Interactions.* ACS Nano, 2012. **6**(4): p. 3318-3326.
97. Chen, M. and A. von Mikecz, *Formation of nucleoplasmic protein aggregates impairs nuclear function in response to SiO2 nanoparticles.* Experimental Cell Research, 2005. **305**(1): p. 51-62.
98. Conroy, J., et al., *CdTe nanoparticles display tropism to core histones and histone-rich cell organelles.* Small, 2008. **4**(11): p. 2006-15.
99. Asharani, P., et al., *Differential regulation of intracellular factors mediating cell cycle, DNA repair and inflammation following exposure to silver nanoparticles in human cells.* Genome Integr, 2012. **3**(1): p. 2.
100. Singh, N., et al., *NanoGenotoxicology: The DNA damaging potential of engineered nanomaterials.* Biomaterials, 2009. **30**(23–24): p. 3891-3914.
101. Balansky, R., et al., *Transplacental clastogenic and epigenetic effects of gold nanoparticles in mice.* Mutation Research/Fundamental and Molecular Mechanisms of Mutagenesis, 2013. **751–752**: p. 42-48.
102. Choi, A.O., et al., *Quantum dot-induced epigenetic and genotoxic changes in human breast cancer cells.* J Mol Med (Berl), 2008. **86**(3): p. 291-302.
103. Gong, C., et al., *SiO2 nanoparticles induce global genomic hypomethylation in HaCaT cells.* Biochemical and Biophysical Research Communications, 2010. **397**(3): p. 397-400.
104. Stoccoro, A., et al., *Epigenetic effects of nano-sized materials.* Toxicology, 2013. **313**(1): p. 3-14.
105. Lynch, I., A. Salvati, and K.A. Dawson, *Protein-nanoparticle interactions: What does the cell see?* Nat Nano, 2009. **4**(9): p. 546-547.
106. Sniadecki, N.J., *Minireview: A Tiny Touch: Activation of Cell Signaling Pathways with Magnetic Nanoparticles.* Endocrinology, 2010. **151**(2): p. 451-457.
107. Eom, H.-J. and J. Choi, *p38 MAPK Activation, DNA Damage, Cell Cycle Arrest and Apoptosis As Mechanisms of Toxicity of Silver Nanoparticles in Jurkat T Cells.* Environmental Science & Technology, 2010. **44**(21): p. 8337-8342.

108. Hyun-Jeong Eom, J.C., *Oxidative stress of CeO2 nanoparticles via p38-Nrf-2 signaling pathway in human bronchial epithelial cell, Beas-2B.* Toxicology Letters, 2009. **187**(2): p. 77-83.
109. King, K.R., et al., *A high-throughput microfluidic real-time gene expression living cell array.* Lab on a Chip, 2007. **7**(1): p. 77-85.
110. Prasad, R.Y., et al., *Investigating oxidative stress and inflammatory responses elicited by silver nanoparticles using high-throughput reporter genes in HepG2 cells: Effect of size, surface coating, and intracellular uptake.* Toxicology in Vitro, 2013. **27**(6): p. 2013-2021.
111. Stepkowski, T.M., K. Brzoska, and M. Kruszewski, *Silver nanoparticles induced changes in the expression of NF-kappaB related genes are cell type specific and related to the basal activity of NF-kappaB.* Toxicol In Vitro, 2014. **28**(4): p. 473-8.
112. Chen, J., et al., *Inflammatory MAPK and NF-κB signaling pathways differentiated hepatitis potential of two agglomerated titanium dioxide particles.* Journal of Hazardous Materials, 2016. **304**: p. 370-378.
113. Oeckinghaus, A. and S. Ghosh, *The NF-kappaB family of transcription factors and its regulation.* Cold Spring Harb Perspect Biol, 2009. **1**(4): p. a000034.
114. Ghosh, S. and M.S. Hayden, *Celebrating 25 years of NF-κB research.* Immunological Reviews, 2012. **246**(1): p. 5-13.
115. Hayden, M.S. and S. Ghosh, *NF-kappaB, the first quarter-century: remarkable progress and outstanding questions.* Genes Dev, 2012. **26**(3): p. 203-34.
116. Karin, M. and A. Lin, *NF-kappaB at the crossroads of life and death.* Nat Immunol, 2002. **3**(3): p. 221-7.
117. Bottero, V., et al., *Monitoring NF-kappa B transactivation potential via real-time PCR quantification of I kappa B-alpha gene expression.* Mol Diagn, 2003. **7**(3-4): p. 187-94.
118. Bonizzi, G. and M. Karin, *The two NF-κB activation pathways and their role in innate and adaptive immunity.* Trends in Immunology, 2004. **25**(6): p. 280-288.
119. Hayden, M.S. and S. Ghosh, *Shared principles in NF-kappaB signaling.* Cell, 2008. **132**(3): p. 344-62.
120. Joris, F., et al., *Assessing nanoparticle toxicity in cell-based assays: influence of cell culture parameters and optimized models for bridging the in vitro-in vivo gap.* Chemical Society Reviews, 2013. **42**(21): p. 8339-8359.
121. Schrurs, F. and D. Lison, *Focusing the research efforts.* Nat Nano, 2012. **7**(9): p. 546-548.
122. Poland, C.A., et al., *The elephant in the room: reproducibility in toxicology.* Part Fibre Toxicol, 2014. **11**: p. 42.
123. Marquis, B.J., et al., *Analytical methods to assess nanoparticle toxicity.* Analyst, 2009. **134**(3): p. 425-39.
124. Alivisatos, A.P., W. Gu, and C. Larabell, *Quantum dots as cellular probes.* Annu Rev Biomed Eng, 2005. **7**: p. 55-76.
125. Arora, S., et al., *Interactions of silver nanoparticles with primary mouse fibroblasts and liver cells.* Toxicol Appl Pharmacol, 2009. **236**(3): p. 310-8.

126. Theumer, A., et al., *Superparamagnetic iron oxide nanoparticles exert different cytotoxic effects on cells grown in monolayer cell culture versus as multicellular spheroids.* Journal of Magnetism and Magnetic Materials, 2015. **380**: p. 27-33.
127. Sung Ju Cho, D.M., Manasi Jain, Beate Ro and F.o.M. Winnik, *Long-Term Exposure to CdTe Quantum Dots Causes Functional Impairments in Live Cells.* Langmuir, 2007. **23**: p. 1974-1980.
128. Piret, J.P., et al., *Copper(II) oxide nanoparticles penetrate into HepG2 cells, exert cytotoxicity via oxidative stress and induce pro-inflammatory response.* Nanoscale, 2012. **4**(22): p. 7168-84.
129. Sikora, B., et al., *Transport of NaYF 4 :Er 3+ , Yb 3+ up-converting nanoparticles into HeLa cells.* Nanotechnology, 2013. **24**(23): p. 235702.
130. Lankoff, A., et al., *The effect of agglomeration state of silver and titanium dioxide nanoparticles on cellular response of HepG2, A549 and THP-1 cells.* Toxicol Lett, 2012. **208**(3): p. 197-213.
131. Havrdova, M., et al., *Field emission scanning electron microscopy (FE-SEM) as an approach for nanoparticle detection inside cells.* Micron, 2014. **67**: p. 149-154.
132. Peckys, D.B. and N. de Jonge, *Gold nanoparticle uptake in whole cells in liquid examined by environmental scanning electron microscopy.* Microsc Microanal, 2014. **20**(1): p. 189-97.
133. Meena, R., et al., *Nano-TiO2-Induced Apoptosis by Oxidative Stress-Mediated DNA Damage and Activation of p53 in Human Embryonic Kidney Cells.* Applied Biochemistry and Biotechnology, 2012. **167**(4): p. 791-808.
134. Connor, E.E., et al., *Gold nanoparticles are taken up by human cells but do not cause acute cytotoxicity.* Small, 2005. **1**(3): p. 325-7.
135. Panyam, J., et al., *Fluorescence and electron microscopy probes for cellular and tissue uptake of poly(d,l-lactide-co-glycolide) nanoparticles.* International Journal of Pharmaceutics, 2003. **262**(1–2): p. 1-11.
136. Gojova, A., et al., *Induction of inflammation in vascular endothelial cells by metal oxide nanoparticles: effect of particle composition.* Environ Health Perspect, 2007. **115**(3): p. 403-9.
137. Deering, C., et al., *A novel method to detect unlabeled inorganic nanoparticles and submicron particles in tissue by sedimentation field-flow fractionation.* Particle and Fibre Toxicology, 2008. **5**(1): p. 18.
138. Kreyling, W.G., et al., *Size dependence of the translocation of inhaled iridium and carbon nanoparticle aggregates from the lung of rats to the blood and secondary target organs.* Inhalation Toxicology, 2009. **21**(sup1): p. 55-60.
139. Sun, C., et al., *Tumor-targeted drug delivery and MRI contrast enhancement by chlorotoxin-conjugated iron oxide nanoparticles.* Nanomedicine (Lond), 2008. **3**(4): p. 495-505.
140. Ma, W., et al., *Silver nanoparticle exposure induced mitochondrial stress, caspase-3 activation and cell death: amelioration by sodium selenite.* Int J Biol Sci, 2015. **11**(8): p. 860-7.
141. Lu, S., et al., *Comparison of cellular toxicity caused by ambient ultrafine particles and engineered metal oxide nanoparticles.* Part Fibre Toxicol, 2015. **12**: p. 5.

142. Ruyra, A., et al., *Synthesis, culture medium stability, and in vitro and in vivo zebrafish embryo toxicity of metal-organic framework nanoparticles.* Chemistry, 2015. **21**(6): p. 2508-18.
143. Hsieh, H.-C., et al., *ROS-induced toxicity: exposure of 3T3, RAW264.7, and MCF7 cells to superparamagnetic iron oxide nanoparticles results in cell death by mitochondria-dependent apoptosis.* Journal of Nanoparticle Research, 2015. **17**(2).
144. Bowman, L., V. Castranova, and M. Ding, *Single cell gel electrophoresis assay (comet assay) for evaluating nanoparticles-induced DNA damage in cells.* Methods Mol Biol, 2012. **906**: p. 415-22.
145. Lima, R.d., et al., *Iron oxide nanoparticles show no toxicity in the comet assay in lymphocytes: A promising vehicle as a nitric oxide releasing nanocarrier in biomedical applications.* Journal of Physics: Conference Series, 2013. **429**(1): p. 012021.
146. Bhol, K.C. and P.J. Schechter, *Topical nanocrystalline silver cream suppresses inflammatory cytokines and induces apoptosis of inflammatory cells in a murine model of allergic contact dermatitis.* Br J Dermatol, 2005. **152**(6): p. 1235-42.
147. Halappanavar, S., et al., *Pulmonary response to surface-coated nanotitanium dioxide particles includes induction of acute phase response genes, inflammatory cascades, and changes in microRNAs: a toxicogenomic study.* Environ Mol Mutagen, 2011. **52**(6): p. 425-39.
148. Huo, L., et al., *Silver nanoparticles activate endoplasmic reticulum stress signaling pathway in cell and mouse models: The role in toxicity evaluation.* Biomaterials, 2015. **61**: p. 307-315.
149. Rinna, A., et al., *Effect of silver nanoparticles on mitogen-activated protein kinases activation: role of reactive oxygen species and implication in DNA damage.* Mutagenesis, 2015. **30**(1): p. 59-66.
150. Kermanizadeh, A., et al., *Hepatic toxicology following single and multiple exposure of engineered nanomaterials utilising a novel primary human 3D liver microtissue model.* Particle and Fibre Toxicology, 2014. **11**(1): p. 56.
151. LeCluyse, E.L., et al., *Organotypic liver culture models: meeting current challenges in toxicity testing.* Crit Rev Toxicol, 2012. **42**(6): p. 501-48.
152. Registration, E., Authorisation & restriction of CHemicals (REACH). *http://www.hse.gov.uk/reach/index.htm*.
153. Hartung, T., *Food for thought... on animal tests.* Altex, 2008. **25**(1): p. 3-16.
154. Shanks, N., R. Greek, and J. Greek, *Are animal models predictive for humans?* Philosophy, Ethics, and Humanities in Medicine, 2009. **4**(1): p. 2.
155. Whiteside, G.T., A. Adedoyin, and L. Leventhal, *Predictive validity of animal pain models? A comparison of the pharmacokinetic-pharmacodynamic relationship for pain drugs in rats and humans.* Neuropharmacology, 2008. **54**(5): p. 767-775.
156. Godin, B. and E. Touitou, *Transdermal skin delivery: Predictions for humans from in vivo, ex vivo and animal models.* Advanced Drug Delivery Reviews, 2007. **59**(11): p. 1152-1161.
157. Hartung, T., *Toxicology for the twenty-first century.* Nature, 2009. **460**.

158. Weaver, V.M., et al., *Reversion of the Malignant Phenotype of Human Breast Cells in Three-Dimensional Culture and In Vivo by Integrin Blocking Antibodies.* The Journal of Cell Biology, 1997. **137**(1): p. 231-245.
159. Abbott, A., *Cell culture: biology's new dimension.* Nature, 2003. **424**(6951): p. 870-2.
160. Griffith, L.G. and M.A. Swartz, *Capturing complex 3D tissue physiology in vitro.* Nat Rev Mol Cell Biol, 2006. **7**(3): p. 211-24.
161. Knight, E. and S. Przyborski, *Advances in 3D cell culture technologies enabling tissue-like structures to be created in vitro.* Journal of Anatomy, 2015. **227**(6): p. 746-756.
162. Francesco Pampaloni, E.G.R.a.E.H.K.S., *The third dimension bridges the gap between cell culture and live tissue.* nature rewievs, 2007.
163. Breslin, S. and L. O'Driscoll, *Three-dimensional cell culture: the missing link in drug discovery.* Drug Discov Today, 2013. **18**(5-6): p. 240-9.
164. Lin, R.Z. and H.Y. Chang, *Recent advances in three-dimensional multicellular spheroid culture for biomedical research.* Biotechnol J, 2008. **3**(9-10): p. 1172-84.
165. Roose, T., S.J. Chapman, and P.K. Maini, *Mathematical Models of Avascular Tumor Growth.* SIAM Review, 2007. **49**(2): p. 179-208.
166. Hu, G. and D. Li, *Three-dimensional modeling of transport of nutrients for multicellular tumor spheroid culture in a microchannel.* Biomedical Microdevices, 2007. **9**(3): p. 315-323.
167. Shirmanova, M.V., et al., *Intracellular pH imaging in cancer cells in vitro and tumors in vivo using the new genetically encoded sensor SypHer2.* Biochimica et Biophysica Acta (BBA) - General Subjects, 2015. **1850**(9): p. 1905-1911.
168. Raleigh, J.A., M.W. Dewhirst, and D.E. Thrall, *Measuring tumor hypoxia.* Seminars in Radiation Oncology, 1996. **6**(1): p. 37-45.
169. Hashem, M., et al., *Electron spin resonance microscopic imaging of oxygen concentration in cancer spheroids.* Journal of Magnetic Resonance, 2015. **256**: p. 77-85.
170. Censi, R., et al., *Hydrogels for protein delivery in tissue engineering.* Journal of Controlled Release, 2012. **161**(2): p. 680-692.
171. Siepmann, J. and N.A. Peppas, *Modeling of drug release from delivery systems based on hydroxypropyl methylcellulose (HPMC).* Advanced Drug Delivery Reviews, 2012. **64, Supplement**: p. 163-174.
172. Hamidi, M., et al., *Taguchi orthogonal array design for the optimization of hydrogel nanoparticles for the intravenous delivery of small-molecule drugs.* Journal of Applied Polymer Science, 2012. **126**(5): p. 1714-1724.
173. Mohd Amin, M.C.I., et al., *Synthesis and characterization of thermo- and pH-responsive bacterial cellulose/acrylic acid hydrogels for drug delivery.* Carbohydrate Polymers, 2012. **88**(2): p. 465-473.
174. Watson, B.M., et al., *Biodegradable, phosphate-containing, dual-gelling macromers for cellular delivery in bone tissue engineering.* Biomaterials, 2015. **67**: p. 286-296.
175. Hoffman, A.S., *Hydrogels for biomedical applications.* Advanced Drug Delivery Reviews, 2012. **64, Supplement**: p. 18-23.
176. DeForest, C.A. and K.S. Anseth, *Advances in bioactive hydrogels to probe and direct cell fate.* Annu Rev Chem Biomol Eng, 2012. **3**: p. 421-44.

177. Thiele, J., et al., *25th anniversary article: Designer hydrogels for cell cultures: a materials selection guide.* Adv Mater, 2014. **26**(1): p. 125-47.
178. Boere, K.W., et al., *Thermogelling and Chemoselectively Cross-Linked Hydrogels with Controlled Mechanical Properties and Degradation Behavior.* Biomacromolecules, 2015. **16**(9): p. 2840-51.
179. Galler, K.M., et al., *Self-assembling peptide amphiphile nanofibers as a scaffold for dental stem cells.* Tissue Eng Part A, 2008. **14**(12): p. 2051-8.
180. Zhong, M., Y.-T. Liu, and X.-M. Xie, *Self-healable, super tough graphene oxide-poly(acrylic acid) nanocomposite hydrogels facilitated by dual cross-linking effects through dynamic ionic interactions.* Journal of Materials Chemistry B, 2015. **3**(19): p. 4001-4008.
181. Mellott, M.B., K. Searcy, and M.V. Pishko, *Release of protein from highly cross-linked hydrogels of poly(ethylene glycol) diacrylate fabricated by UV polymerization.* Biomaterials, 2001. **22**(9): p. 929-941.
182. Xiao, W., et al., *Synthesis and characterization of photocrosslinkable gelatin and silk fibroin interpenetrating polymer network hydrogels.* Acta Biomaterialia, 2011. **7**(6): p. 2384-2393.
183. D'Errico, G., et al., *Structural and Mechanical Properties of UV-Photo-Cross-Linked Poly(N-vinyl-2-pyrrolidone) Hydrogels.* Biomacromolecules, 2008. **9**(1): p. 231-240.
184. Hennink, W.E. and C.F. van Nostrum, *Novel crosslinking methods to design hydrogels.* Advanced Drug Delivery Reviews, 2012. **64, Supplement**: p. 223-236.
185. Seliktar, D., *Designing Cell-Compatible Hydrogels for Biomedical Applications.* Science, 2012. **336**(6085): p. 1124-1128.
186. Drury, J.L. and D.J. Mooney, *Hydrogels for tissue engineering: scaffold design variables and applications.* Biomaterials, 2003. **24**(24): p. 4337-4351.
187. Dinerman, A.A., et al., *Swelling behavior of a genetically engineered silk-elastinlike protein polymer hydrogel.* Biomaterials, 2002. **23**(21): p. 4203-4210.
188. Ruedinger, F., et al., *Hydrogels for 3D mammalian cell culture: a starting guide for laboratory practice.* Appl Microbiol Biotechnol, 2015. **99**(2): p. 623-36.
189. Zhu, J. and R.E. Marchant, *Design properties of hydrogel tissue-engineering scaffolds.* Expert Rev Med Devices, 2011. **8**(5): p. 607-26.
190. Parenteau-Bareil, R., R. Gauvin, and F. Berthod, *Collagen-Based Biomaterials for Tissue Engineering Applications.* Materials, 2010. **3**(3): p. 1863-1887.
191. Shoulders, M.D. and R.T. Raines, *Collagen structure and stability.* Annual review of biochemistry, 2009. **78**: p. 929-958.
192. Yung, C.W., et al., *Transglutaminase crosslinked gelatin as a tissue engineering scaffold.* J Biomed Mater Res A, 2007. **83**(4): p. 1039-46.
193. Paguirigan, A. and D.J. Beebe, *Gelatin based microfluidic devices for cell culture.* Lab Chip, 2006. **6**(3): p. 407-13.
194. Kleinman, H.K. and G.R. Martin, *Matrigel: basement membrane matrix with biological activity.* Semin Cancer Biol, 2005. **15**(5): p. 378-86.

195. Neto, A.I., et al., *A novel hanging spherical drop system for the generation of cellular spheroids and high throughput combinatorial drug screening*. Biomaterials Science, 2015. **3**(4): p. 581-585.
196. Raghavan, S., et al., *Formation of stable small cell number three-dimensional ovarian cancer spheroids using hanging drop arrays for preclinical drug sensitivity assays*. Gynecologic Oncology, 2015. **138**(1): p. 181-189.
197. Tung, Y.C., et al., *High-throughput 3D spheroid culture and drug testing using a 384 hanging drop array*. Analyst, 2011. **136**(3): p. 473-8.
198. Frey, O., et al., *Reconfigurable microfluidic hanging drop network for multi-tissue interaction and analysis*. Nat Commun, 2014. **5**.
199. Zhang, S., et al., *The effects of spheroid formation of adipose-derived stem cells in a microgravity bioreactor on stemness properties and therapeutic potential*. Biomaterials, 2015. **41**: p. 15-25.
200. Rebelo, S.P., et al., *Three-dimensional co-culture of human hepatocytes and mesenchymal stem cells: improved functionality in long-term bioreactor cultures*. Journal of Tissue Engineering and Regenerative Medicine, 2015: p. n/a-n/a.
201. Ebrahimkhani, M.R., et al., *Bioreactor technologies to support liver function in vitro*. Advanced Drug Delivery Reviews, 2014. **69–70**: p. 132-157.
202. Silber, P.M., et al., *Hepatocyte bioreactor system for long term culture of functional hepatocyte spheroids*. 2011, Google Patents.
203. Pörtner, R., et al., *Bioreactor design for tissue engineering*. Journal of Bioscience and Bioengineering, 2005. **100**(3): p. 235-245.
204. Martin, I., D. Wendt, and M. Heberer, *The role of bioreactors in tissue engineering*. Trends in Biotechnology, 2004. **22**(2): p. 80-86.
205. Yip, D. and C.H. Cho, *A multicellular 3D heterospheroid model of liver tumor and stromal cells in collagen gel for anti-cancer drug testing*. Biochemical and Biophysical Research Communications, 2013. **433**(3): p. 327-332.
206. Meng, Q., *Three-dimensional culture of hepatocytes for prediction of drug-induced hepatotoxicity*. Expert Opinion on Drug Metabolism & Toxicology, 2010. **6**(6): p. 733-746.
207. Uchea, C., S.F. Owen, and J.K. Chipman, *Functional xenobiotic metabolism and efflux transporters in trout hepatocyte spheroid cultures*. Toxicol Res (Camb), 2015. **4**(2): p. 494-507.
208. Gunness, P., et al., *3D organotypic cultures of human HepaRG cells: a tool for in vitro toxicity studies*. Toxicol Sci, 2013. **133**(1): p. 67-78.
209. Mehta, G., et al., *Opportunities and challenges for use of tumor spheroids as models to test drug delivery and efficacy*. Journal of Controlled Release, 2012. **164**(2): p. 192-204.
210. Yamada, M., et al., *Controlled formation of heterotypic hepatic micro-organoids in anisotropic hydrogel microfibers for long-term preservation of liver-specific functions*. Biomaterials, 2012. **33**(33): p. 8304-8315.
211. Yoon No, D., et al., *3D liver models on a microplatform: well-defined culture, engineering of liver tissue and liver-on-a-chip*. Lab on a Chip, 2015. **15**(19): p. 3822-3837.
212. Lee, J., M.J. Cuddihy, and N.A. Kotov, *Three-dimensional cell culture matrices: state of the art*. Tissue Eng Part B Rev, 2008. **14**(1): p. 61-86.

213. Kyburz, K. and K. Anseth, *Synthetic Mimics of the Extracellular Matrix: How Simple is Complex Enough?* Annals of Biomedical Engineering, 2015. **43**(3): p. 489-500.
214. Lutolf, M.P. and J.A. Hubbell, *Synthetic biomaterials as instructive extracellular microenvironments for morphogenesis in tissue engineering*. Nat Biotech, 2005. **23**(1): p. 47-55.
215. Verhulsel, M., et al., *A review of microfabrication and hydrogel engineering for micro-organs on chips*. Biomaterials, 2014. **35**(6): p. 1816-1832.
216. Rouwkema, J., N.C. Rivron, and C.A. van Blitterswijk, *Vascularization in tissue engineering*. Trends in Biotechnology, 2008. **26**(8): p. 434-441.
217. Novosel, E.C., C. Kleinhans, and P.J. Kluger, *Vascularization is the key challenge in tissue engineering*. Advanced Drug Delivery Reviews, 2011. **63**(4–5): p. 300-311.
218. Mironov, V., et al., *Organ printing: computer-aided jet-based 3D tissue engineering*. Trends in Biotechnology, 2003. **21**(4): p. 157-161.
219. Ruedinger, F., et al., *Hydrogels for 3D mammalian cell culture: a starting guide for laboratory practice*. Applied Microbiology and Biotechnology, 2015. **99**(2): p. 623-636.
220. Shamir, E.R. and A.J. Ewald, *Three-dimensional organotypic culture: experimental models of mammalian biology and disease*. Nat Rev Mol Cell Biol, 2014. **15**(10): p. 647-664.
221. Ortega, M.H. and J.C. Clevers, *Liver organoid, uses thereof and culture method for obtaining them*. EP 2412800 A1, 2012.
222. Pampaloni, F., E.H. Stelzer, and A. Masotti, *Three-dimensional tissue models for drug discovery and toxicology*. Recent Pat Biotechnol, 2009. **3**(2): p. 103-17.
223. Van de Bovenkamp, M., et al., *Liver fibrosis in vitro: cell culture models and precision-cut liver slices*. Toxicol In Vitro, 2007. **21**(4): p. 545-57.
224. Uygun, B.E., et al., *Organ reengineering through development of a transplantable recellularized liver graft using decellularized liver matrix*. Nat Med, 2010. **16**(7): p. 814-820.
225. Baptista, P.M., et al., *The use of whole organ decellularization for the generation of a vascularized liver organoid*. Hepatology, 2011. **53**(2): p. 604-17.
226. Tyson, L.Y.G.T.A.F.A.W., *Cell-based sensing: From 2D to 3D cell culture*. ECS Transactions. , 2014. **64**(1): p. 125-132.
227. Mosmann, T., *Rapid colorimetric assay for cellular growth and survival: Application to proliferation and cytotoxicity assays*. Journal of Immunological Methods, 1983. **65**(1–2): p. 55-63.
228. Stalder, A.F., et al., *A snake-based approach to accurate determination of both contact points and contact angles*. Colloids and Surfaces A: Physicochemical and Engineering Aspects, 2006. **286**(1-3): p. 92-103.
229. Dean, R.L., *Kinetic studies with alkaline phosphatase in the presence and absence of inhibitors and divalent cations*. Biochemistry and Molecular Biology Education, 2002. **30**(6): p. 401-407.
230. Pfaffl, M.W., *A new mathematical model for relative quantification in real-time RT–PCR*. Nucleic Acids Research, 2001. **29**(9): p. e45.
231. Monteiro-Riviere, N.A., A.O. Inman, and L.W. Zhang, *Limitations and relative utility of screening assays to assess engineered nanoparticle*

toxicity in a human cell line. Toxicology and Applied Pharmacology, 2009. **234**(2): p. 222-235.
232. J. M. Worle-Knirsch, K.P., and H. F. Krug, *Oops They Did It Again! Carbon Nanotubes Hoax Scientists in Viability Assays.* Nano Letters, 2006. **6**(6): p. 1261-1268.
233. Ong, K.J., et al., *Widespread nanoparticle-assay interference: implications for nanotoxicity testing*. PLoS One, 2014. **9**(3): p. e90650.
234. Warheit, D.B., *Debunking some misconceptions about nanotoxicology.* Nano Lett, 2010. **10**(12): p. 4777-82.
235. Arkin, A.P., *A wise consistency: engineering biology for conformity, reliability, predictability*. Curr Opin Chem Biol, 2013. **17**(6): p. 893-901.
236. Nohynek, G.J., et al., *Safety assessment of personal care products/cosmetics and their ingredients*. Toxicol Appl Pharmacol, 2010. **243**(2): p. 239-59.
237. Cedervall, T., et al., *Detailed Identification of Plasma Proteins Adsorbed on Copolymer Nanoparticles.* Angewandte Chemie International Edition, 2007. **46**(30): p. 5754-5756.
238. DelRaso, N.J., *Cadmium Uptake Kinetics in Rat Hepatocytes: Correction for Albumin Binding*. Toxicological Sciences, 2003. **72**(1): p. 19-30.
239. Beg, A.A., et al., *Tumor necrosis factor and interleukin-1 lead to phosphorylation and loss of I kappa B alpha: a mechanism for NF-kappa B activation.* Mol Cell Biol, 1993. **13**(6): p. 3301-10.
240. Schütze, S., et al., *TNF activates NF-κB by phosphatidylcholine-specific phospholipase C-induced "Acidic" sphingomyelin breakdown.* Cell, 1992. **71**(5): p. 765-776.
241. Bouwmeester, T., et al., *A physical and functional map of the human TNF-[alpha]/NF-[kappa]B signal transduction pathway.* Nat Cell Biol, 2004. **6**(2): p. 97-105.
242. Bellezzo, J.M., et al., *LPS-mediated NF-kappa beta activation in rat Kupffer cells can be induced independently of CD14.* American Journal of Physiology - Gastrointestinal and Liver Physiology, 1996. **270**(6): p. G956-G961.
243. Bressenot, A., et al., *Assessment of Apoptosis by Immunohistochemistry to Active Caspase-3, Active Caspase-7, or Cleaved PARP in Monolayer Cells and Spheroid and Subcutaneous Xenografts of Human Carcinoma.* Journal of Histochemistry and Cytochemistry, 2009. **57**(4): p. 289-300.
244. Soldani, C. and A.I. Scovassi, *Poly(ADP-ribose) polymerase-1 cleavage during apoptosis: An update.* Apoptosis. **7**(4): p. 321-328.
245. Niwa, D., et al., *Heterofunctional nanosheet controlling cell adhesion properties by collagen coating.* J Biomater Appl, 2012. **27**(2): p. 131-41.
246. Dolatshahi-Pirouz, A., et al., *Cell shape and spreading of stromal (mesenchymal) stem cells cultured on fibronectin coated gold and hydroxyapatite surfaces.* Colloids Surf B Biointerfaces, 2011. **84**(1): p. 18-25.
247. Salmeron-Sanchez, M., et al., *Role of material-driven fibronectin fibrillogenesis in cell differentiation.* Biomaterials, 2011. **32**(8): p. 2099-105.
248. Christopher J. Tape, I.C.N., Jonathan D. Worboys, Lindsay Lim, and a.C.J. Douglas A. Lauffenburger, *Cell-specific Labeling Enzymes for*

Analysis of Cell–Cell Communication in Continuous Co-culture. Molecular & Cellular Proteomics, 2014. **13**: p. 1866-1876.
249. Tian, H., et al., *Enhanced proliferation of bone marrow mesenchymal stem cells by co-culture with TM4 mouse Sertoli cells: involvement of the EGF/PI3K/AKT pathway*. Mol Cell Biochem, 2014. **393**(1-2): p. 155-64.
250. Astashkina, A. and D.W. Grainger, *Critical analysis of 3-D organoid in vitro cell culture models for high-throughput drug candidate toxicity assessments*. Adv Drug Deliv Rev, 2014. **69-70**: p. 1-18.
251. Discher, D.E., P. Janmey, and Y.L. Wang, *Tissue cells feel and respond to the stiffness of their substrate*. Science, 2005. **310**(5751): p. 1139-43.
252. O'Brien, F.J., et al., *The effect of pore size on cell adhesion in collagen-GAG scaffolds*. Biomaterials, 2005. **26**(4): p. 433-41.
253. Geckil, H., et al., *Engineering hydrogels as extracellular matrix mimics*. Nanomedicine (Lond), 2010. **5**(3): p. 469-84.
254. Vats, K. and D.S. Benoit, *Dynamic manipulation of hydrogels to control cell behavior: a review*. Tissue Eng Part B Rev, 2013. **19**(6): p. 455-69.
255. Wei, J., et al., *Influence of surface wettability on competitive protein adsorption and initial attachment of osteoblasts*. Biomedical Materials, 2009. **4**(4): p. 045002.
256. Yildirim, E.D., et al., *Accelerated differentiation of osteoblast cells on polycaprolactone scaffolds driven by a combined effect of protein coating and plasma modification*. Biofabrication, 2010. **2**(1): p. 014109.
257. Ko, T.-J., et al., *Adhesion behavior of mouse liver cancer cells on nanostructured superhydrophobic and superhydrophilic surfaces*. Soft Matter, 2013. **9**(36): p. 8705-8711.
258. Rozga, J., T. Piatek, and P. Malkowski, *Human albumin: old, new, and emerging applications*. Ann Transplant, 2013. **18**: p. 205-17.
259. Garcovich, M., M.A. Zocco, and A. Gasbarrini, *Clinical use of albumin in hepatology*. Blood Transfus, 2009. **7**(4): p. 268-77.
260. Zheng, Y.-R., et al., *Pt(IV) Prodrugs Designed to Bind Non-Covalently to Human Serum Albumin for Drug Delivery*. Journal of the American Chemical Society, 2014. **136**(24): p. 8790-8798.
261. Gerlier, D. and N. Thomasset, *Use of MTT colorimetric assay to measure cell activation*. Journal of Immunological Methods, 1986. **94**(1): p. 57-63.
262. O'Brien, J., et al., *Investigation of the Alamar Blue (resazurin) fluorescent dye for the assessment of mammalian cell cytotoxicity*. Eur J Biochem, 2000. **267**(17): p. 5421-6.
263. Bonnier, F., et al., *Cell viability assessment using the Alamar blue assay: a comparison of 2D and 3D cell culture models*. Toxicol In Vitro, 2015. **29**(1): p. 124-31.
264. Essani, N.A., M.A. Fisher, and H. Jaeschke, *Inhibition of NF-kappa B activation by dimethyl sulfoxide correlates with suppression of TNF-alpha formation, reduced ICAM-1 gene transcription, and protection against endotoxin-induced liver injury*. Shock, 1997. **7**(2): p. 90-6.
265. Chang, C.K., S. Llanes, and W. Schumer, *Inhibitory effect of dimethyl sulfoxide on nuclear factor-kappa B activation and intercellular*

adhesion molecule 1 gene expression in septic rats. J Surg Res, 1999. **82**(2): p. 294-9.
266. Guo, L., et al., *Similarities and Differences in the Expression of Drug-Metabolizing Enzymes between Human Hepatic Cell Lines and Primary Human Hepatocytes.* Drug Metabolism and Disposition, 2011. **39**(3): p. 528-538.
267. Wilkening, S., F. Stahl, and A. Bader, *Comparison of primary human hepatocytes and hepatoma cell line Hepg2 with regard to their biotransformation properties.* Drug Metab Dispos, 2003. **31**(8): p. 1035-42.
268. Guillouzo, A., et al., *The human hepatoma HepaRG cells: A highly differentiated model for studies of liver metabolism and toxicity of xenobiotics.* Chemico-Biological Interactions, 2007. **168**(1): p. 66-73.
269. Bokhari, M., et al., *Culture of HepG2 liver cells on three dimensional polystyrene scaffolds enhances cell structure and function during toxicological challenge.* Journal of Anatomy, 2007. **211**(4): p. 567-576.
270. Bokhari, M., et al., *Novel cell culture device enabling three-dimensional cell growth and improved cell function.* Biochem Biophys Res Commun, 2007. **354**(4): p. 1095-100.
271. Lan, S.-F., B. Safiejko-Mroczka, and B. Starly, *Long-term cultivation of HepG2 liver cells encapsulated in alginate hydrogels: A study of cell viability, morphology and drug metabolism.* Toxicology in Vitro, 2010. **24**(4): p. 1314-1323.
272. Li, C.L., et al., *Survival advantages of multicellular spheroids vs. monolayers of HepG2 cells in vitro.* Oncol Rep, 2008. **20**(6): p. 1465-71.
273. Pruksakorn, D., et al., *Metabolic alteration of HepG2 in scaffold-based 3-D culture: proteomic approach.* Proteomics, 2010. **10**(21): p. 3896-904.
274. Goepfert, C., et al., *Functional Characterisation of Human Hepatoma Cell Line HepG2 in 3D Culture*, in *Proceedings of the 21st Annual Meeting of the European Society for Animal Cell Technology (ESACT), Dublin, Ireland, June 7-10, 2009*, N. Jenkins, N. Barron, and P. Alves, Editors. 2012, Springer Netherlands. p. 241-246.
275. Stępkowski, T.M., K. Brzóska, and M. Kruszewski, *Silver nanoparticles induced changes in the expression of NF-κB related genes are cell type specific and related to the basal activity of NF-κB.* Toxicology in Vitro, 2014. **28**(4): p. 473-478.
276. Huang, J., et al., *Genetic modification of mesenchymal stem cells overexpressing CCR1 increases cell viability, migration, engraftment, and capillary density in the injured myocardium.* Circ Res, 2010. **106**(11): p. 1753-62.
277. Teeguarden, J.G., et al., *Particokinetics in vitro: dosimetry considerations for in vitro nanoparticle toxicity assessments.* Toxicol Sci, 2007. **95**(2): p. 300-12.
278. Lison, D., et al., *Nominal and effective dosimetry of silica nanoparticles in cytotoxicity assays.* Toxicol Sci, 2008. **104**(1): p. 155-62.
279. Deguchi, S., et al., *Stabilization of C60 nanoparticles by protein adsorption and its implications for toxicity studies.* Chem Res Toxicol., 2007. **20**(6): p. 854-858.

280. Vippola, M., et al., *Preparation of nanoparticle dispersions for in-vitro toxicity testing*. 2009(1477-0903 (Electronic)).
281. Lim, J., et al., *Characterization of magnetic nanoparticle by dynamic light scattering*. Nanoscale Research Letters, 2013. **8**(1): p. 1-14.
282. Li, L., et al., *Dissolution and aggregation of Cu nanoparticles in culture media: effects of incubation temperature and particles size*. Journal of Nanoparticle Research, 2015. **17**(1): p. 1-11.
283. Allouni, Z.E., et al., *Agglomeration and sedimentation of TiO2 nanoparticles in cell culture medium*. Colloids and Surfaces B: Biointerfaces, 2009. **68**(1): p. 83-87.
284. Fang, C., et al., *Functionalized Nanoparticles with Long-Term Stability in Biological Media*. Small, 2009. **5**(14): p. 1637-1641.
285. Kroll, A., et al., *Interference of engineered nanoparticles with in vitro toxicity assays*. Archives of Toxicology, 2012. **86**(7): p. 1123-1136.
286. Elkayam, T., et al., *Enhancing the drug metabolism activities of C3A--a human hepatocyte cell line--by tissue engineering within alginate scaffolds*. 2006(1076-3279 (Print)).
287. Xu, J., M. Ma, and W.M. Purcell, *Characterisation of some cytotoxic endpoints using rat liver and HepG2 spheroids as in vitro models and their application in hepatotoxicity studies. I. Glucose metabolism and enzyme release as cytotoxic markers*. Toxicology and Applied Pharmacology, 2003. **189**(2): p. 100-111.
288. Wrzesinski, K. and S.J. Fey, *After trypsinisation, 3D spheroids of C3A hepatocytes need 18 days to re-establish similar levels of key physiological functions to those seen in the liver*. Toxicology Research, 2013. **2**(2): p. 123.
289. Horning, J.L., et al., *3-D Tumor Model for In Vitro Evaluation of Anticancer Drugs*. Molecular Pharmaceutics, 2008. **5**(5): p. 849-862.
290. Desoize, B. and J.-C. Jardillier, *Multicellular resistance: a paradigm for clinical resistance?* Critical Reviews in Oncology/Hematology, 2000. **36**(2–3): p. 193-207.
291. Schreck, R., K. Albermann, and P.A. Baeuerle, *Nuclear Factor Kb: An Oxidative Stress-Responsive Transcription Factor of Eukaryotic Cells (A Review)*. Free Radical Research Communications, 1992. **17**(4): p. 221-237.
292. Wagner, M., et al., *Mechanisms of cell activation by heavy metal ions*. Journal of Biomedical Materials Research, 1998. **42**(3): p. 443-452.

9 APPENDIX

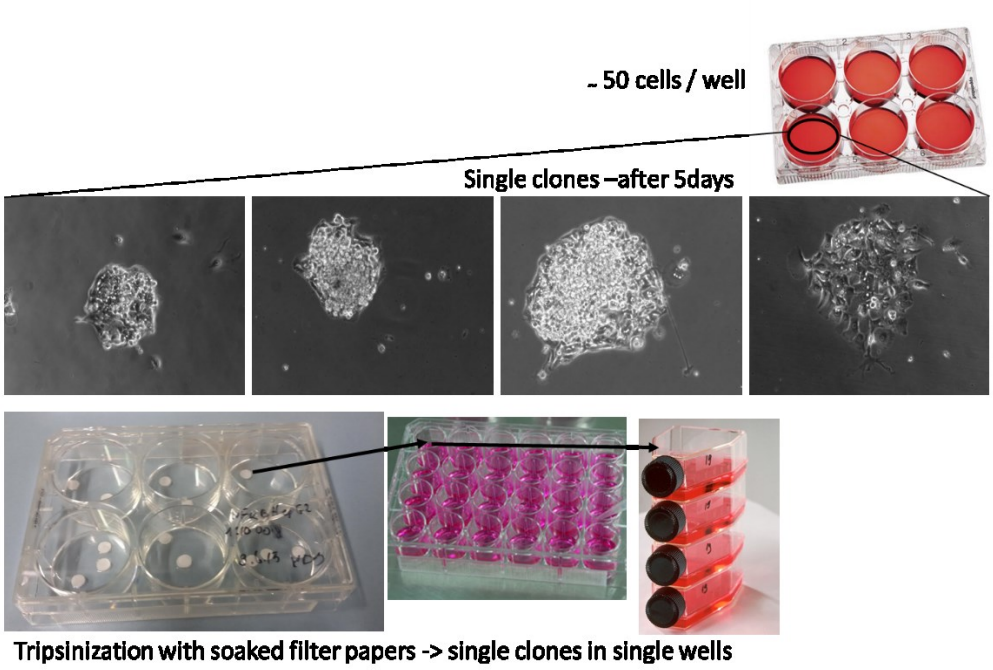

Figure A. 1 Schematic overview of single colony selection. Transfected cells were supplemented with selective medium supplemented with 300 µg/ml zeocin. After, cells reached ~100% confluency, were trypsinized and highly diluted plated on a 6-wellplate (~50 cells / well). After 8 days of cultivation single colonies were picked up with sterile filter paper soaked with trypsin and transferred to single well.

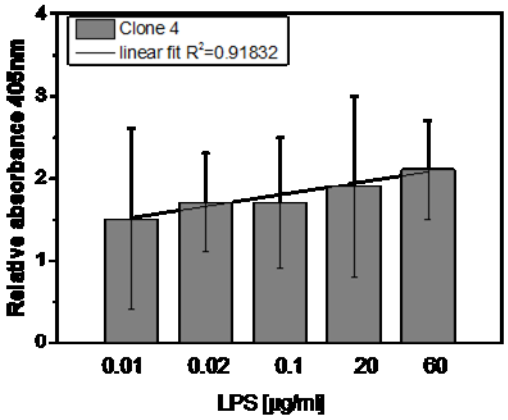
Clone 4
linear fit R²=0.91832
Relative absorbance 405nm
0.01
0.02
0.1
20
60
LPS [µg/ml]

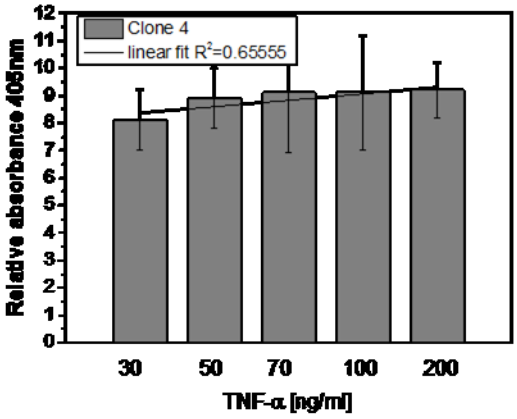
Clone 4
linear fit R²=0.65555
Relative absorbance 405nm
30
50
70
100
200
TNF-α [ng/ml]

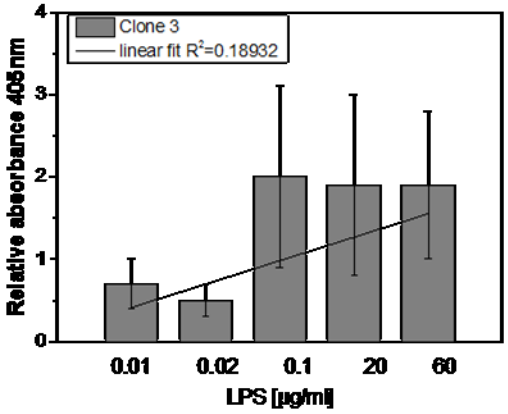
Clone 3
linear fit R²=0.18932
Relative absorbance 405nm
0.01
0.02
0.1
20
60
LPS [µg/ml]

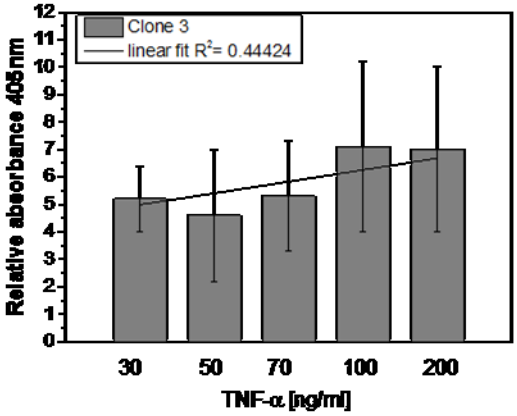
Clone 3
linear fit R²= 0.44424
Relative absorbance 405nm
30
50
70
100
200
TNF-α [ng/ml]

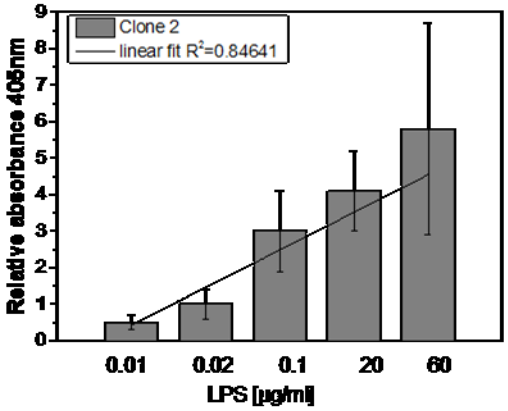
Clone 2
linear fit R²=0.84641
Relative absorbance 405nm
0.01
0.02
0.1
20
60
LPS [µg/ml]

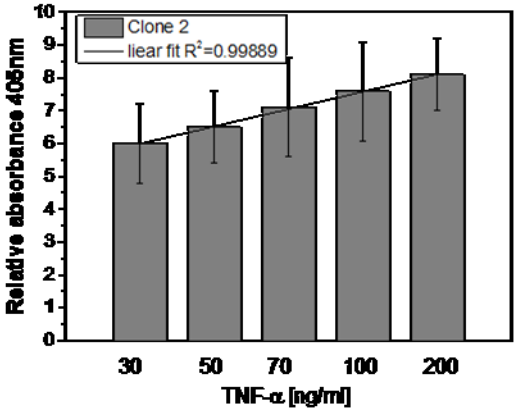
Clone 2
liear fit R²=0.99889
Relative absorbance 405nm
30
50
70
100
200
TNF-α [ng/ml]

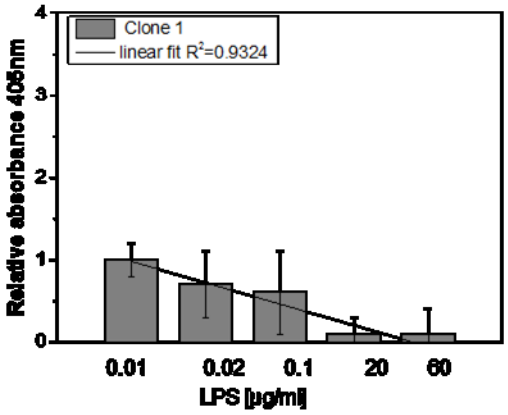
Clone 1
linear fit R²=0.9324
Relative absorbance 405nm
0.01
0.02
0.1
20
60
LPS [µg/ml]

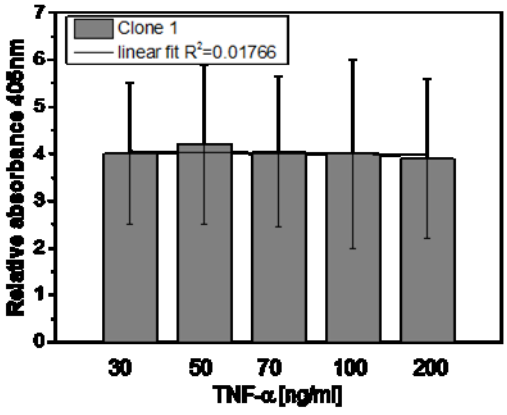
Clone 1
linear fit R²=0.01766
Relative absorbance 405nm
30
50
70
100
200
TNF-α [ng/ml]

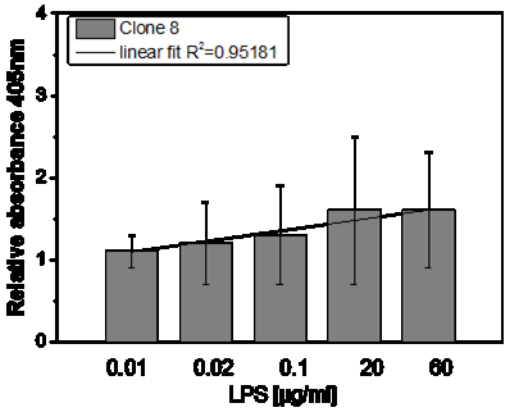
Clone 8
linear fit R²=0.95181
Relative absorbance 405nm
0.01
0.02
0.1
20
60
LPS [µg/ml]

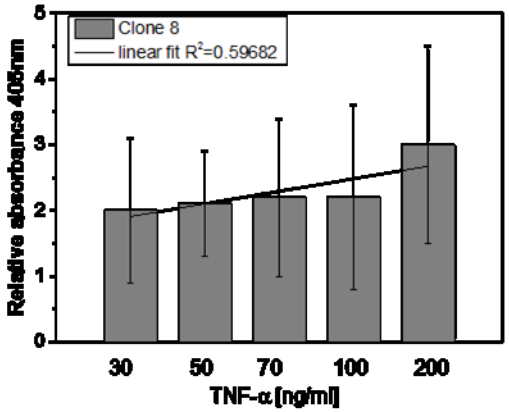
Clone 8
linear fit R²=0.59682
Relative absorbance 405nm
30
50
70
100
200
TNF-α [ng/ml]

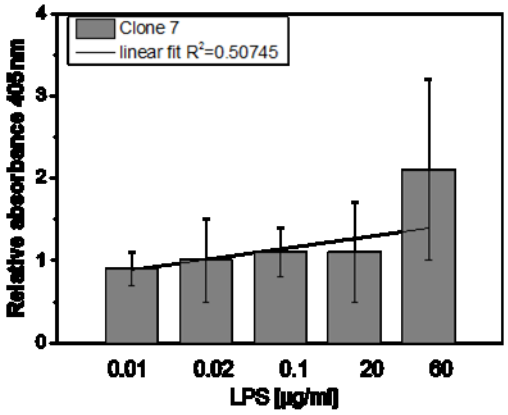
Clone 7
linear fit R²=0.50745
Relative absorbance 405nm
0.01
0.02
0.1
20
60
LPS [µg/ml]

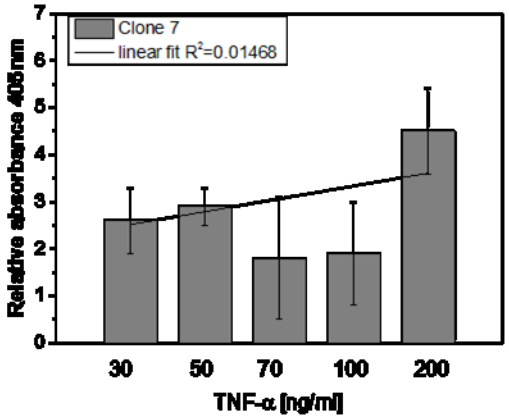
Clone 7
linear fit R²=0.01468
Relative absorbance 405nm
30
50
70
100
200
TNF-α [ng/ml]

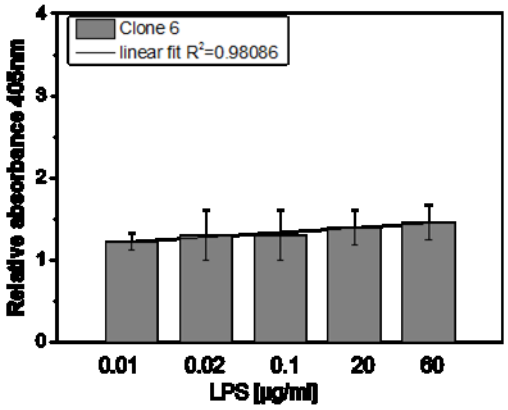
Clone 6
linear fit R²=0.98086
Relative absorbance 405nm
0.01
0.02
0.1
20
60
LPS [µg/ml]

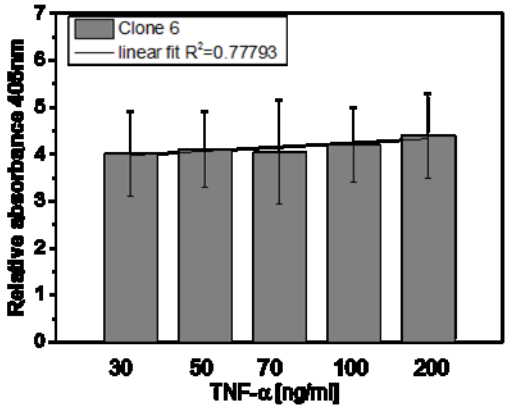
Clone 6
linear fit R²=0.77793
Relative absorbance 405nm
30
50
70
100
200
TNF-α [ng/ml]

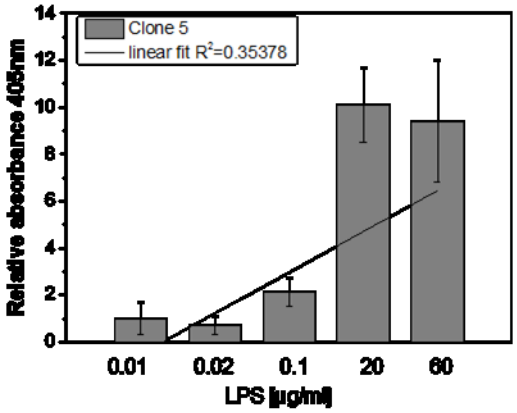
Clone 5
linear fit R²=0.35378
Relative absorbance 405nm
0.01
0.02
0.1
20
60
LPS [µg/ml]

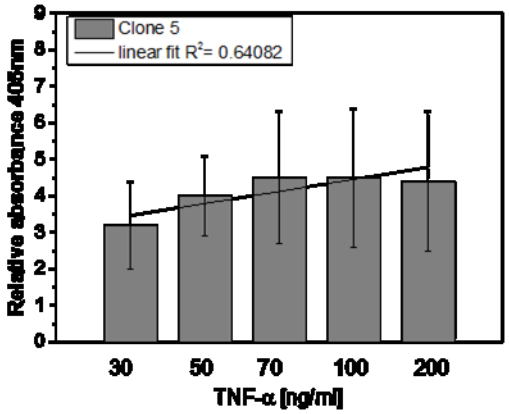
Clone 5
linear fit R²= 0.64082
Relative absorbance 405nm
30
50
70
100
200
TNF-α [ng/ml]

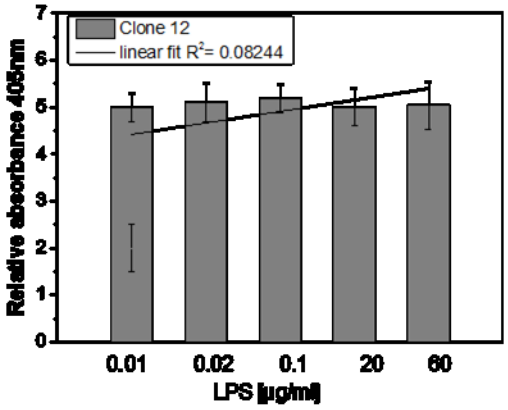
Clone 12
linear fit R²= 0.08244
Relative absorbance 405nm
0.01
0.02
0.1
20
60
LPS [µg/ml]

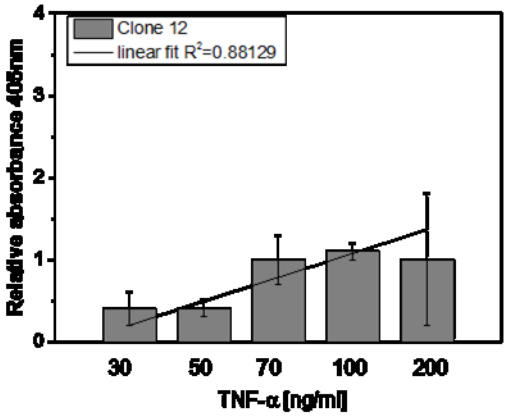
Clone 12
linear fit R²=0.88129
Relative absorbance 405nm
30
50
70
100
200
TNF-α [ng/ml]

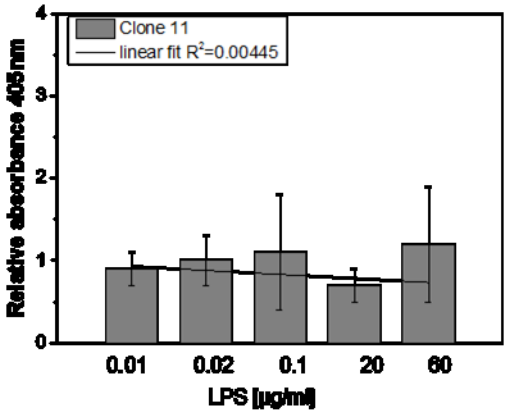
Clone 11
linear fit R²=0.00445
Relative absorbance 405nm
0.01
0.02
0.1
20
60
LPS [µg/ml]

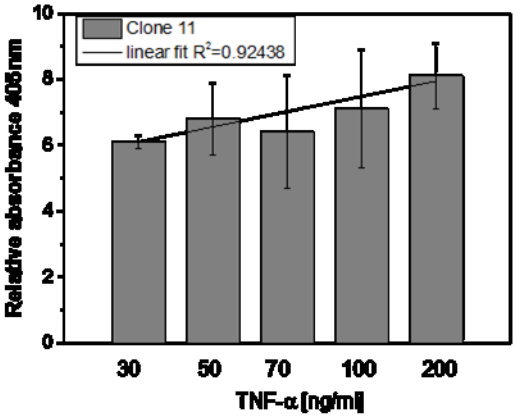
Clone 11
linear fit R²=0.92438
Relative absorbance 405nm
30
50
70
100
200
TNF-α [ng/ml]

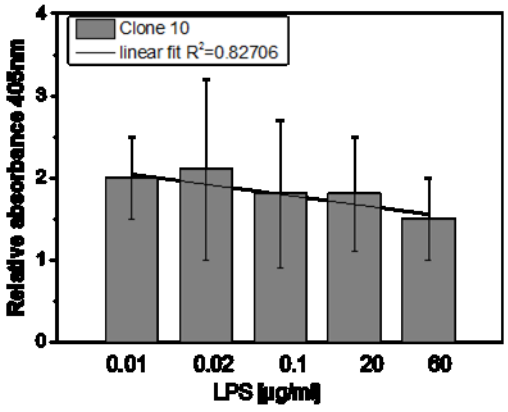
Clone 10
linear fit R²=0.82706
Relative absorbance 405nm
0.01
0.02
0.1
20
60
LPS [µg/ml]

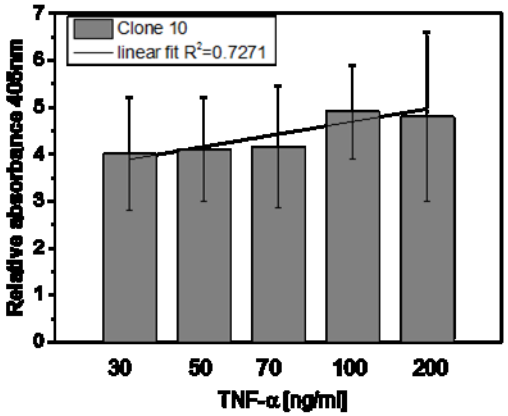
Clone 10
linear fit R²=0.7271
Relative absorbance 405nm
30
50
70
100
200
TNF-α [ng/ml]

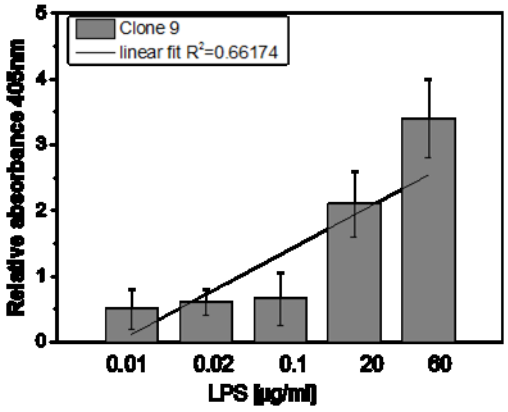
Clone 9
linear fit R²=0.66174
Relative absorbance 405nm
0.01
0.02
0.1
20
60
LPS [µg/ml]

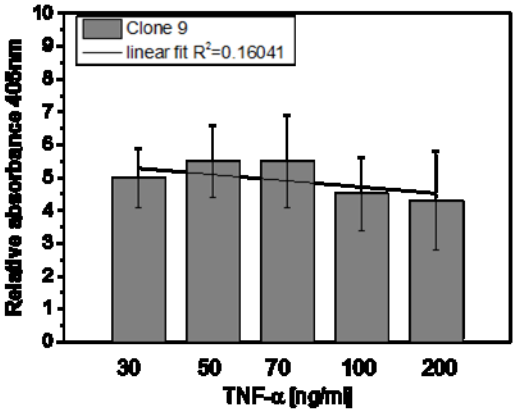
Clone 9
linear fit R²=0.16041
Relative absorbance 405nm
30
50
70
100
200
TNF-α [ng/ml]

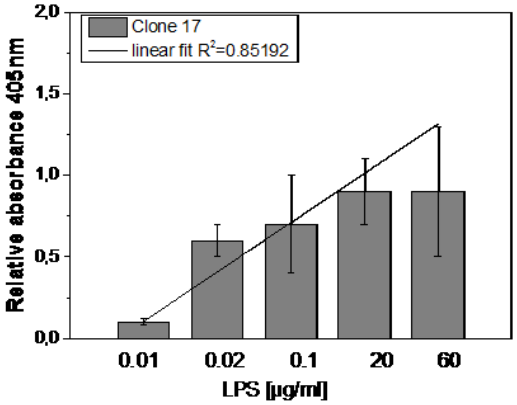
Clone 17
linear fit R²=0.85192
Relative absorbance 405nm
2,0
1,5
1,0
0,5
0,0
0.01
0.02
0.1
20
60
LPS [µg/ml]

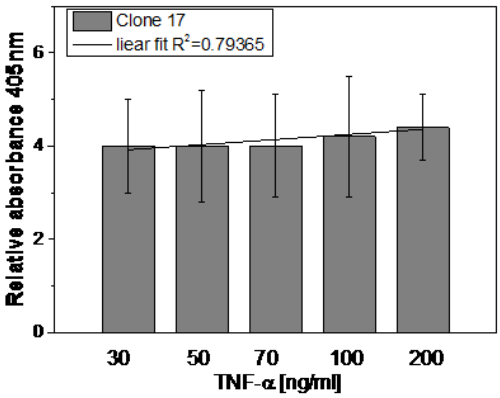
Clone 17
liear fit R²=0.79365
Relative absorbance 405nm
6
4
2
0
30
50
70
100
200
TNF-α [ng/ml]

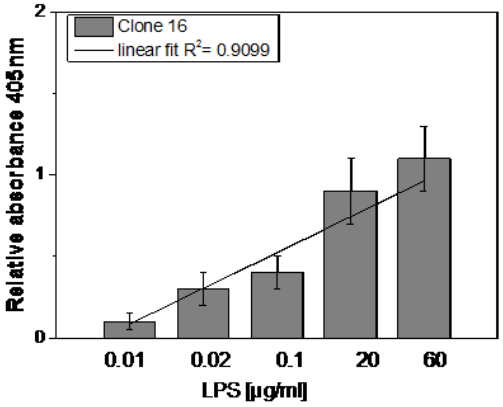
Clone 16
linear fit R²= 0.9099
Relative absorbance 405nm
2
1
0
0.01
0.02
0.1
20
60
LPS [µg/ml]

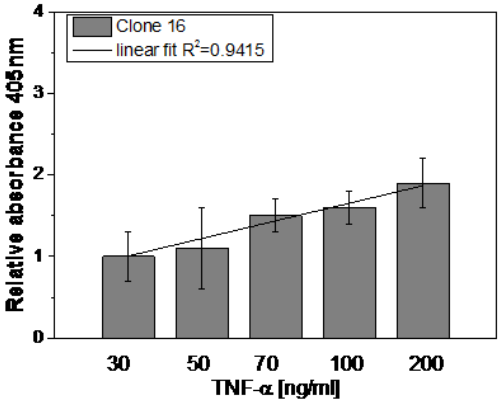
Clone 16
linear fit R²=0.9415
Relative absorbance 405nm
4
3
2
1
0
30
50
70
100
200
TNF-α [ng/ml]

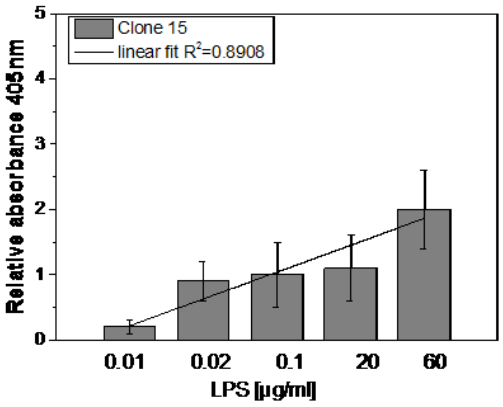
Clone 15
linear fit R²=0.8908
Relative absorbance 405nm
5
4
3
2
1
0
0.01
0.02
0.1
20
60
LPS [µg/ml]

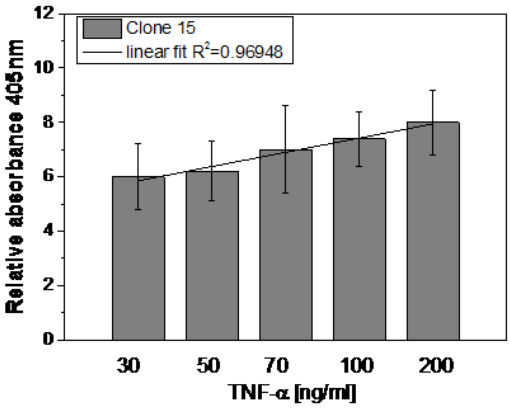
Clone 15
linear fit R²=0.96948
Relative absorbance 405nm
12
10
8
6
4
2
0
30
50
70
100
200
TNF-α [ng/ml]

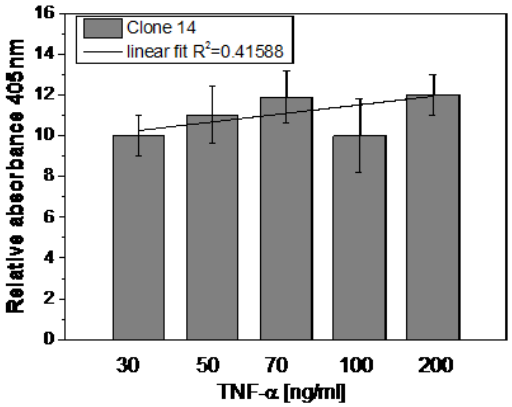
Clone 14
linear fit R²=0.41588
Relative absorbance 405nm
16
14
12
10
8
6
4
2
0
30
50
70
100
200
TNF-α [ng/ml]

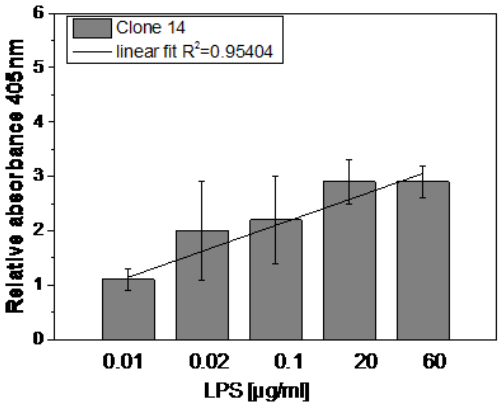
Clone 14
linear fit R²=0.95404
Relative absorbance 405nm
6
5
4
3
2
1
0
0.01
0.02
0.1
20
60
LPS [µg/ml]

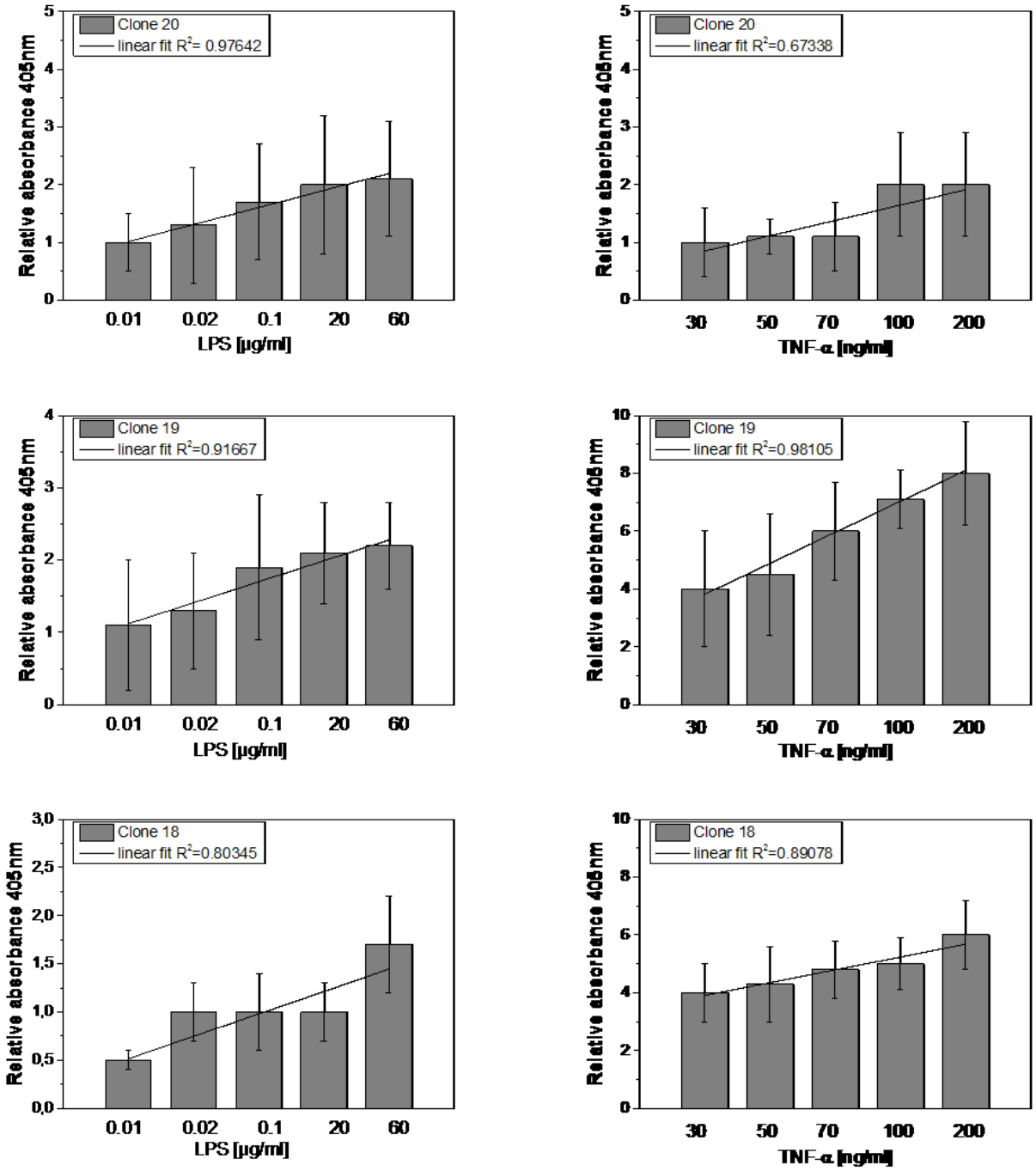

Figure A. 2. Screening of clones after stimulation with TNF-α and LPS; t= 6h; (n= 3 ± SD).

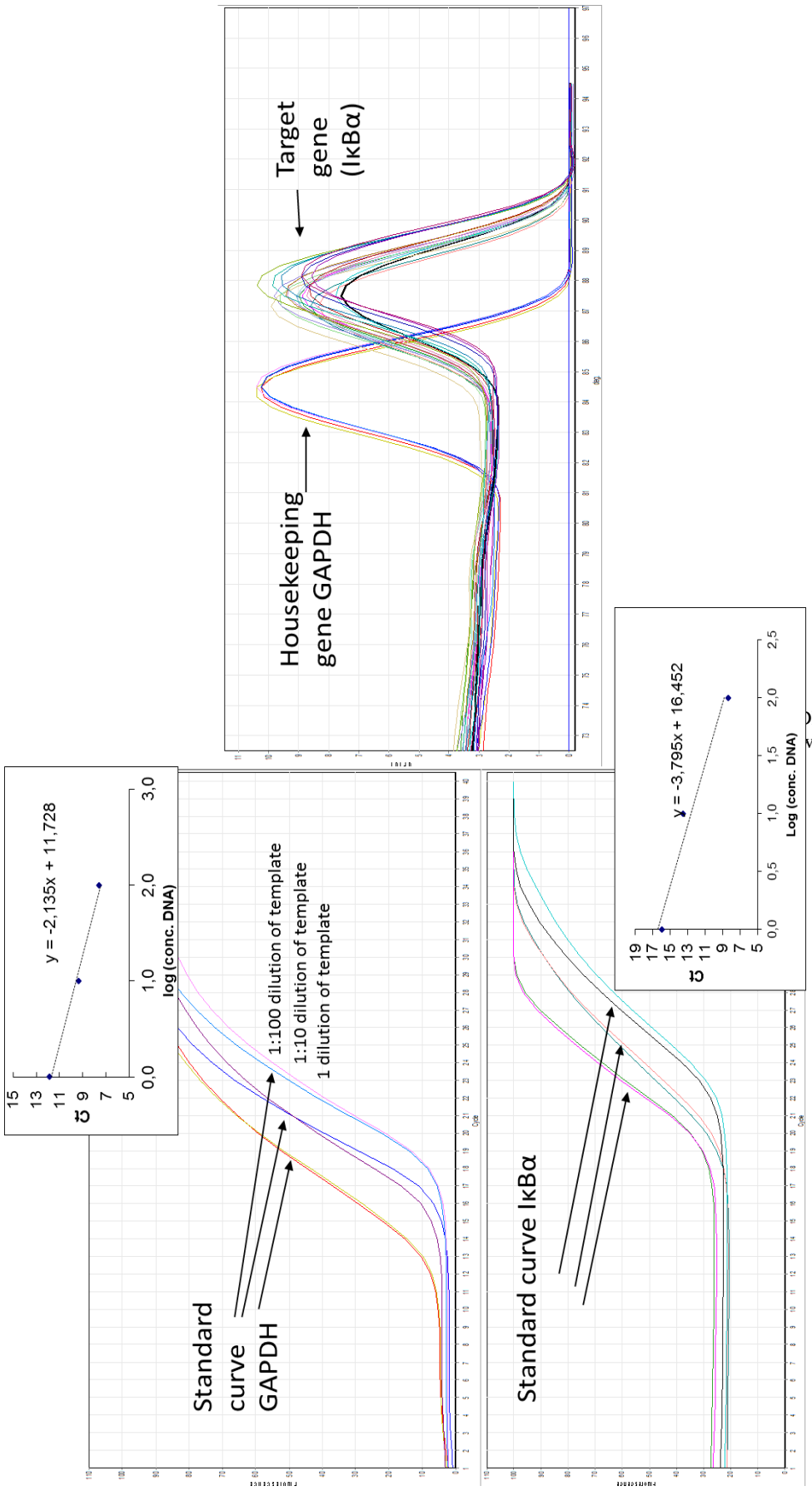

DH) and target gene (IκBα) (axis Y –fl
vare Rotor-Gene 6000 Series Software

Cross linking with glutaraldehyde

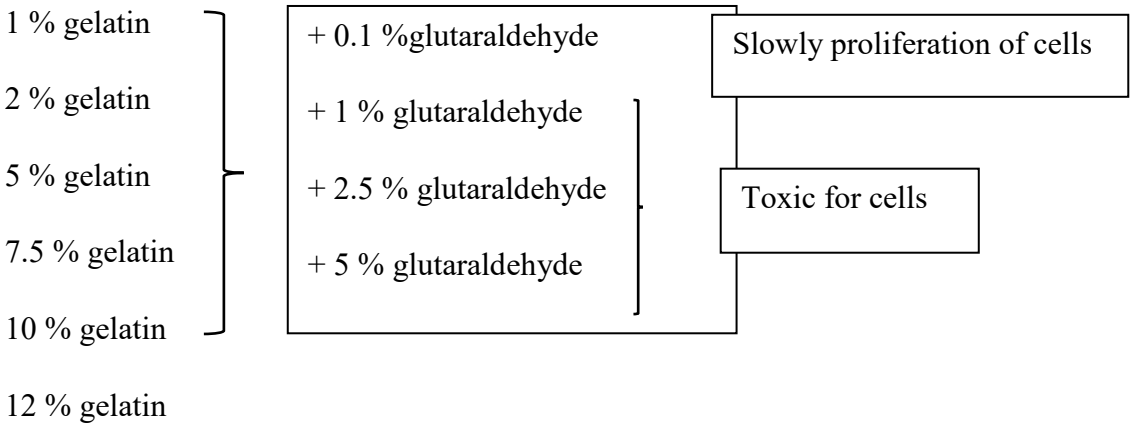

Cross linking with acetic acid

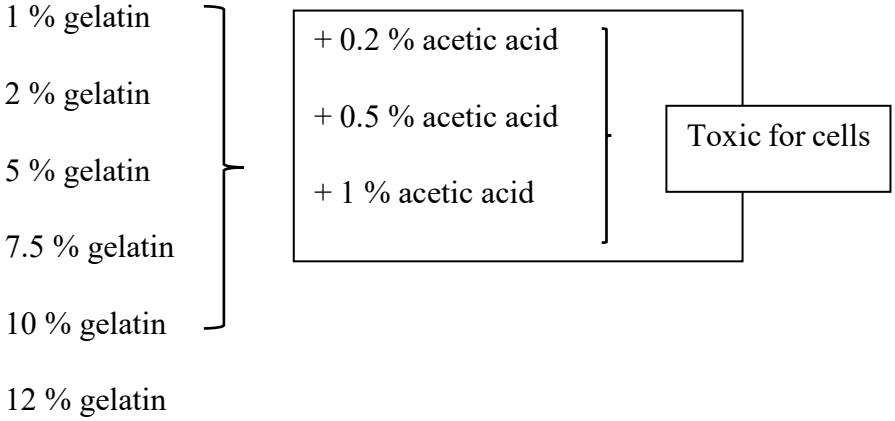

Figure A. 4 Schematic overview of the workflow of cross-linking gelatin development. Acetic acid and glutaraldehyde in different concentrations as cross-linking agents were examined with different concentrations of gelatin. However, both of them were problematic due to difficulties to remove their excess, which resulted in cell cytotoxicity.

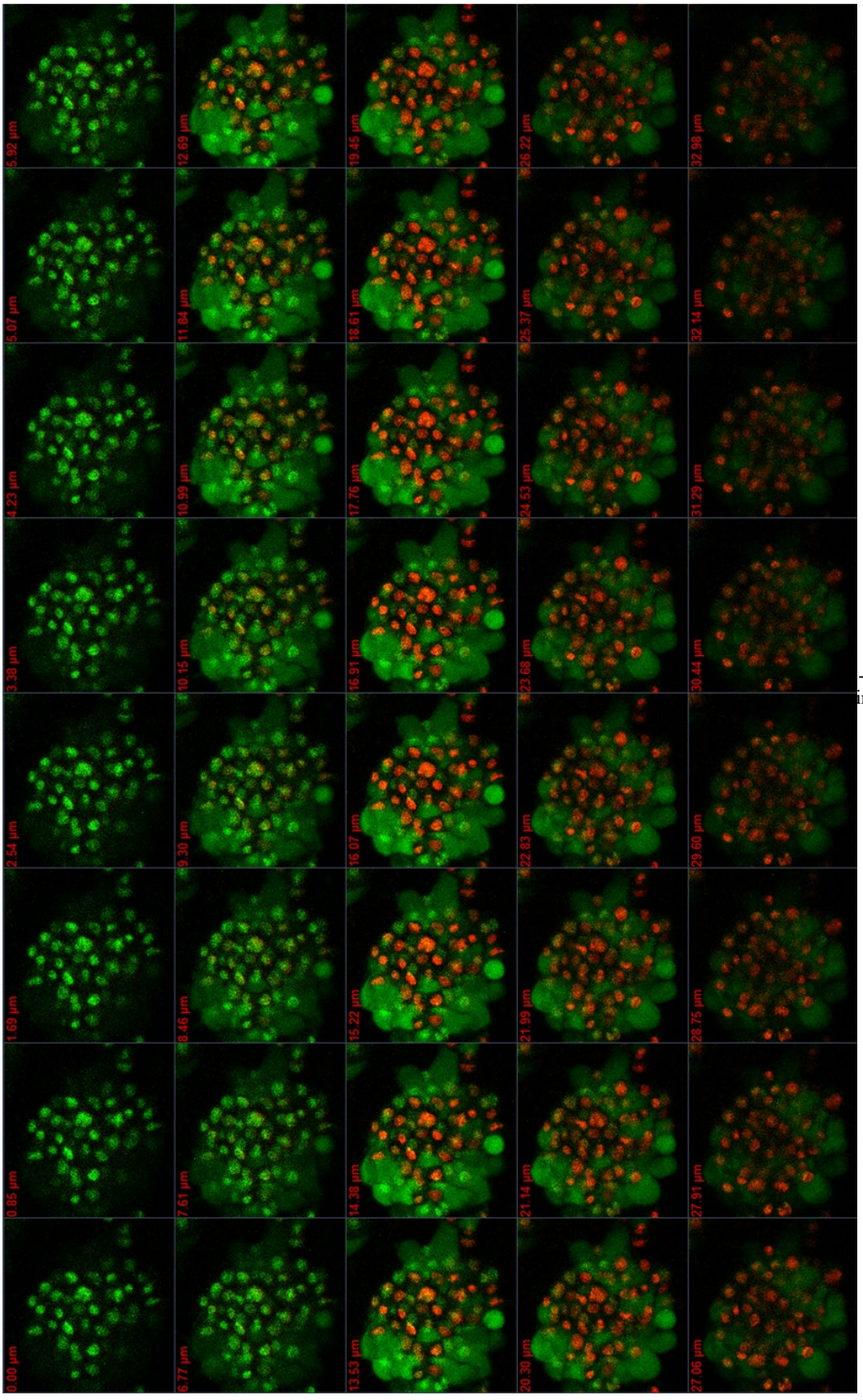

-stuck series from outer part of spher
in AM (green, viable cells) and propi

10 ACKNOWLEDGEMENTS

I am grateful to Prof. Karl-Heinz Feller for suggesting the topic and the opportunity to write this thesis under his guidance. I am indebted for allowing me to take part in valuable training schools, secondments and present progress of my project at numerous international scientific conferences. I really appreciate that your office door were open, especially during my last year. Thank you that you allowed me to grow in this group and develop my own ideas.

I thank to Prof. Thomas Winckler for scientific discussions, help with papers writing, patience, valuable comments, immediate responses to my email enquiry and nice contact during meetings.

I am indebted to my SAMOSS fellows Maureen, Leena, Guido, Riikka, Silvia, Maria, Frank, Koni, Sergio, Surjana, Ola, Heman, Laura and Sandro for the excellent working atmosphere and the scientific and sometimes maybe not so scientific discussions. Of course, I thank to all supervisors in SAMOSS network Prof. Maria Moreno-Bondi, Prof. Guillermo Orellana (Complutense University of Madrid), Prof. Karsten Haupt (University of Technology of Compiègne), Prof. Sabeth Verpoorte (University of Groningen), Prof. Levi Gheber (Ben-Gurion University of the Negev), Ursula Sauer (Austrian Institute of Technology GmbH) and Prof. Karl-Heinz Feller (Ernst Abbe University of Applied Sciences) for comments to results of my project during SAMOSS International Meetings, well organized training schools and friendly working environment. I truly feel that I have learned a lot from a brilliant researchers.

Thank to Assistance Professor Martin Jonsön-Niedziolka for organizing my stay in Institute of Physical Chemistry PAN (Polish Academy of Sciences) in Warsaw and for help with SEM images, DLS and contact angle measurements. Thanks a lot for cooperation and paper writing.

I also want acknowledge Dr. Günter Brader and again Ursula Sauer from Austrian Institute of Technology GmbH for training in molecular biology and Dr. Laura Moro, Mehmed Turemis, Dr. Maria-Teresa Giardi for excellent working environment during my secondment in Biosensor Company in Rome and scientifically fruitful period.

I thank all past and present colleagues in Instrumental Analysis Group at Ernst Abbe University of Applied Sciences. Thank to Ola, Dirk, Christiane and Konrad for friendly

conversations, I really felt support from you when I was in need. Ute your work was my inspiration. Astrid, I appreciate talks with you in the office, thank that you established in our lab Alamar Blue assay and always supported me with all difficulties in work with microscopes. Basti thank you for transfer of knowledge about bio-printing and positive spirit in general. Susi you was friendly companion in the lab, Krems, Regensburg and thanks that you always took seriously and answered for millions of my more and less important questions. Dr. Bartzsch thank you for very nice contact.

Acknowledgements for my former supervisors Prof. Zbigniew Madeja from Jagiellonian University in Cracow and Dr. Kirti Kaul from German Diabetes Center in Düsseldorf, you both taught me wide variety of research skills, you showed the magnificence of science, you helped to believe me in my own capabilities, you both are for me examples of Ideal Scientists. It was a big pleasure to be your student.

Thank to Marcel Noßmann (Ernst Abbe University of Applied Sciences) for advices in qPCR, Prof. Thomas Munder (Ernst Abbe University of Applied Sciences) for making possible to work in his lab, Eva Kling (Friedrich Schiller University Jena) for the help with Western Blot.

Finally, I am deeply grateful to my best friend and husband Jakub Szepietowski without your support this PhD-thesis would be never ended. At any time I was doubtful you were with me. Thank you that you accept I have done so far and you motivate me all the time to be strong enough to fight and realize my dreams. Now, I promise you the new era of our life with me more often present at home is starting.

Last but not least, thank to my mother Anna Dubiak for your life wisdom, you are my inspiration.

11 DECLARATION

I declare that presented PhD-thesis contains any material which has been accepted or submitted for other degree or diploma in my name, in any university or other tertiary institution and, to the best of my knowledge and belief, contains any material previously published written by another person, except where due reference has been made in the text. In addition, I certify that any part of this work will, in the future, be used in a submission in my name, for any other degree or diploma in any university or other tertiary institution. The same or similar work was not published elsewhere by other people. PhD- thesis was written by myself and all kind of contributions from other people are mentioned in acknowledgment part. Presented PhD-thesis partially contain in methods, results, discussion and summary parts already published data under my name (doi:10.1016/j.taap.2016.01.016 and second manuscript with results included in PhD-Thesis is in preparation). Nobody demanded from me, nor received financial compensation as part of conducted research or supervision. I declare that I read documents regarded dissertation and defense (Promotionsordnung) at Department of Pharmaceutical Biology in Jena from 4th December 2012.

Jena 12.05.2016

……..……..

Monika Dubiak-Szepietowska

12 CURRICULUM VITAE

PERSONAL INFORMATION

First name(s) / Surname(s)	**Monika Maria Dubiak-Szepietowska**
Address	Alte Wiesenstr. 5A, 07749 Jena (Germany)
Mobile	4915231070723
E-mail(s)	dubiak.monika@gmail.com
Nationality	Polish
Date of birth	3rd April 1989
Gender	Female
Marital status	Married

EDUCATION

10/2008 → 6/2011

Biotechnology at Jagiellonian University (faculty of Biochemistry, Biophysics, and Biotechnology), Cracow (Poland)

Bachelor's degree

10/2010 → 6/2013

Pharmacy at Jagiellonian University Medical College, Cracow (Poland)

10/2011 →6/2013

Biotechnology at Jagiellonian University (Faculty of Biochemistry, Biophysics, and Biotechnology), Cracow (Poland)

Master degree

11/2013 → present

PhD student in the frame of a Marie Curie Initial Training Network (ITN): Sample In – Answer Out Optochemical Sensing Systems (SAMOSS); Early Stage Researcher at Ernst Abbe University of Applied Sciences Jena / Friedrich Schiller University Jena (Germany)

TRAINING SCHOOLS

July 2014 Synthesis and characterization of new sensing materials (Complutense University of Madrid; Spain)

May 2015 Microfluidics (University of Groningen; The Netherlands)

October 2015 Light Microscopy and Fluorescence Techniques (Ben Gurion University of the Negev; Israel)

June 2016 Optical Biochips (Austrian Institute of Technology GmbH)

TRAINING/ SCIENTIFIC COOPERATION

July 2010 - August 2010 trainee in Poviat Sanitary-Epidemiological Station in Sieradz (Poland)
Responsibilities: Bacterial cultures from the biological material, parasitology, SPORAL *atrophaeus*, SPORAL *Stearothemophilus* assay.

October 2010- June 2011voluntary work in the Department of Microbiology Laboratory in addition to academic education.

October 2011 – February 2013 voluntary work in the Department of Cell Biology Laboratory in addition to academic education.

February 2013 – May 2013 trainee in German Diabetes Centre in Düsseldorf under supervision of Dr. Kirti Kaul
Responsibilities: Reactive oxygen species measurements (Amplex red method), oxygen consumption measurements (oxygraph), protein concentration measurements (BCA assay, Fluram assay), mitochondrial membrane potential measurements (TPP assay).

October 2014 cooperation with Assistance Professor Martin Jönsson-Niedziolka from Department of Electrode Processes at Polish Academy of Science in Warsaw (Poland)
Responsibilities: biological sample preparation for SEM, dynamic light scattering measurements.

April 2015 – May 2015 cooperation with Ursula Sauer and Dr. Günter Brader in Austrian Institute of Technology GmbH (AIT) in Tulln (Austria)
Responsibilities: plasmid amplification, Real-Time PCR, PCR, electrophoresis, primer design, preparation of competent prokaryotic cells.

March 2016 cooperation with Dr. Laura Moro, Dr. Maria Teresa Giauri and Mehmet Turemis in Biosensor Srl company in Rome (Italy)
Responsibilities: development cytotoxicity measurements with mutants of algae cells with fluorescence and absorbance readout.

CONFERENCES

- EASD Bariatrix 2013 in Barcelona (Spain). Coautor of presentation: *Hepatic mitochondrial function in human obesity: association with insulin sensitivity and oxidative stress.* Chrysi Koliaki, Julia Szendroedi, Kirti Kaul, Tomas Jelenik, Peter J. Nowotny, **Monika Dubiak** Markus Krausch, Wolfram Trudo Knoefel, Frank Jankowiak, Matthias Schlensak, Michael Roden

- BioNanoMed 2014 in Krems (Austria). Poster: *Bioengineering liver sensor cell line and cytotoxicity analysis of therapeutically used nanoparticles in 3D environment.* **Monika Dubiak-Szepietowska**, K.H. Feller

- EACR CONFERENCE SERIES 2014, Goodbye flat biology: 3D Models and the tumor microenvironment in Berlin (Germany). Poster: *Live cell-based biosensor as a cytotoxicity detector in 3D environment.* **Monika Dubiak-Szepietowska**, K.H. Feller

- 11th BBMEC 2015 in Regensburg (Germany). Poster and oral presentation: *Three dimensional environment for whole cell-based biosensor.* **Monika Dubiak-Szepietowska**, Martin Jönsson-Niedziolka, K.H. Feller

- 3D Cell Culture 2016: How close to 'in vivo' can we get? Models, applications & translation in Freiburg (Germany). Poster: *Cell-based biosensor as a cytotoxicity detector in 3D environment.* **Monika Dubiak-Szepietowska**, Martin Jönsson-Niedziolka, K.H. Feller

PUBLICATIONS RELATED TO PRESENTED PhD THESIS

- **Dubiak-Szepietowska, Monika**, Karczmarczyk, Aleksandra, Jönsson-Niedziółka, Martin, Winckler, Thomas. Feller, Karl-Heinz. (2016). *Development of complex-shaped liver multicellular spheroids as a human-based model for nanoparticle*

toxicity assessment in vitro. Toxicol Appl Pharmacol 294: 78-85.

- **Monika Dubiak-Szepietowska,** Aleksandra Karczmarczyk, Thomas Winckler, Karl-Heinz Feller. *Development of whole cell-based biosensor in 3D milieu as a detector for nanomaterials cytotoxicity detection.* In preparation

OTHER PUBLICATIONS

- Chrysi Koliaki, Julia Szendroedi, Kirti Kaul, Tomas Jelenik, Peter J. Nowotny, **Monika Dubiak,** Markus Krausch, Wolfram Trudo Knoefel, Frank Jankowiak, Matthias Schlensak, Michael Roden. (2013). *Hepatic mitochondrial function in human obesity: association with insulin sensitivity and oxidative stress* Diabetologia 56:[Suppl1]S1–S566, number of abstract: 198 DOI 10.1007/s00125-013-3012-z

- Aleksandra Karczmarczyk, **Monika Dubiak-Szepietowska**, Mariia Vorobii, Cesar Rodriguez-Emmenegger, Jakub Dostálek, Karl-Heinz Feller. (2016). *Sensitive and rapid detection of Aflatoxin M1 in milk utilizing enhanced SPR and p(HEMA) brushes.* Biosensors and Bioelectronics 81: 159-165.

- Aleksandra Karczmarczyk, Ciril Reiner-Rozman, **Monika Dubiak-Szepietowska** , Jakub Dostálek, Karl-Heinz Feller (2016). *Fast and sensitive biosensor for detection of Ochratoxin A (OTA) in red wine utilizing enhanced surface plasmon resonance (SPR) spectroscopy.* Submitted to Food Chemistry

ADDITIONAL INFORMATION

AWARD scholarship for the best student at Jagiellonian University

AWARD scholarship (CIRS/ ERASMUS organisation) for promising young scientist to perform research abroad (realized in German Diabetes Centre in Düsseldorf)

Marie-Curie Fellowship in SAMOSS network

1th place in poster award 11th BBMEC 2015 in Regensburg (Germany)

OUTREACH ACTIVITIES

Article in a local newspaper *Ostthüringer Zeitung* (20.11.2013)

Meeting with the rector of the University of Applied Sciences Jena and the state secretary of Thuringia where the SAMOSS project was presented, November 2013

Presentation of SAMOSS project in a local TV programme (Jena TV), November 2013

Guided tour for pupils through the science laboratories of Prof. Feller (07.02.2014)

Lecture during Year Of The Light in Jena, open day

All experiments are part of SAMOSS project

www.samoss.eu

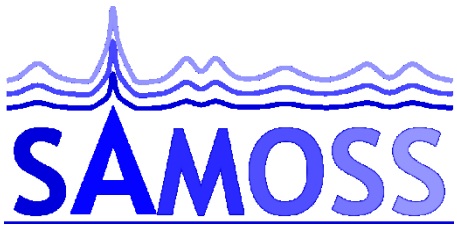

Founded: